



DOCTORAL PROGRAMME IN ELECTRONIC ENGINEERING

DOCTORAL THESIS

INDUSTRIAL DOCTORATE MENTION

Study of magnetic absorber sheets for EMI control in electronic devices

Author:

Jorge Victoria Ahuir

Supervisors:

Dr.Eng. José Torres País

Dr.Eng. Adrián Suárez Zapata

Universitat de València (UV)

Department of Electronic Engineering

Valencia, Spain – March 2024

VNIVERSITAT
DE VALÈNCIA

 Escola Tècnica Superior
d'Enginyeria ETSE-UV

Declaration

D. JOSÉ TORRES PAÍS, Doctor en Ingeniería Electrónica, Profesor Titular del Departamento de Ingeniería Electrónica de la Escola Tècnica Superior d'Enginyeria de la Universitat de València

D. ADRIÁN SUÁREZ ZAPATA, Doctor en Ingeniería Electrónica, Profesor Ayudante Doctor del Departamento de Ingeniería Electrónica de la Escola Tècnica Superior d'Enginyeria de la Universitat de València

HACEN CONSTAR QUE:

D. JORGE VICTORIA AHUIR, Ingeniero Técnico de Telecomunicación especialidad Sistemas Electrónicos e Ingeniero Electrónico, ha realizado bajo su dirección el trabajo titulado "Study of magnetic absorber sheets for EMI control in electronic devices", que se presenta en esta memoria para optar al grado de Doctor por la Universitat de València.

Y para que así conste a los efectos oportunos, y dando su conformidad para la presentación de este trabajo delante del Tribunal de Tesis Doctoral que corresponda, firma el presente certificado, en Valencia, a 22 de marzo de 2024.



Fdo. D. José Torres País



Fdo. D. Adrián Suárez Zapata

UNIVERSITAT DE VALÈNCIA
ESCOLA TÈCNICA SUPERIOR D'ENGINYERIA
Departamento de Ingeniería Electrónica

Av. De la Universidad s/n, 46100 Burjassot (Valencia)

Acta de Calificación de Tesis Doctoral

Tesis Doctoral: STUDY OF MAGNETIC ABSORBER SHEETS FOR EMI CONTROL
IN ELECTRONIC DEVICES

Autor: JORGE VICTORIA AHUIR

Director: Dr. JOSÉ TORRES PAÍS, Dr. ADRIÁN SUÁREZ ZAPATA

El Tribunal nombrado para juzgar la Tesis Doctoral citada anteriormente, compuesto por los doctores:

Presidente: _____

Vocal: _____

Secretario: _____

Acuerda otorgarle la calificación de _____

Y para que así conste a los efectos oportunos, firmamos el presente certificado.

En Valencia, el _____ de _____ de 2024

Note to the Reader

According to the University of Valencia Doctorate Regulation¹ this Ph.D. dissertation is presented as a compendium of at least three publications in international journals containing the results of the conducted work.

This is an Industrial Doctorate developed within the Würth Elektronik eiSos research and innovation strategy and the scientific environment of the University of Valencia.

Furthermore, in accordance with the aforementioned regulation and with the aim of fostering the language of the University of Valencia in research and education activity, this Ph.D. dissertation starts with an extended abstract in one of the official languages of the Valencian Community (Spanish). Page XXI includes a short abstract in English followed by the research context, motivation, objectives, theoretical fundamentals, methodology, results, and conclusions.

¹Reglament sobre depòsit, avaluació i defensa de la tesi doctoral aprovat pel Consell de Govern de 28 de Juny de 2016. ACGUV 172/2016.

Pla d'increment de la docència en valencià (ACGUV 129/2012) aprovat i modificat pel Consell de Govern de 22 de desembre de 2016. ACGUV 308/2016.

Resumen

1. Contexto de investigación y motivación

El control de las interferencias electromagnéticas (EMI) entre dispositivos, subsistemas y componentes electrónicos es una tarea necesaria y compleja, sujeta continuamente a nuevos y mayores retos. La investigación, desarrollo y transferencia a la sociedad de soluciones a dichos retos es el objetivo de la Cátedra de Compatibilidad Electromagnética (EMC) creada por Würth Elektronik eiSos y la Universitat de València.

Este Doctorado Industrial se desarrolla en este ámbito de cooperación entre empresa y Universidad, enfocado en la innovación y la transferencia de soluciones de apantallamiento electromagnético.

El apantallamiento electromagnético es una solución extremadamente eficaz, capaz de atenuar las interferencias electromagnéticas en decenas de decibelios (dB) sin necesidad de rediseñar los circuitos electrónicos y sin reducir su velocidad de conmutación.

Sin embargo, la proliferación de sistemas de comunicación basados en el acoplamiento magnético (p.ej. *Near Field Communication* (NFC), *Wireless Power Communication* (WPC)) o en altas frecuencias (p.ej. 5G) generan la necesidad de nuevas soluciones y materiales de apantallamiento. Estos nuevos materiales deben ser capaces de evitar las EMI sin afectar a los rangos de frecuencia necesarios para la comunicación.

Las láminas de absorción electromagnética (MAS) basadas en ferritas pueden ser diseñadas para solucionar estas nuevas problemáticas, pero para ello es necesario un buen conocimiento, no solo de su composición, sino de su comportamiento en frecuencia sobre la aplicación final. En este trabajo se estudian tanto las láminas de ferrita sinterizada (FSFS) como las láminas de polímero con partículas de ferrita embebidas (NSS).

Tradicionalmente estas láminas vienen caracterizadas por su permeabilidad inicial (a 10 kHz o 1 MHz) o por la gráfica de la permeabilidad compleja en función de la frecuencia. Estos valores nos permiten estimar la capacidad del material para desacoplar un campo magnético, o los rangos de frecuencia en los que el material permite redirigir o absorber el flujo magnético. En cambio, no nos aportan ninguna información sobre la influencia del espesor o la forma de la lámina, su superficie de contacto o la distancia en relación con el circuito electrónico en el que se aplica.

Esta falta de información y comprensión del comportamiento de las láminas de absorción electromagnética lleva a que el diseñador electrónico deba elegir el producto

final mediante el método de prueba/error y que en muchas ocasiones desestime este tipo de solución debido a su aparente complejidad.

Esta tesis doctoral se basa en la hipótesis de que las láminas de absorción electromagnéticas adecuadamente diseñadas, pueden ofrecer solución a nivel de circuito impreso a los retos de EMI de creciente complejidad y rango de frecuencia.

Se pretende además aportar las herramientas y el conocimiento necesario para caracterizar las láminas de absorción electromagnéticas, no sólo en cuanto a su composición sino también en su comportamiento para cada aplicación en la que puede resultar útil, así como herramientas de simulación y medida para diseñar y verificar una solución eficaz ante las EMI.

Los resultados obtenidos se transfieren a la sociedad a través de la Cátedra EMC Wurth Elektronik – Universitat de València y la empresa Wurth Elektronik eiSos en forma de publicaciones científicas, seminarios, información técnica y productos.

2. Objetivos

Teniendo en cuenta el contexto de la investigación, la motivación y la hipótesis anteriormente definidos, el objetivo general de la presente tesis doctoral se define de la siguiente manera:

Estudiar, analizar y evaluar la idoneidad de las láminas de absorción electromagnética como solución a diversos problemas de EMI, y caracterizar los materiales mediante parámetros y modelos de simulación que permitan optimizar el diseño final.

En este sentido, se proponen los siguientes objetivos específicos (O.E.) para realizar la investigación de estos estudios doctorales que permitan dar solución a las dificultades previamente planteadas:

- **O.E.1:** Caracterización de los absorbentes magnéticos mediante sus propiedades electromagnéticas. Implementación de los sistemas de medida.
- **O.E.2:** Caracterización del comportamiento de los absorbentes magnéticos frente a las EMI en aplicaciones de filtrado, desacoplo, absorción y apantallamiento electromagnético. Diseño e implementación de los sistemas de medida.
- **O.E.3:** Creación de modelos de simulación para predecir los efectos de los absorbentes magnéticos, basados en sus propiedades físicas (forma, tamaño, espesor) y electromagnéticas (permeabilidad, permitividad, conductividad).

- **O.E.4:** Validación de los modelos comparando la simulación de sistemas de medida con los resultados experimentales.
- **O.E.5:** Validación de la utilidad de los modelos sobre una aplicación real: Optimizar sistemas de comunicación en campo cercano.
- **O.E.6:** Diseñar, optimizar y evaluar una nueva lámina de absorción magnética para aplicaciones de apantallamiento electromagnético en el circuito impreso (*Board-Level Shielding* (BLS)), validando así la hipótesis de partida de la presente tesis.
- **O.E.7:** Generar un producto final con la configuración óptima, composición y espesor que permitan reducir las EMI en un amplio rango de frecuencias. Se completa así la transferencia a la empresa y a la sociedad de esta solución a un problema tecnológico de relevancia objeto del presente Doctorado Industrial.

3. Metodología

La presente tesis doctoral se basa en un compendio de publicaciones científicas las cuales han superado una revisión por pares internacionales. El cuerpo de la tesis incluye un total de tres artículos publicados en revistas indexadas en el *Journal Citation Reports* (JCR), tres artículos presentados en congresos internacionales y un artículo presentado en un congreso nacional. Cada uno de ellos describe la investigación llevada a cabo para alcanzar cada uno de los objetivos específicos planteados en la sección anterior.

En base a este formato de tesis por compendio, la metodología se desarrolla en 5 capítulos que se abordan empezando por una revisión de los conceptos y contenidos tratados en este estudio (**Capítulo 2**). En el **Capítulo 3** se describe la caracterización de las láminas de absorción magnética mediante dos contribuciones a congreso. En el **Capítulo 4** se simula el comportamiento de las láminas para solucionar problemas tecnológicos concretos en la primera publicación científica en revista y la tercera contribución a congreso. Finalmente, se desarrolla y evalúa una nueva solución basada en láminas absorbentes en el segundo y tercer artículo científico y la cuarta contribución a congreso (**Capítulo 5**). En el **Capítulo 6** se resumen las conclusiones de la tesis y la transferencia del conocimiento generado.

Capítulo 3 - Artículo de contribución a congreso I: Characterization of electromagnetic noise suppression sheet for Aerospace applications.

En el primer artículo, presentado en el “IEEE ESA Workshop on Aerospace EMC” en 2016, se implementan los principales métodos de caracterización de absorbentes electromagnéticos y se analizan los resultados obtenidos con diferentes materiales y espesores.

Los absorbentes electromagnéticos son caracterizados por su permeabilidad electromagnética, pero su efecto sobre una aplicación determinada depende en gran medida de sus dimensiones y geometría, así como de las propiedades de la fuente de EMI. En este artículo se presentan tres métodos de caracterización destinados a evaluar el comportamiento de los absorbentes en diferentes aplicaciones, considerando los diferentes parámetros. Con ellos analizamos múltiples muestras con diferentes características y evaluamos su capacidad para solucionar problemas de EMI en líneas de transmisión, cavidades resonantes y acoplamiento magnético entre circuitos o componentes próximos.

Con el método de la línea de transmisión, colocamos la muestra de absorbente sobre un circuito impreso (PCB) con una línea conductora diseñada para mantener una impedancia constante de $50\ \Omega$ en un amplio rango de frecuencia. Medimos la atenuación producida por el absorbente entre un extremo y otro de la línea mediante un analizador de redes, caracterizando así su efecto como filtro paso-bajo. Al medir muestras con diferentes espesores y materiales vemos que el efecto de filtrado se incrementa con el espesor, y con el valor de la permeabilidad. Al aumentar el espesor observamos también que la frecuencia de corte del filtro se reduce.

Mediante una línea coaxial, colocando las muestras frente a un material reflectante en la terminación, podemos medir su capacidad de absorción al medir la energía reflejada con el analizador de redes. Esta medida nos permite evaluar la utilidad de los diferentes materiales y espesores para reducir o eliminar las resonancias electromagnéticas producidas en el interior de un dispositivo electrónico, debido a las reflexiones múltiples generadas por la radiación producida por el funcionamiento del propio dispositivo. En las medidas obtenidas se aprecia un aumento en la absorción con el aumento de espesor, así como un desplazamiento en el pico de absorción hacia frecuencias más bajas.

Con el objetivo de evaluar el apantallamiento magnético de los absorbentes para prevenir la aparición de EMI por acoplamiento entre el generador de EMI y su víctima, reproducimos dicha situación mediante nuestro diseño experimental. Diseñamos dos antenas de baja impedancia, y utilizamos una como emisor (conectándola a la salida del analizador de redes) y otra como receptor (conectándola a la entrada), las colocamos en paralelo a una distancia fija e introducimos la muestra de absorbente entre ellas. Medimos así la capacidad de desacoplo. En los resultados se observa una dependencia directa con la permeabilidad y el espesor de las muestras.

Con los diferentes sistemas de medida implementados se puede seleccionar el material idóneo para cada aplicación en función de las frecuencias críticas y su nivel de energía. Los resultados aportan información sobre el efecto del espesor, y son consecuentes con las medidas de permeabilidad.

Capítulo 3 – Artículo de contribución a congreso II: Characterization of Flexible Absorber Sheets with an EMC Scanner System

En este artículo presentado en el “Seminario Anual de Automática, Electrónica Industrial e Instrumentación (SAAEI)” en 2017, diseñamos un experimento para analizar el efecto de los absorbentes magnéticos en la reducción de EMI a nivel de PCB.

Diseñamos un circuito que genera interferencias de alta frecuencia, y trazamos las pistas de modo que se maximice la radiación. Utilizamos un equipo de medida basado en una matriz de sondas de campo cercano (EMScan), conectado a un analizador de redes, que nos permite medir la distribución del campo magnético en cada frecuencia.

En los resultados observamos que los absorbentes magnéticos son capaces de reducir el campo magnético de manera significativa en un determinado rango de frecuencias. Esta habilidad puede ser útil para resolver problemas de EMI a nivel de PCB (BLS) sin necesidad de rediseñar el circuito ni modificar componentes, lo que representa un gran beneficio para los diseñadores en la etapa de certificación de sus dispositivos.

Se demuestra también la utilidad del EMScan tanto para localizar las zonas críticas de la PCB como para evaluar el impacto de las medidas correctivas aplicadas, como en este caso el apantallamiento mediante láminas de absorción magnética.

Capítulo 4 - Artículo científico I: Improving the efficiency of NFC systems through optimizing the Sintered Ferrite Sheet thickness selection

En este artículo se analiza el uso de absorbentes magnéticos, en este caso láminas de ferritas sinterizadas, para mejorar la eficiencia de sistemas de comunicación en campo cercano.

Los sistemas de comunicación NFC se basan en el principio de inducción magnética desde la antena emisora a la receptora. La presencia de superficies eléctricamente conductoras a su alrededor puede interferir hasta el punto de impedir su correcto funcionamiento. El campo magnético generado por el emisor puede inducir corriente en un plano metálico (*Eddy currents*), esta corriente genera a su vez un campo magnético en sentido opuesto. Esta alteración afecta a la magnitud del campo magnético, a la distancia máxima de comunicación y al ajuste de la frecuencia de resonancia a la que emisor y receptor se comunican (13.56 MHz para NFC).

Las láminas flexibles de ferrita sinterizada, colocadas entre la antena y el plano conductor, pueden prevenir estas interferencias electromagnéticas gracias a su capacidad de redirigir el flujo magnético. La FSFS evita que el flujo atraviese el plano y el efecto de las *Eddy currents*. Para ello, es importante que la FSFS seleccionada presente

a 13.56 MHz una permeabilidad alta (μ') y unas bajas pérdidas (μ'') para no reducir el flujo.

En este trabajo analizamos el rendimiento de las FSFS para compensar el efecto de un plano conductor en una antena NFC en función de su espesor, de manera que la frecuencia de comunicación de la antena no se vea alterada y la comunicación se mantenga sintonizada.

Para ello diseñamos una antena NFC en un circuito impreso, a la que podemos añadir los diferentes espesores de FSFS, una lámina de aluminio a una distancia controlada, o una batería para simular una situación real.

Un analizador de redes nos permite medir la frecuencia de resonancia original de la antena, su valor cuando se añade la lámina conductora y se intercala la FSFS. Mediante una configuración de medida basada en la matriz de sondas magnéticas EMSCan y un analizador de espectros, observamos la distribución del campo magnético y el efecto producido por las diferentes combinaciones de planos conductores con FSFS.

Simulando la antena, y usando los modelos de los materiales, podemos obtener tanto la frecuencia de resonancia como la magnitud y distribución del campo magnético. Los resultados son comparados con los obtenidos experimentalmente.

Este trabajo nos permite concluir que las FSFS pueden solucionar los problemas de interferencia de planos metálicos en sistemas NFC, que es crítica la selección de su espesor para garantizar una comunicación óptima, y que las simulaciones basadas en elementos finitos y los modelos generados en este trabajo resultan de gran utilidad y precisión para este propósito.

Capítulo 4 - Artículo de contribución a congreso III: Design approach for high efficiency NFC systems with magnetic shielding materials

En esta contribución presentada en el congreso “IEEE EMC Europe” de 2020 analizamos el uso de láminas de compuesto ferrita-polímero, conocidas como *Noise Suppression Sheet* (NSS) para la solución de problemas relacionados con la presencia de metales en sistemas de NFC no apantallados magnéticamente.

Las láminas de ferrita tienen una alta permeabilidad, lo que en ocasiones puede provocar un exceso de inductancia en las antenas y en consecuencia un desajuste en la frecuencia de resonancia (13.56 MHz). Las NSS estudiadas aquí, con una baja permeabilidad ($\mu_r = 25$) a la frecuencia de comunicación, nos permiten ajustar con mayor precisión la inductancia necesaria para robustecer el sistema sin afectar a la comunicación. Esto puede resultar especialmente útil con planos metálicos ligeramente alejados de la antena, o materiales con una conductividad menor.

Para ello, evaluamos diferentes espesores colocados entre la antena NFC y un plano metálico a 0.5 mm de distancia, y analizamos el circuito equivalente y la frecuencia de resonancia en cada situación.

Los resultados están basados en medidas con la carta de Smith mediante un analizador de redes, y simulaciones realizadas con los modelos desarrollados en esta tesis y el software de simulación electromagnética ANSYS HFSS.

De ellos se concluye que la presencia de una superficie metálica disminuye la inductancia de la antena, desplazando la frecuencia de resonancia e imposibilitando la comunicación del sistema. Una NSS debidamente dimensionada permite aumentar la inductancia, sin aumentar la resistencia, devolviendo dicha frecuencia a su valor idóneo. Se demuestra asimismo la utilidad y la precisión en la fase de diseño tanto de las medidas con carta de Smith como de las simulaciones con los modelos creados.

Capítulo 5 – Artículo científico II: Transmission Attenuation Power Ratio Analysis of Flexible Electromagnetic Absorber Sheets Combined with a Metal Layer

En este artículo se propone la combinación de una lámina de absorbente magnético con otra de metal para aumentar el efecto en la eliminación de las EMI sobre una línea de transmisión.

Utilizamos un diseño experimental basado en el standard IEC 62333-2. Nuestro circuito simula una línea de transmisión entre los puertos S_1 y S_2 de nuestro analizador de redes. Al aplicar sobre la línea una lámina absorbente se puede cuantificar la atenuación producida en las diferentes frecuencias mediante los parámetros S_{21} (energía transmitida del puerto 1 al puerto 2) y S_{11} (energía reflejada al puerto 1 por la discontinuidad en la línea de transmisión generada por la introducción del absorbente). Esta atenuación presenta un perfil de filtro paso-bajo que permite la reducción de las EMI a altas frecuencias.

Combinamos diferentes materiales y espesores tanto de absorbente como de metal para analizar su efecto sobre la magnitud y la distribución en frecuencia de la atenuación obtenida.

Al añadir una capa metálica, paralela tanto a la línea como al plano de masa del circuito, corremos el riesgo de que la señal sea radiada por la misma debido al acoplamiento capacitivo o a los campos magnéticos generados por las *Eddy currents* en el metal.

Para medir la re-radiación implementamos un nuevo diseño experimental. Añadimos una sonda de campo cercano colocada directamente sobre la capa metálica y la conectamos al puerto 2 del analizador de redes. Terminamos nuestra línea de transmisión

con una carga de $50\ \Omega$ y medimos la transmisión S_{21} , que en este caso representa que parte de la energía transmitida por el puerto 1 es radiada a la sonda de campo magnético conectada al puerto 2 para cada frecuencia.

Los resultados obtenidos demuestran que la combinación del absorbente con el metal ofrece mayor atenuación y rango de frecuencia que el absorbente original. En los casos en que la permeabilidad del absorbente es muy alta y el espesor es mayor, este efecto se ve reducido debido a que el campo electromagnético que llega a la capa metálica es menor.

También se comprueba que tanto cobre como aluminio ofrecen resultados similares, y que no se producen efectos significativos de re-radiación en ningún caso.

Capítulo 5 – Artículo de contribución a congreso IV: Board-level shielding with magnetic absorber sheet

Esta contribución fue presentada en el congreso “IEEE EMC Europe” de 2022. En ella evaluamos la posibilidad, basada en los resultados del artículo previo, del uso de la combinación de una lámina NSS, una lámina de metal y una lámina adhesiva para el apantallamiento electromagnético en circuitos impresos (BLS).

La solución clásica para el BLS es una caja metálica abierta por un lado, que cubre la zona de la PCB que se quiere apantallar. Debe ir soldada a un plano de masa que cubra la sexta cara de la caja formando así una celda de Faraday. Con la combinación de la absorción magnética de las NSS y los efectos de reflexión y absorción por *Eddy currents* de la capa metálica pretendemos obtener una solución de eficacia equivalente y con mejoras prácticas en cuanto a diseño y aplicación.

Para evaluar y comparar el apantallamiento electromagnético (SE) de ambas soluciones diseñamos un experimento basado en un circuito impreso que genera campos electromagnéticos en un amplio rango de frecuencia y que permite insertar las diferentes soluciones. Las medidas se miden con un dispositivo EMScan conectado a un analizador de espectros.

Se comparan los resultados de apantallamiento obtenidos con una caja metálica soldada al plano de masa (solución clásica de BLS), láminas NSS y diversas combinaciones de NSS de diferentes espesores y láminas aluminio y cobre. Se concluye que la combinación de NSS con metal produce mayor atenuación en un mayor rango de frecuencias que la NSS y que no hay diferencias significativas entre el uso de aluminio o cobre. Los resultados del compuesto híbrido son comparables, aunque inferiores a los obtenidos con la caja metálica. A cambio el compuesto presenta la ventaja de no necesitar un circuito impreso diseñado específicamente para su correcta soldadura al

plano de referencia, por lo que resulta una solución interesante sin necesidad de rediseño.

Capítulo 5 – Artículo científico III: Advanced Characterization of a Hybrid Shielding Solution for Reducing Electromagnetic Interferences at Board Level

En el último artículo publicado diseñamos y validamos la solución híbrida para BLS.

En primer lugar, caracterizamos la NSS seleccionada mediante su permeabilidad y permitividad, así como el apantallamiento (SE) de los materiales para la capa metálica aluminio y cobre.

Para cuantificar el SE de la solución final diseñamos e implementamos un nuevo sistema de medida. Utilizamos una línea de transmisión de 20 mm conectada a un generador de señal como fuente de emisiones electromagnéticas, y una sonda de campo magnético a una distancia fija como receptor. Aplicando diferentes soluciones de BLS medimos la magnitud del SE en cada frecuencia.

Creamos un modelo de elementos finitos del sistema diseñado y, utilizando los modelos de las NSS generados en esta tesis, simulamos el apantallamiento de las diferentes combinaciones: NSS, solución híbrida NSS con lámina metálica y caja metálica soldada al plano de masa. Comparando los resultados experimentales con los simulados se demuestra la validez de nuestros modelos.

La simulación generada nos permite optimizar el espesor del NSS para obtener una máxima SE al combinarlo con la lámina metálica.

Finalmente, gracias a la simulación, analizamos la distribución del campo magnético en las diferentes situaciones. Observamos que existe un riesgo de re-radiación en los bordes de la solución híbrida, y que este se elimina aumentando el área cubierta de forma que se cubra en exceso la fuente de radiación.

En este artículo se demuestra tanto la validez de la simulación y los modelos, como su utilidad en el diseño y el análisis de las diversas soluciones. Se comprueba también que la solución híbrida diseñada ofrece unos resultados de SE comparables a los de la solución clásica, añadiendo grandes ventajas en cuanto a la aplicación, el espacio y la facilidad de uso sin la necesidad de rediseño.

4. Conclusiones

Los absorbentes magnéticos han sido estudiados, analizados y evaluados en profundidad en esta tesis doctoral, demostrando su utilidad para el control de las EMI. Además, esta tesis doctoral proporciona una caracterización completa de los materiales a través de diferentes métodos de medida experimentales y modelos de simulación que

permite determinar su rendimiento desde el punto de vista de las propiedades magnéticas, dimensiones, y posición en el dispositivo electrónico a proteger.

Las medidas de permeabilidad, resistividad y permitividad nos han permitido caracterizar las propiedades electromagnéticas de los materiales. Hemos podido caracterizar el rendimiento de las láminas absorbentes para la prevención de EMI gracias a las medidas implementadas de pérdidas de transmisión, absorción y desacoplo. También hemos utilizado una matriz de sondas de campo magnético (EMScan) para medir el efecto de los diferentes absorbentes sobre la distribución del campo magnético. Además, hemos diseñado un sistema para cuantificar la efectividad del apantallamiento electromagnético, y compararla con otras soluciones de BLS.

Utilizando las medidas de caracterización realizadas, hemos generado modelos de simulación por elementos finitos de las diferentes láminas de absorción estudiado (FSFS, NSS, solución híbrida). También hemos simulado los sistemas de medida, lo que nos ha permitido validar los modelos comparando los resultados obtenidos en la simulación con los experimentales. Los modelos nos han servido para solucionar de manera óptima problemas de EMI en sistemas de comunicación en campo cercano (NFC). Las soluciones obtenidas mediante simulación han sido también corroboradas por medidas experimentales, y utilizadas en combinación con la Carta de Smith y el circuito equivalente del sistema de comunicación.

Los métodos experimentales diseñados, y los modelos de simulación validados, nos han permitido diseñar y evaluar una nueva solución para el apantallamiento electromagnético en los circuitos impresos. Esta solución se basa en la combinación de una NSS y una capa de aluminio. Tanto la selección de los materiales como sus espesores han sido realizado con los conocimientos, simulaciones y medidas presentadas en este trabajo. La simulación nos permite además observar el efecto de esta solución híbrida sobre la distribución de los campos electromagnéticos, lo que nos permite optimizar sus dimensiones para cada problema dado.

Queda así demostrada la hipótesis de la presente tesis doctoral, las láminas de absorción electromagnéticas permiten la solución de problemas complejos de EMI a nivel PCB. Las herramientas de medida y simulación generadas, unidas a la flexibilidad en el desarrollo de nuevos compuestos basados en materiales ferrimagnéticos, sientan las bases para el desarrollo de soluciones a presentes y futuros retos en el campo de la compatibilidad electromagnética.

La transferencia tecnológica de los resultados de esta tesis doctoral se ha realizado a varios niveles.

Todos los sistemas de medida diseñados han sido instalados en alguno de los diferentes laboratorios de la empresa Würth Elektronik en su sede central de Waldenburg

(Alemania), su centro de calidad en Shenzhen (China) o en el laboratorio de la Cátedra EMC Würth Elektronik – Universitat de València. Las medidas obtenidas han sido introducidas en sus bases de datos y pueden ser consultadas en las hojas de datos de los productos o en la aplicación para selección de productos RedExpert.

Los modelos de simulación generados y validados, además de ser transferidos a las bases de datos de la empresa, son accesibles a través de su página web y han sido incluidos en las librerías del software de simulación ANSYS.

La solución híbrida diseñada para BLS se ha convertido en un producto ofrecido al mercado por Würth Elektronik con el nombre de EMI Patch™.

Además, el conocimiento generado ha servido como contenido de publicaciones, notas de aplicación y seminarios en los diversos países en los que la empresa Würth Elektronik está presente (52 en 2024).

Abstract

The choice of materials for electromagnetic interference (EMI) suppression application is determined by the frequency of the interference or disturbance and the operational frequency that the material must pass.

Ferrites behave at low frequencies as suitable inductors but are quite lossy at high frequencies, making them valuable materials for EMI solutions. They are commonly used for LC filters of several types, using ferrite beads over traces or toroids to encircle cables, absorb the offending noise, and reduce the incoming radiated fields by magnetic shielding. This research will study the implementation of ferrites into thin, flexible sheets and their properties and applications in EMI.

Magnetic Absorber Sheets (MAS) can be produced by embedding ferrite particles in a polymer material, these are known as Noise Suppression Sheets (NSS), or by sintering a thin layer of ferrite and protecting it with plastic layers on both sides, Flexible Sintered Ferrite Sheet (FSFS).

We first characterize the MAS through their electromagnetic properties: permeability, permittivity, and resistivity. In the second step, we measure their performance when used as a countermeasure for EMI, such as absorbers, filters, and magnetic shields, including the influence of the material composition and the thickness of the sheets.

Simulation models are created using electromagnetic properties. We validate the models through measurements and use them in EMI challenges like optimizing and protecting near-field communication systems (NFC).

Finally, we use the knowledge, measurement configurations, and modeling procedures generated to develop a new board-level shielding solution. This hybrid solution combines an NSS, an aluminum layer, and an electrically isolating adhesive.

Keywords: electromagnetic interference (EMI) suppressors, electromagnetic compatibility (EMC), magnetic shielding, noise suppression sheet (NSS), finite element method (FEM) simulation, relative permeability, shielding effectiveness (SE), insertion loss.

Acknowledgements

This thesis is the result of a long journey, during which I have been fortunate to enjoy the support and collaboration of phenomenal individuals and institutions.

First and foremost, I would like to thank my thesis advisors, José Torres and Adrián Suárez, who have motivated, accompanied, and guided me from the first to the last day. I hope we continue to share projects for many more years because we make a great team.

I also want to express my gratitude to my colleagues at Würth Elektronik. To my boss, Steffen Muetsch, who has allowed me to balance my doctoral studies with my daily work. To my partner in the struggles with FAS and FSFS, Antonio Alcarria, who will surely continue this research and add his own doctoral thesis. To the growing team of Shielding & Thermal, with Víctor and Sebas at the helm, and Iván, Toni, Lisa, and María bailing water.

Thanks also to the colleagues from the Catedra. To Pedro Martínez, a genius in design and simulation, I hope my work motivates you (if I could, so can you). To Andrea, a researcher with an incredible future, to Roberto, who has brought a whole new world of equations to absorbers, and to the DSDC group (Jesús, Julio, Rai) with their always wise advice.

I am grateful for the unwavering support of my family. To my parents, Juan and Vicen, I thank them for their love, patience, and constant encouragement over the years. To my siblings, Juanma and Angeles, for the tough burden of being my siblings. To my children, Darah, Kira, and Maia, I thank them for never stopping playing, arguing, shouting, interrupting, and laughing, regardless of their father's thesis, because they are children, after all.

I also want to thank TU Graz University, especially professors Deutschman, Winkler, and Pommerenke, and KU Leuven University, with Professor Pissort at the helm. Their selfless collaboration has allowed me to use equipment and acquire knowledge that I thought was beyond my reach.

I will also always be grateful to two people who sparked my interest in electromagnetic compatibility, and then made it fun and passionate. First, Professor Henry W. Ott with his book "Electromagnetic Compatibility," and then Professor Arturo Mediano with his courses, presentations, and conversations at events, conferences, and spontaneous encounters.

Last but not least, I want to thank all those who, in one way or another, contributed to this work, even if they are not specifically mentioned here. Their influence has left an indelible mark on this project.

Agradecimientos

Esta tesis es el fruto de una carrera de fondo, durante la que he tenido la suerte de disfrutar del apoyo y la colaboración de fenomenales personas e instituciones.

En primer lugar, quiero agradecer a mis directores de tesis, José Torres y Adrián Suárez, que me han motivado, acompañado y orientado desde el primer hasta el último día. Espero que sigamos compartiendo proyectos muchos años más porque hacemos un gran equipo.

También quiero agradecer a mis colegas en Würth Elektronik. Al jefe, Steffen Muetsch, que me ha permitido compatibilizar el doctorado con mi trabajo diario. A mi compañero de fatigas con las FAS y las FSFS, Antonio Alcarria, que seguro continuará con la investigación y le sumará su propia tesis doctoral. Al creciente equipo de Shielding & Thermal, con Víctor y Sebas a la cabeza, e Iván, Toni, Lisa y María achicando agua.

Gracias también a los compañeros de la Cátedra. A Pedro Martínez, un crack del diseño y la simulación, espero que mi trabajo te motive (si yo he podido tú también). A Andrea, una investigadora con un futuro increíble, a Roberto que ha traído a los absorbers un mundo nuevo de ecuaciones, y al grupo de DSDC (Jesús, Julio, Rai) con sus siempre sabios consejos.

Agradezco el apoyo incondicional de mi familia. A mis padres, Juan y Vicen, les agradezco su amor, paciencia y aliento constante a lo largo de los años. A mis hermanos, Juanma y Ángeles, la dura carga de ser mis hermanos. A mis hijos, Darah, Kira y Maia, les agradezco que no hayan parado ni un momento de jugar, discutir, gritar, interrumpir y reír, sin importarles lo más mínimo la tesis de su padre, que para eso son niños.

Quiero agradecer también a la universidad TU Graz, en especial a los profesores Deutschman, Winkler y Pommerenke, a la universidad KU Leuven con el Profesor Pissoot a la cabeza. Su desinteresada colaboración me ha permitido utilizar equipamiento y adquirir conocimientos que creía fuera de mi alcance.

Estaré también siempre agradecido a dos personas que consiguieron que me interesara por la compatibilidad electromagnética, y que luego me divirtiera y apasionara. Primero el Profesor Henry W. Ott con su libro “Electromagnetic Compatibility”, y después el Profesor Arturo Mediano con sus cursos, presentaciones y conversaciones en eventos, congresos y encuentros improvisados.

Por último, pero no menos importante, quiero agradecer a todas aquellas personas que, de una forma u otra, contribuyeron a este trabajo, aunque no estén mencionadas específicamente aquí. Su influencia ha dejado una marca indeleble en este proyecto.

Table of contents

Declaration	III
Acta de Calificación de Tesis Doctoral	V
Note to the Reader	VII
Resumen.....	IX
1. Contexto de investigación y motivación.....	IX
2. Objetivos	X
3. Metodología	XI
4. Conclusiones.....	XVII
Abstract.....	XXI
Acknowledgements	XXIII
Table of contents	XXVII
List of figures	XXX
Chapter 1. INTRODUCTION	33
1.1 Research context and motivation	33
1.2 Research objectives	34
1.3 Thesis structure.....	35
1.4 Thesis framework.....	36
Chapter 2. BACKGROUND	37
2.1 Electromagnetic Interference (EMI).....	37
2.1.1 Inter-system EMI.....	38
2.1.2 Intra-system EMI.....	39
2.2 Ferrites.....	42
2.3 Ferrite properties.....	44
2.4 Magnetic Absorber Sheets (MAS)	49
2.4.1 Flexible Sintered Ferrite Sheets (FSFS).....	50

2.4.2 Noise Suppression Sheets (NSS)	53
2.5 Summary	55
Chapter 3. CHARACTERIZATION METHODOLOGIES FOR MAGNETIC ABSORBER SHEETS	57
3.1 Intrinsic Parameters	57
3.1.1 Permeability	57
3.1.2 Resistivity	59
3.1.3 Permittivity	60
3.2 Scientific conference article I: Performance characterization	62
3.3 Scientific conference article II: Field distribution in complex circuits	70
3.4 Summary	77
Chapter 4. MODELLING AND SIMULATION OF MAGNETIC ABSORBER SHEETS	79
4.1 Simulation Model Design	79
4.2 Scientific article I: Modelling an FSFS	81
4.3 Scientific conference article III: Modelling an NSS	94
4.4 Summary	101
Chapter 5. DESIGN OF A HYBRID SHEET FOR ELECTROMAGNETIC SHIELDING AT THE PRINTED CIRCUIT LEVEL	103
5.1 Hybrid shielding sheet design	103
5.2 Scientific article II: Material properties definition	104
5.3 Scientific conference article IV: Designing the layers structure	120
5.4 Scientific article III: Design and validation of the hybrid solution	127
5.5 Summary	144
Chapter 6. CONCLUSIONS AND TECHNOLOGICAL TRANSFER	145
6.1 Conclusions	145
6.2 Technological transfer	146
6.2.1 Measurement setups	146
6.2.2 Simulation models	147
6.2.3 Education	148
6.2.4 Product design and development: EMI Patch™	149

REFERENCES 151

Appendix A. SCIENTIFIC CONTRIBUTIONS 153

A.1 Peer-reviewed scientific articles in journals153

A.2 Peer-reviewed scientific articles in conferences153

Appendix B. LIST OF ABBREVIATIONS 155

List of figures

Figure 2.1. Radiated emissions test	38
Figure 2.2. Conducted emissions test	39
Figure 2.3. Diagram of common line impedance coupling	40
Figure 2.4. Diagram of common ground impedance coupling	40
Figure 2.5. Diagram of capacitive coupling	41
Figure 2.6. Diagram of magnetic coupling	41
Figure 2.7. Magnetic domains: (a) Lines of force in a particle of a single domain; (b, c) reduction of magnetostatic energy by the formation of domains	43
Figure 2.8. DC magnetization curve: domain dynamics during various parts of the magnetization curve	44
Figure 2.9. Hysteresis loop: relation of the sine-wave current driving the magnetization through one hysteresis loop per sine-wave cycle	45
Figure 2.10. Relative permeability representation of a magnetic absorber sheet	46
Figure 2.11. Relative permittivity representation of a magnetic absorber sheet	47
Figure 2.12. Customized samples of a magnetic absorber sheet	50
Figure 2.13. Layers structure of FSFS	50
Figure 2.14. FSFS permeability representation: (a) Permeability of NiZn; (b) MnZn (right) FSFS	51
Figure 2.15. FSFS manufacturing process	52
Figure 2.16. FSFS sample	53
Figure 2.17. SEM of a noise suppression sheet	53

Figure 2.18. Permeability response of different NSS	54
Figure 2.19. NSS manufacturing process	54
Figure 2.20. NSS samples	55
Figure 3.1. Measurement setup to measure the permeability parameter	58
Figure 3.2. Measured permeability parameter with the defined measurement setup	59
Figure 3.3. Measurement setup to determine the volume resistivity	59
Figure 3.4. Measurement setup to determine the permittivity parameter	61
Figure 3.5. Relative permittivity representation of a noise suppression sheet	61
Figure 4.1. FEM simulation model for the measurement setup	79
Figure 6.1. Measurement setup designed to determine the SE parameter	147
Figure 6.2. H-field results obtained from the simulation model created for the new hybrid shielding solution: (a) EMI source reference; (b) EMI source shielded with the EMI Patch	147
Figure 6.3. WE internal process diagram	149
Figure 6.4. Manufacturing procedure for the EMI Patch product (hybrid shielding sheet).	149
Figure 6.5. EMI Patch product (hybrid shielding sheet): a) layers structure without isolating the top metal layer; b) layers structure isolating the top metal layer; c) final product sample	150

Chapter 1. INTRODUCTION

This introductory chapter sets out the context and unresolved challenges of the research topic covered in this doctoral thesis. Thereby, the initial hypothesis and the expected achievements in the objectives of the thesis are presented.

1.1 Research context and motivation

Controlling electromagnetic interference (EMI) among devices, subsystems, and electronic components is a necessary and complex task constantly subject to new and more complex challenges. The Electromagnetic Compatibility Chair, created by Würth Elektronik eiSos and the University of Valencia, aims to research, develop, and transfer solutions to these challenges to society. This Industrial Doctorate has been developed through a collaboration between the University and the company, focusing on innovation and the transfer of solutions for electromagnetic shielding.

Electromagnetic shielding is a highly effective solution, capable of attenuating electromagnetic noise by tens of decibels (dB) without redesigning electronic circuits and reducing their switching speed. However, the proliferation of communication systems based on magnetic coupling (e.g., Near Field Communication (NFC), Wireless Power Communication (WPC)) or high frequencies (e.g., 5G) creates the need for new shielding solutions and materials. These new materials must prevent EMI without affecting the frequency ranges necessary for communication.

Magnetic absorption sheets (MAS) based on ferrites can be designed to address these new challenges, but this requires a good understanding of their composition and frequency behavior in the final application. This work studies sintered ferrite sheets (FSFS) and polymer sheets with embedded ferrite particles (NSS).

Traditionally characterized by their initial permeability (at 100 kHz or 1 MHz) or by the graph of complex permeability as a function of frequency, these values allow us to estimate the material's ability to decouple a magnetic field or the frequency ranges in which the material allows redirecting or absorbing magnetic flux. However, they do not

provide information about the influence of the sheet's thickness or shape, contact surface, or the distance to the electronic circuit where it is applied.

This lack of information and understanding of the behavior of electromagnetic absorption sheets leads electronic designers to choose the final product through trial and error. They may often dismiss this type of solution due to its apparent complexity.

This doctoral thesis is based on the hypothesis that properly designed electromagnetic absorption sheets can offer a circuit-level solution to EMI's increasingly complex and wide-ranging challenges. The aim is also to provide the tools and knowledge necessary to characterize electromagnetic absorption sheets, not only in terms of their composition but also in their behavior for each application where they may be useful, as well as simulation and measurement tools to design and verify an effective solution against EMI.

1.2 Research objectives

Taking into account the context of the research, motivation, and the previously defined hypothesis, the general objective of this doctoral thesis is as follows:

To study, analyze, and evaluate the suitability of electromagnetic absorption sheets as a solution to various EMI problems, and to characterize the materials using parameters and simulation models that allow optimizing the final design.

In this regard, the following specific objectives (S.O.) are proposed to conduct the research for this doctoral study to address the previously stated difficulties:

- **S.O.1:** Characterization of magnetic absorbers through their electromagnetic properties. Implementation of measurement systems.
- **S.O.2:** Characterization of the behavior of magnetic absorbers against EMI in applications such as filtering, decoupling, absorption, and electromagnetic shielding. Design and implementation of measurement systems.
- **S.O.3:** Creation of models to predict the effects of magnetic absorbers based on their physical (shape, size, thickness) and electromagnetic properties (permeability, permittivity, conductivity).
- **S.O.4:** Validation of the models by comparing the simulation of measurement systems with experimental results.
- **S.O.5:** Validation of the utility of the models in a real-world application: Optimizing near-field communication (NFC) systems.

- **S.O.6:** Design, optimize, and evaluate a new magnetic absorption sheet for electromagnetic shielding applications in printed circuit boards (Board-Level Shielding), thereby validating this thesis's initial hypothesis.
- **S.O.7:** Generate a final product with the optimal configuration, composition, and thickness to reduce EMI across a wide range of frequencies. Thus completing the transfer of this solution to a relevant technological problem addressed in this Industrial Doctorate to the company and society.

1.3 Thesis structure

This doctoral thesis is organized into six chapters covering the evolution of the implemented research work. The main body comprises a collection of three peer-reviewed scientific articles and two peer-reviewed scientific conference articles that address the research objectives listed in Section 1.2.

Chapter 1 introduces the overall context, motivation, and objectives of this research topic, together with a description of its structure.

Chapter 2 provides a summary of the theoretical background and literature review to provide the basis on which this Ph.D. study has been developed. These fundamentals firstly cover a brief overview of the ferrites and their use to solve problems derived from Electromagnetic Interference Phenomena. Subsequently, ferrite-based magnetic absorber sheets are introduced in both configurations: flexible sintered ferrite sheets (FSFS) and noise suppression sheets (NSS). Composition and production processes are finally described.

Chapter 3 focuses on the study of the characterization methodologies for electromagnetic absorber sheets. First, we characterize the intrinsic electromagnetic properties: permeability, permittivity, and conductivity. Then, we define and implement measurement methods to characterize their performance against EMI issues in different situations: filters, magnetic shields, and absorbers. With these techniques, we can evaluate not only the material but also the effect of the thickness of the sheets.

Chapter 4 approaches the modeling and simulation of the MAS and its applications. Using the results described in Chapter 3, simulation models are created based on Finite Elements Methodology (FEM). The measurement setups are also simulated, and the simulation and measurement results are compared for the validation of the models. Finally, the validated models are used to solve critical EMI challenges mostly covered with MAS: optimization of NFC communication systems and countermeasure of EMI produced by metallic planes.

Chapter 5 covers the study of different compositions for a hybrid sheet for electromagnetic shielding at the printed circuit level (BLS). Using the measurement systems defined and implemented in Chapter 3 and the models created and validated in Chapter 4, different combinations of MAS and metal sheets are evaluated. The use of such a combination allows the BLS to be on a broad frequency range without affecting useful low-frequency signals. Adding an electrically isolated adhesive layer, this hybrid solution can be used directly on the PCB without the need of redesign.

Chapter 6 summarizes the general and specific conclusions drawn from this doctoral thesis. In addition, this chapter presents the technological transfer of the results of this work through the company Würth Elektronik eiSos and the Catedra EMC WE-UV.

1.4 Thesis framework

The present industrial doctoral thesis summarizes its author's research efforts from 2016 to 2024 as a Product Manager for Shielding Materials at Würth Elektronik eiSos and a Ph.D. candidate at the University of Valencia.

Specifically, this doctoral study has been carried out within the Catedra EMC WE-UV framework, representing a collaboration agreement between the University of Valencia and the company Würth Elektronik eiSos. The Catedra EMC is a wide and long-term academic collaboration that reaches one or more areas of knowledge and extends its activities to all the areas of the university activity:

- Teaching and dissemination of science, technology, and culture.
- Training and attraction of talent.
- Research and Innovation.

Thereby, this Ph.D. study is covered by the Research and Innovation area of the Catedra. It has been supported by the company's expertise and university experts, as well as their installations, materials, and laboratory resources. In this context, the author has carried out an appropriate amount of state-of-the-art developments, including magnetic absorber analysis, instrumentation, and calibration, mechanical designs, design and development of magnetic absorber sheets characterization setups, laboratory and field experiments, advanced data analysis, and finite element method based numerical simulations.

Throughout these research experiences, the author has presented and discussed the research work's status and prepared working plans to carry out some of the experiments derived in the publications appended to this thesis.

Chapter 2. BACKGROUND

This chapter introduces the theoretical background and literature review to provide the basis on which this Ph.D. study has been developed. Firstly, an overview of the electromagnetic interference phenomena and its challenges. Then, ferrite materials and the parameters needed to describe their behavior are described. Finally, Sintered Ferrite Sheets and Noise Suppression Sheets are described.

2.1 Electromagnetic Interference (EMI)

Electronic devices generate electromagnetic fields due to the alternating voltages and currents they work with. These fields can negatively impact other devices, causing electromagnetic interference.

Contemporary devices are consistently incorporating increasingly intricate and advanced functionalities. This progression entails elevating operating frequencies, shrinking electronic designs, achieving high component integration, reducing printed circuit board size and thickness, and utilizing signals with extremely low voltage amplitude. While these design principles are commonly employed to enhance device performance and features, they concurrently heighten the probability of encountering complex electromagnetic interference issues. The susceptibility of electronics to the surrounding electromagnetic environment is notable, as they can both react to and emit noise. Hence, effective management of electromagnetic noise becomes crucial to prevent undesired electromagnetic interactions with neighboring systems. Some common methods to reduce EMI include:

- LC filters: These filters redirect disturbing currents and are effective in reducing EMI.
- Electromagnetic shielding: This method is used to avoid unintended field coupling and is effective in reducing EMI.
- Ferrite beads, toroids, or other shapes: Ferrite materials can be placed over or around traces and cables, absorbing the offending noise and reducing EMI.

2.1.1 Inter-system EMI

Electromagnetic interference can lead to malfunctions with potentially harmful consequences, prompting the establishment of comprehensive laws in numerous countries to mitigate these risks. One notable regulatory framework is found within the European Union (EU), which imposes specific requirements on electronic equipment marketed in the European Community [1]. These regulations emphasize two crucial aspects:

- Non-Interference: Electronic equipment must not interfere with other devices, ensuring a harmonious coexistence within the technological ecosystem.
- Immunity to EMI Emissions: Devices must exhibit immunity to electromagnetic interference emissions, safeguarding their operational integrity in the presence of external electromagnetic disturbances.

These regulations are pivotal in maintaining the reliability and performance of electronic devices within the European market. Moreover, similar regulatory measures are instituted globally, reflecting the widespread recognition of EMI prevention as a crucial concern.

The mechanisms through which inter-system EMI manifests are primarily categorized into two forms:

- Radiated Emissions in Air: EMI can occur through radiated emissions in the air, where electromagnetic signals propagate and potentially interfere with nearby electronic systems.

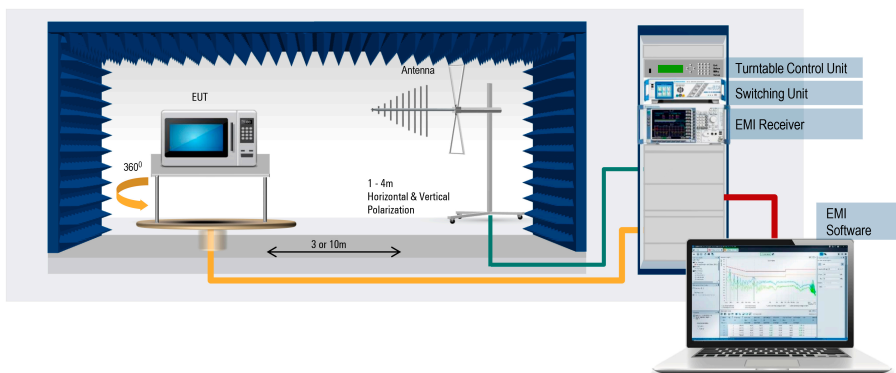


Figure 2.1. Radiated emissions test [2].

- Conducted Emissions in the Power Line: Conducted emissions in the power line represent another avenue for inter-system EMI, where electromagnetic disturbances travel through power lines, impacting connected devices.

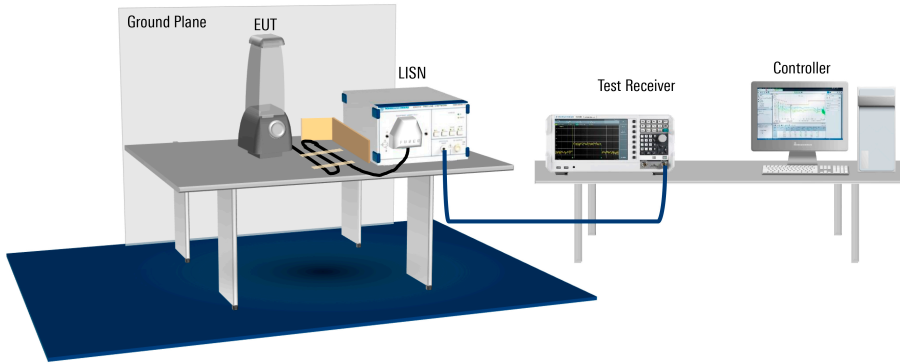


Figure 2.2. Conducted emissions test [2].

In response to these challenges, the EU sets specific limits for both radiated and conducted emissions, tailoring these restrictions to different frequency ranges and operational environments. This approach ensures a comprehensive and adaptive regulatory framework that addresses the diverse ways in which EMI can manifest.

Parallel initiatives in other countries, such as the United States and China, mirror the global recognition of EMI prevention as an imperative. Harmonizing these regulations on an international scale underscores the collective effort to create a technologically resilient landscape where electronic devices can coexist without compromising each other's functionality. In essence, EMI prevention has become an integral aspect of global governance in the realm of electronic devices, reflecting the interconnected nature of today's technology-driven world.

2.1.2 Intra-system EMI

Every device needs internal electromagnetic compatibility to ensure the reliability of its functions. Therefore, circuit boards, components, and subsystems must be designed and combined accordingly.

Intra-system critical EMI is mostly generated by:

- Conducted noise-interfering data lines and power lines.
- Unintended magnetic or capacitive coupling between subsystems, cables, traces, and components.

Conducted coupling

When disparate circuits coexist on a shared line, the electrical current produced by one circuit has the potential to interfere with the voltage characteristics of the others. This phenomenon becomes particularly pronounced in power lines and ground planes, especially at higher frequencies where impedance deviates significantly from zero. In such instances, unforeseen voltage drops may manifest, and there is an increased susceptibility to the induction of common mode noise [3]. This underscores the importance of carefully managing the interaction of circuits on shared lines, especially in scenarios with fast switching signals (high di/dt).

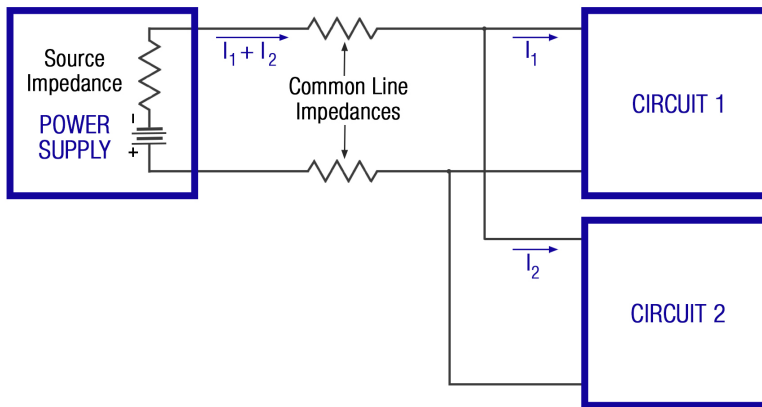


Figure 2.3. Diagram of common line impedance coupling.

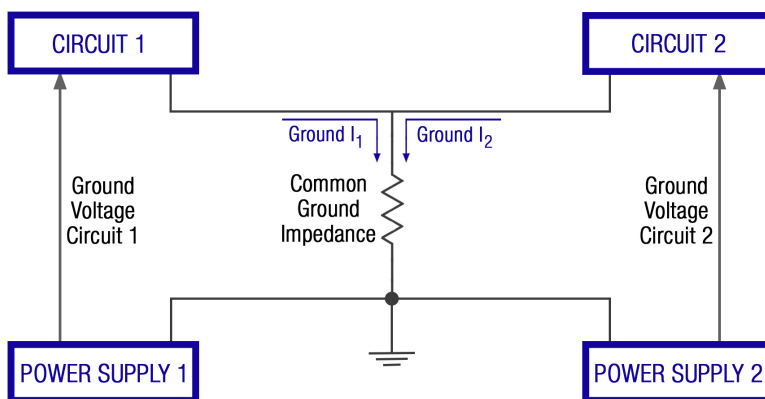


Figure 2.4. Diagram of common ground impedance coupling.

Capacitive coupling

Conductor lines in close proximity, such as board traces or cables, and neighboring planes like ground and power planes induce stray capacitance. The extent of this capacitance amplifies in correlation with the closeness and size of the conductors. Functioning as a conduit, this capacitance enables the interconnection of high-frequency electric fields, thereby facilitating energy coupling from one conductor to another [2].

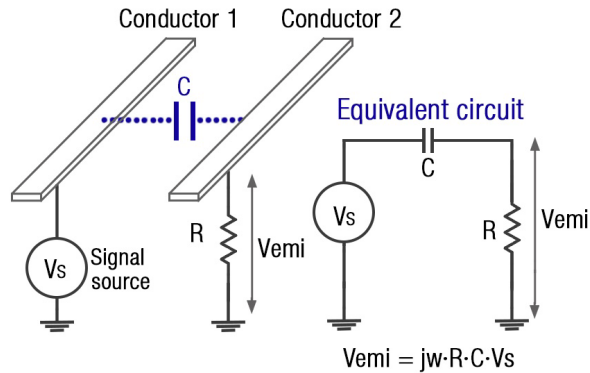


Figure 2.5. Diagram of capacitive coupling.

Magnetic coupling

The circulation of currents within a circuit induces a magnetic flux directly proportional to the current and the area encompassed by the circuit. This magnetic flux possesses the potential to couple with other circuits having a substantial area through the mechanism of magnetic coupling, resulting in the generation of unforeseen voltages [2].

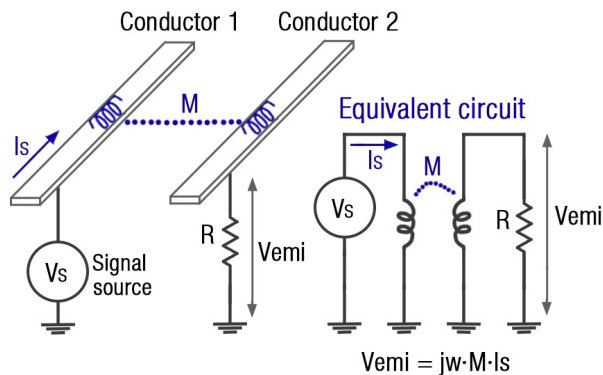


Figure 2.6. Diagram of magnetic coupling.

Historically, the management of intra-system EMI has relied on fundamental techniques, including physically separating source and victim circuits, altering their

orientations, or enclosing one of them within a metallic case to ensure effective shielding. However, the contemporary drive towards miniaturization in electronic devices aimed at enhancing functionalities introduces a paradigm shift. This shift involves the adoption of embedded systems operating at high frequencies, the integration of communication circuits, and a consequent reduction in device housing. This reduction extends to the size and thickness of PCBs, facilitating increased component integration.

As a consequence of these evolving design parameters, traditional shielding methods become impractical. Basic techniques such as physical separation or metallic enclosures are no longer viable due to the constraints imposed by miniaturization. Consequently, there is a growing reliance on alternative measures, with magnetic shielding emerging as a viable solution to address the challenges posed by the intricate and compact nature of modern electronic designs.

Continuous development of new materials, components, and solutions is essential to facilitate the seamless integration of emerging technologies into increasingly compact and intricate devices.

2.2 Ferrites

Ferrites are ferrimagnetic materials widely used in high-frequency applications, including EMI prevention. They are ceramics with a crystal structure sintered by various metal oxides, and they have high values of permeability, resistivity, and magnetic losses.

Ferrites are iron oxides combined with other materials, like nickel and manganese. These compositions enhance the atomic spin effect, which results from the cooperative interactions of atomic spins when they are aligned in parallel in a region known as a domain.

Within ferrites, the spontaneous formation of magnetic domains occurs independently of external magnetic field application. These domains serve as distinct regions within the ferrite material, where magnetization uniformly aligns in a specific direction. This alignment reflects the synchronization of individual magnetic moments of the atoms, all pointing in the same direction. This inherent process is driven by the goal of reducing the magnetic potential energy contained in the flux lines that connect the north and south poles of the material.

Each magnetic domain acts as a magnet composed of smaller magnets, and the intricate interplay among these magnetic domains is a fundamental aspect of the material's behavior. This dynamic interaction significantly influences the ferrite's

magnetic properties and overall performance, providing insight into the material's magnetic behavior and contributing to its functionality in various applications [4].

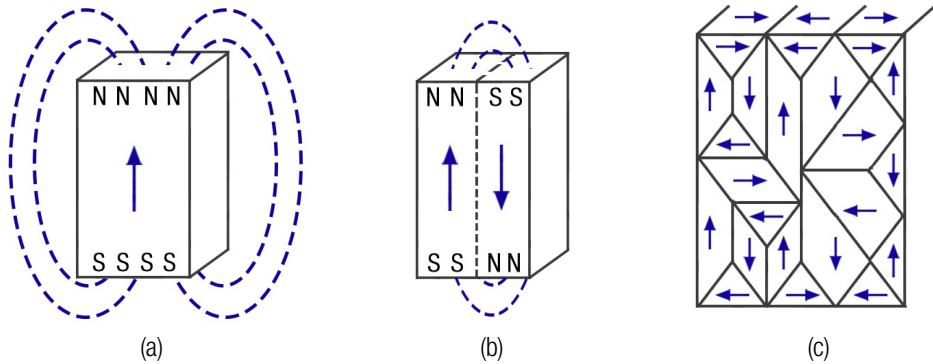


Figure 2.7. Magnetic domains: (a) Lines of force in a particle of a single domain; (b, c) reduction of magnetostatic energy by the formation of domains.

MAGNETIZATION CURVE

Upon the application of an external field, ferrites undergo a transition from a random orientation of domains to a complete alignment in a singular direction, accompanied by the elimination of domain boundaries. This evolution can be observed in the magnetization curve, revealing distinct stages in the process.

In the lower applied field region, the movement of domain walls is reversible, indicating that if the external field is removed, the initial position of the walls will be restored. As the applied field strength increases, the boundaries become irreversibly displaced. In the saturation area, domain walls cease to be discernible as all magnets within the material attain a rotated configuration. This delineation of stages provides insights into the dynamic behavior of ferrites under varying external field conditions [5].

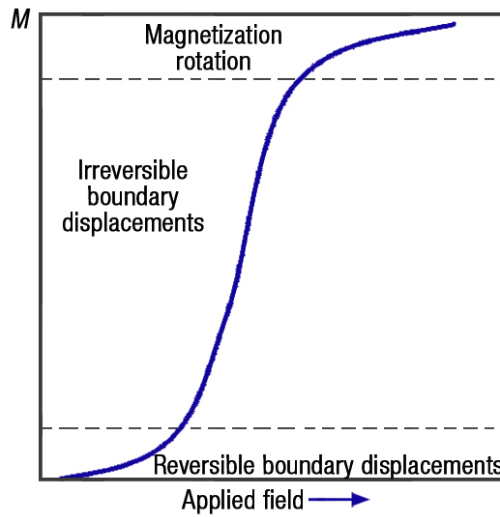


Figure 2.8. DC magnetization curve: domain dynamics during various parts of the magnetization curve [6].

2.3 Ferrite properties

Ferrites are normally used in alternating current situations when a magnetic field is generated by a current varying on some kind of waveform (sinusoidal, square, triangular, etc.).

AC HYSTERESIS LOOP

At low frequencies, the AC magnetization curve closely resembles the DC. However, as the frequency of the excitation field rises, the losses expand the loop's width.

Taking a sinusoidal waveform current as an illustrative example, the magnetization of a ferrite influenced by the induced field undergoes a single hysteresis loop cycle, as depicted in the figure. The area enclosed within this hysteresis loop serves as a measure of the losses incurred by the material during the cyclic magnetization process.

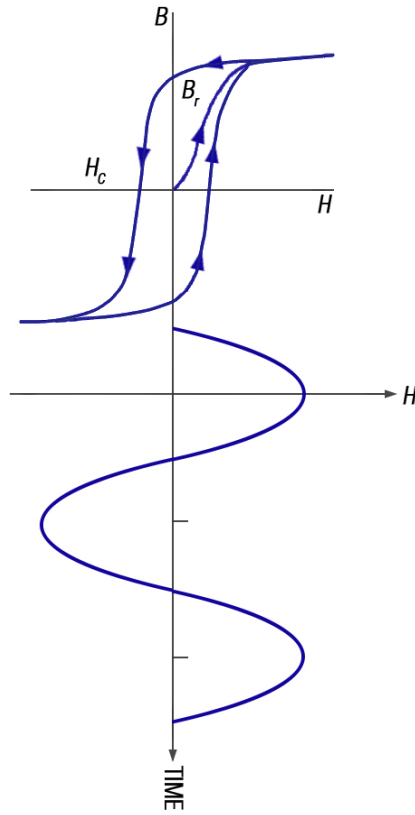


Figure 2.9. Hysteresis loop: relation of the sine-wave current driving the magnetization through one hysteresis loop per sine-wave cycle.

PERMEABILITY

Permeability establishes a connection between a specified medium's magnetic flux density and the magnetic field. Consequently, when introducing an absorber sheet, the magnetic flux becomes concentrated within it. This concentration is determined by the internal properties of the composite material and is expressed through the complex permeability parameter. The losses in magnetic flux can be measured by dissecting it into its complex form. In this breakdown, the real component (μ') is associated with the reflective or inductive aspect, while the imaginary component (μ'') quantifies the material's effectiveness in absorbing magnetic noise:

$$\mu_r = \mu' - j\mu'' \quad (1)$$

It is usually represented versus the frequency and it can be derived from electromagnetic theory as well as obtained experimentally.

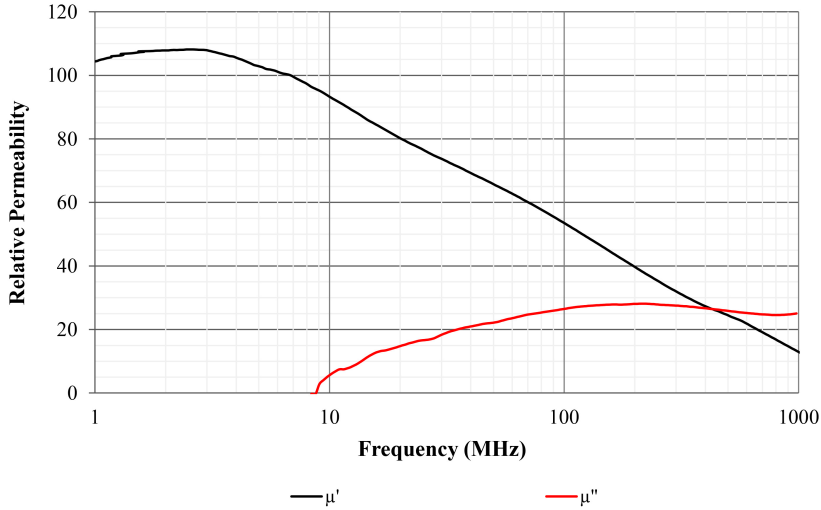


Figure 2.10. Relative permeability representation of a magnetic absorber sheet.

The real component (μ') is associated with the induction generated by the external field, represented by the slope of the magnetization curve. It remains constant with frequency, experiences a slight increase, and then declines rapidly at higher frequencies.

On the other hand, the imaginary component is linked to losses, reflected by the area of the hysteresis loop. It increases gradually, and when μ' starts to decline, it experiences a sudden rise. μ'' reaches its maximum when μ' is approximately half of its original value at the so-called relaxation frequency.

These two curves are interconnected, as the rise in losses leads to a reduction in permeability.

LOSS TANGENT

The loss tangent measures the magnetic system's inefficiency and is the ratio of the imaginary part to the real part of permeability.

$$\tan \delta = \mu'' / \mu' \quad (2)$$

PERMITTIVITY

In the field of electromagnetism, permittivity (ϵ) quantifies the electric polarizability of a dielectric material. A material with high permittivity demonstrates greater polarization in response to an applied electric field than a material with low permittivity, resulting in increased energy storage within the material. Its impact hinges on factors like the applied electric field's frequency, magnitude, and direction.

The relative permittivity, often denoted as ϵ_r , denotes the ratio of absolute permittivity (ϵ) to vacuum permittivity (ϵ_0). This dimensionless quantity is also commonly known as "permittivity."

Similar to permeability, permittivity adopts a complex nature when confronted with time-varying fields present in alternating current circuits or electromagnetic waves. The complex permittivity encompasses both the real part, termed the dielectric constant, and the imaginary part, known as the loss factor.

The real part reflects the storage of energy due to polarization, while the imaginary part accounts for energy dissipation (losses) within the material. In summary, complex permittivity captures the intricate interplay between energy storage and dissipation in ferrite when exposed to electric fields.

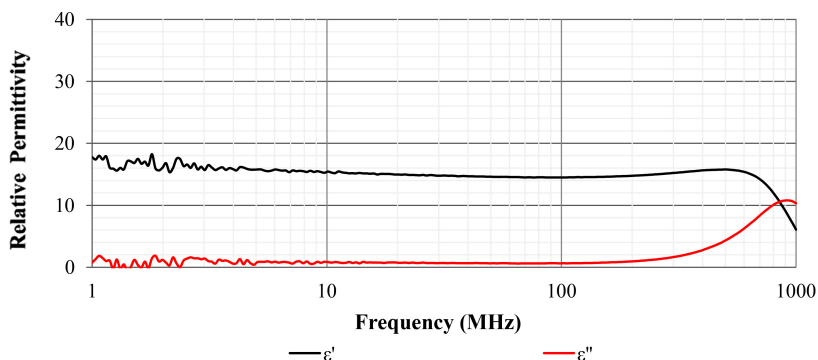


Figure 2.11. Relative permittivity representation of a magnetic absorber sheet.

MAGNETIC LOSSES

Losses in ferrites primarily result from irreversible domain changes, anisotropy, eddy currents, and ferromagnetic resonance. Magnetic domain losses occur when favorably oriented magnetic domains grow at the expense of others, either through the motion of

domain-wall boundaries or the activation of large-scale instabilities related to the nucleation and annihilation of magnetic domains.

Due to the crystalline structure of ferrites, preferred orientations for magnetization exist, requiring energy to rotate the magnetic moments away from them. This phenomenon, known as anisotropy energy, can be heightened not only by the crystallographic structure but also by mechanical and temperature stress processes.

Eddy currents are induced by changes in magnetic induction within the material, as per Faraday's law of induction, and they contribute to damping the motion of magnetic domain walls.

The induced voltage is determined by dB/dt , representing the rate of induction (B) change over time. As the frequency (f) increases, so does the induced voltage, leading to higher eddy current losses. Eddy current losses are present in all materials, but they are most pronounced in magnetic materials due to their higher permeabilities, resulting in a more significant change in induction.

The impact of the eddy current effect heavily relies on the material's resistivity, which influences the resistance within the eddy current for a given induced voltage. Higher resistivity diminishes eddy currents and, consequently, the opposing magnetic field. Given the high resistivity of ferrites, eddy currents become a concern only at higher frequencies.

Table 2.1. Resistivities of ferrites and metallic magnetic materials.

Material	Resistivity ($\Omega\cdot\text{cm}$)
Zn ferrite	10^2
Cu ferrite	10^5
Fe ferrite	4×10^{-3}
Mn ferrite	10^4
NiZn ferrite	10^6
Mg ferrite	10^7
Co ferrite	10^7
MnZn ferrite	$10^2\text{-}10^3$
Yttrium iron garnet	$10^{10}\text{-}10^{12}$
Iron	9.6×10^{-6}
Silicon iron	50×10^{-6}
Silicon nicket	45×10^{-6}

An additional noteworthy class of losses, potentially dominant at specific frequencies, arises from the magnetic phenomenon called ferrimagnetic resonance. This resonance

depends on the inherent composition of the ferrite material. Ferromagnetic resonance (FMR) describes a phenomenon in which an electromagnetic wave efficiently interacts with the magnetization of a medium, leading to a significant dissipation of power within the wave. The material's magnetization absorbs this power, dissipating it as heat [7].

Modifying ferrite properties to align with the demands of the end application involves blending various simple ferrites in an appropriate ratio. The variability in composition stands out as a major advantage of ferrites, and a majority of commercially available ferrites are blends.

After establishing the composition, there is ample opportunity to mold the hysteresis properties by manipulating the microstructure. This includes factors such as grain orientation, particle size, impurities, and a diverse range of physical, structural, and geometrical parameters.

Leveraging the unique effects of each individual ferrite enables the optimization or balancing of specific properties within the final mixed ferrite.

Consequently, ferrite design has become a trending strategy for addressing emerging EMI challenges.

2.4 Magnetic Absorber Sheets (MAS)

Ferrite-based magnetic absorber sheets offer an extension of the advantageous features inherent in ferrite design to the domain of board-level EMI shielding, thanks to their favorable mechanical properties. These thin and flexible sheets present a versatile solution that can be seamlessly adapted and introduced into highly integrated electronic devices without imposing a significant increase in overall size or weight. Their adaptability makes them particularly well-suited for applications where space constraints are a critical consideration.

One notable advantage of these magnetic absorber sheets is their ability to be strategically placed in close proximity to noise sources. By doing so, the sheets' absorption capabilities are maximized, leading to an enhanced shielding effect against unwanted electromagnetic interference. This positioning optimizes the overall shielding performance and contributes to a more efficient and targeted mitigation of electromagnetic noise within electronic systems.

These magnetic absorber sheets (MAS) are manufactured using different approaches. One method involves utilizing pure sintered ferrite ceramic (FSFS), while another involves filling a silicon base with ferrite powder flakes (NSS). Each approach offers unique

benefits, and the choice between them depends on specific application requirements and desired material properties. Whether using pure sintered ferrite ceramic or incorporating ferrite powder flakes into a silicon base, these sheets provide a reliable means of addressing EMI concerns in electronic devices while maintaining a balance between performance, flexibility, and adaptability.

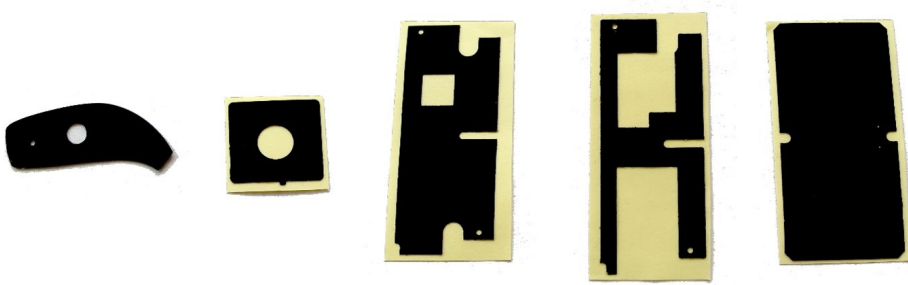


Figure 2.12. Customized samples of a magnetic absorber sheet.

2.4.1 Flexible Sintered Ferrite Sheets (FSFS)

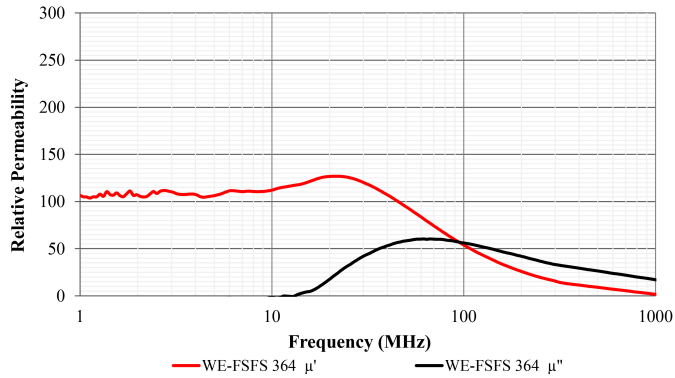
FSFS is composed of three layers:

- PET protective layer: High surface resistivity and adhesive strength to protect the ferrite layer.
- Pre-cracked Sintered Ferrite Layer: It is the core of the product. Its magnetic properties concentrate and control the external magnetic fields.
- Adhesive layer: High adhesive strength to protect the ferrite and to apply the sheet over printed circuit boards, device walls, antenna...

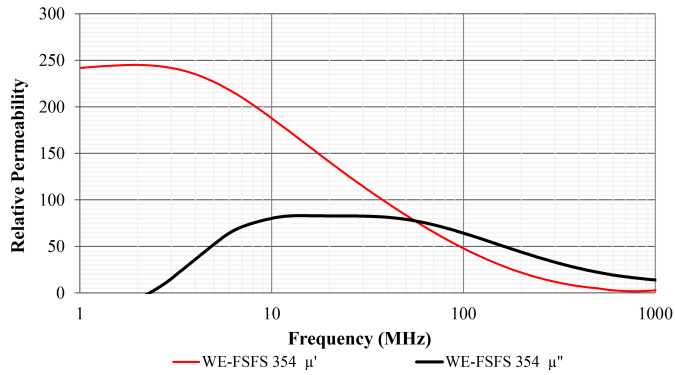


Figure 2.13. Layers structure of FSFS.

This layer configuration is meant to provide protection, high surface resistivity, and isolation from top to bottom sides. Ferrites used for FSFS are based on Nickel Zinc (NiZn) and Manganese Zinc (MnZn) ferrite oxides [8].



(a)



(b)

Figure 2.14. FSFS permeability representation: (a) NiZn composition; (b) MnZn composition.

Manganese zinc-based FSFS present high permeability at low frequencies (up to μ_r 300) and resistivity of $10^4 \Omega$. The eddy current losses are high and start at hundreds of kHz. These properties make it especially useful for:

- Magnetic shielding for low frequencies (up to some MHz).
- Improve the efficiency of wireless power systems (working at 100 kHz) due to the high permeability and low losses at the working frequency.

Nickel-zinc-based FSFS presents lower permeability than MnZn (up to μ_r 150) but a higher resistivity ($10^6 \Omega$) and can, therefore, be useful for higher frequencies.

- Magnetic shielding up to hundreds of MHz.

- Improve the efficiency of near-field communication systems (working at 13,56 MHz).

MANUFACTURING PROCESS

The initial phase involves measuring and combining the base materials in predetermined proportions, followed by a wet mixing process in ball mills to achieve a uniform distribution and desired particle size. Subsequently, a thin layer (0.1 mm thickness) of ferrite paste is cast and pressed. For thicker sheets, multiple layers can be stacked.

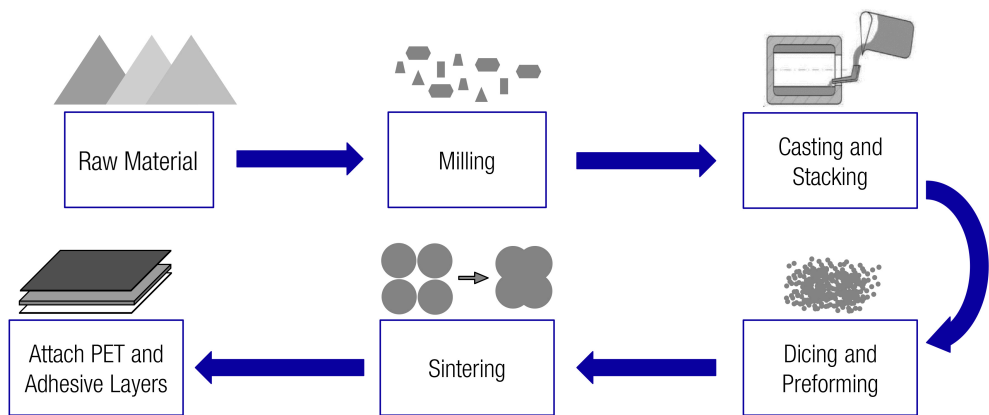


Figure 2.15. FSFS manufacturing process.

The ferrite paste is marked into 2 x 2 mm squares using a laser cutting machine. This strategic marking allows the sheets to be easily broken along this pattern once the sintering process is complete. This step not only defines the final size and shape of the sheet but also facilitates precise cutting compared to dealing with a thin ferrite sintered sheet directly. Calculations are made to account for the expected shrinking during the sintering process, ensuring the final product meets the specified dimensions.

The ferrite paste undergoes sintering in a conventional ceramic oven, following a defined temperature curve reaching 1000 °C. After sintering, the ferrite layers are covered on one side with PET-protecting adhesive and on the other with double-sided adhesive tape. Using a metal roll, the ferrite sintered sheet is then cracked both vertically and horizontally, conforming to the earlier marked 2 x 2 mm squares. The adhesive protection on both sides imparts a degree of flexibility to the final sheet, ensuring durability and ease of handling.



Figure 2.16. FSFS samples.

2.4.2 Noise Suppression Sheets (NSS)

Noise suppression sheets constitute ferrite-polymer composites, utilizing a silicon rubber matrix with incorporated ferrite inclusions. The dimensions of these inclusions and their spatial periods, when significantly smaller than the wavelength of the electromagnetic field produced by the noise source, allow the composite materials to be treated as homogeneous substances.

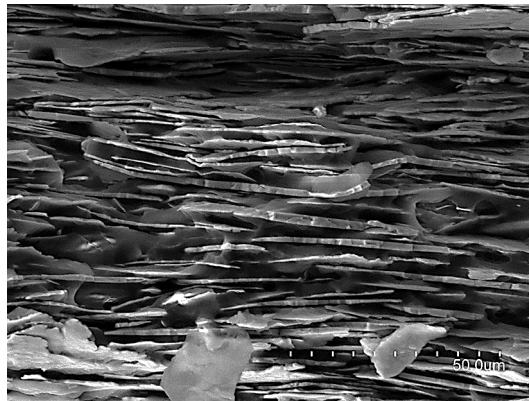


Figure 2.17. SEM of a noise suppression sheet.

As a result, this material category can be thoroughly characterized by investigating the magnetic, geometrical, and physical properties of the ferrite inclusions, the host medium (silicon rubber matrix), and the orientation of the inclusions within the host matrix. This expanded analysis provides more significant opportunities for designing their performance and enhances their potential to address electromagnetic interferences.

NSS can be designed with multiple permeability profiles and wide absorption frequency bands reaching the gigahertz range [9].

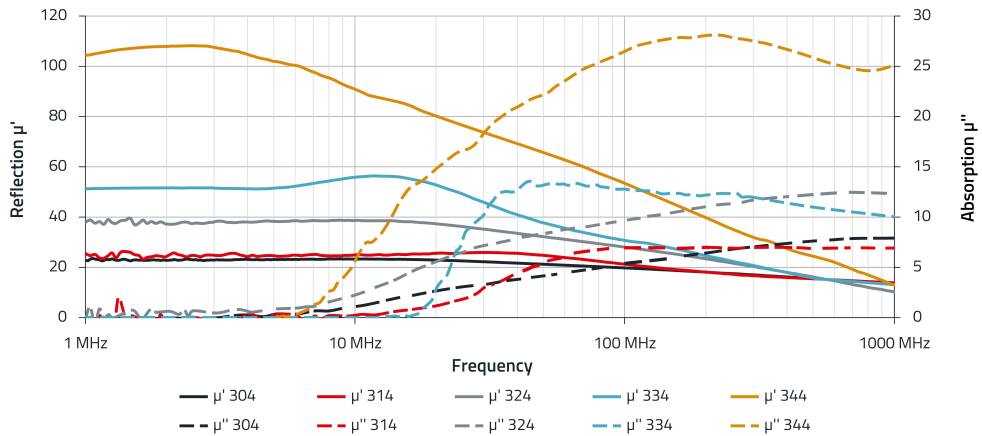


Figure 2.18. Permeability response of different NSS.

MANUFACTURING PROCESS

Following the preparation of the powder with the specified material compositions and proportions, flakes are produced through the mechanical forging of spherical iron powders using an attrition mill. The resulting mixture is distributed, dried, and subjected to a heat process to ensure the formation of a flake structure.

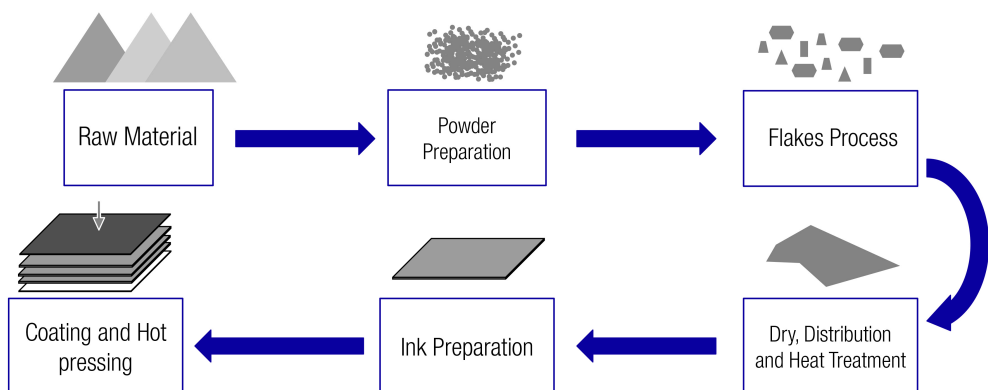


Figure 2.19. NSS manufacturing process.

Subsequently, an ink is created by combining the flakes with a polymer binder. This ink is then applied in 0.05 mm layers to achieve the desired sheet thickness. Finally, the

coated sheets undergo a pressing and curing process in an oven. Double-sided adhesive layers may be affixed to one or both sides through lamination in an optional final step.



Figure 2.20. NSS samples.

2.5 Summary

Electromagnetic interferences are a challenge that is increasing in complexity and importance. Intra-system interferences affect the signal and power integrity of electronic devices due to the electromagnetic coupling between components, circuits, and subsystems, which work closer with faster switching currents and voltages. New trends in electronics require new EMI solutions that can provide effective protection without affecting the performance of all the co-habiting technologies.

Ferrite materials can be designed to solve EMI problems in different frequency ranges, controlling the magnetic fields due to their high permeability and absorbing the energy at the interference frequencies due to their multiple absorption mechanisms.

In this work, we will use the ferrite properties for board-level shielding applications in the shape of flexible, thin adhesive sheets, covering the interference's source or victim. Flexible magnetic absorbers can be produced using pre-cut sintered ferrite plates (FSFS) or embedding ferrite flakes into a polymer (NSS).

Chapter 3. CHARACTERIZATION

METHODOLOGIES FOR ELECTROMAGNETIC

ABSORBER SHEETS

In this chapter, we present the measurement of the intrinsic parameters of MAS. Then, we define and implement measurement methods to characterize their performance against EMI issues in different situations: filters, magnetic shields, and absorbers. We finally evaluated the effect of absorber sheets on a printed circuit board using an EMScan.

3.1 Intrinsic Parameters

The intrinsic parameters of electromagnetic absorber sheets, which define their electromagnetic properties and the behavior of the material, include:

3.1.1 Permeability

As introduced in Chapter 2, permeability measures how easily a material can become magnetized. In the context of electromagnetic absorber sheets, permeability influences their ability to absorb and attenuate electromagnetic interference.

We utilize an E4991A Material Analyzer (Keysight) in conjunction with the 16454A Magnetic Material Test Fixture for our measurements. This fixture, founded on cavity resonance and single-turn inductor principles, facilitates the assessment of a material's magnetic properties. To accommodate the fixture, the sample under examination must possess a toroidal shape, necessitating the creation of a toroidal core using the material of each absorber composition. The toroidal sample boasts an outer diameter of 20 mm, an inner diameter of 8 mm, and a thickness of 1 mm.

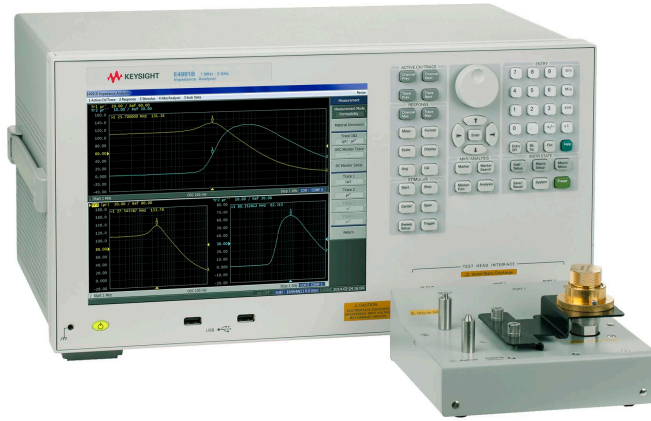


Figure 3.1. Measurement setup to measure the permeability parameter [10].

Once the sample is positioned inside the fixture, it effectively forms an ideal single-turn inductor with no flux leakage. Using the dimensions of the samples and measuring the complex impedance through the frequency, the internal software calculates μ' (proportional to the inductive component of the impedance) and μ'' (proportional to the resistive part) [5].

$$Z = R + j \omega L \quad (3)$$

- Loss component:

$$R = \omega L_0 \mu'' \quad (4)$$

- Inductance component:

$$L = \omega L_0 \mu' \quad (5)$$

where L_0 is a value given by the fixture with no absorber inside and measured during the calibration phase.

The loss tangent is given by:

$$\tan \delta = \mu'' / \mu' \quad (6)$$

As a result, we obtain direct and comprehensive readouts of the complex permeability and tangent loss.

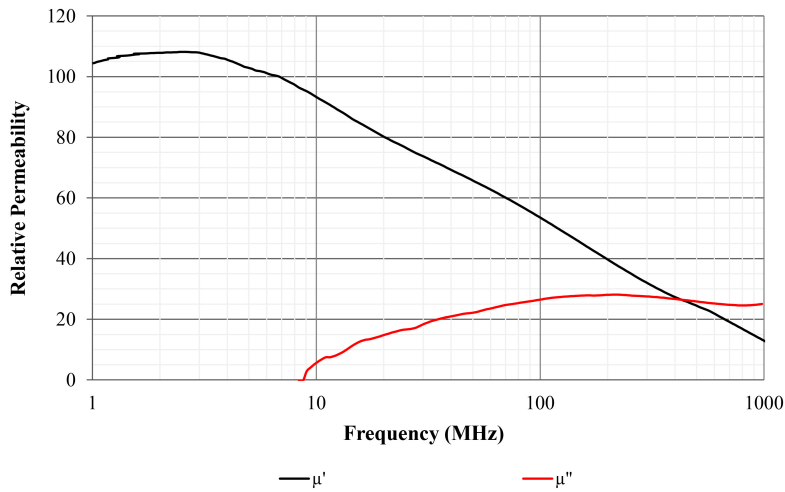


Figure 3.2. Measured permeability parameter with the defined measurement setup.

3.1.2 Resistivity

The measurement setup shown in Fig. 3.3 allows the measurement of the volume resistivity according to standard ASTM D-257. This standard defines it as *the resistance to leakage current through the body of an insulating material*.

The setup consists of a voltage source, an ammeter, a voltmeter, and the specimen holder with two parallel electrodes. A known voltage (500 V) is applied across the electrodes, and voltage and current are measured [11].



Figure 3.3. Measurement setup to determine the volume resistivity [12].

Following Ohm's Law, we calculate the volume resistivity (ρ) using the formula:

$$\rho = V/I \cdot d \quad (7)$$

where V is the applied voltage, I is the measured current, and d is the thickness of the specimen. This method is suitable for materials with resistivity typically in the range of 10^4 to $10^{17} \Omega\cdot\text{cm}$.

Typical values for magnetic absorber sheets are:

- FSFS based on Manganese Zinc: $10^4 \Omega\cdot\text{cm}$
- FSFS based on Nickel Zinc: $10^6 \Omega\cdot\text{cm}$
- Noise suppression sheet based on material WE 344: $10^9 \Omega\cdot\text{cm}$

With the same setup, we measure the surface resistivity, not including the thickness of the sample. Surface resistivity denotes a material's resistance to current leakage across its surface. It gauges the material's effectiveness in impeding current flow along its surface. Typically measured in ohms, it can also be expressed as ohms per square, regardless of the square's dimensions.

The FSFS surface resistivity is given by the PET layer covering the ferrite material, which has a typical value of $10^9 \Omega$.

3.1.3 Permittivity

Another important intrinsic property of materials is their electrical permittivity (ϵ). This parameter characterizes a material's ability to resist the establishment of an electric field within it under the influence of an external field. Electrical permittivity can be further categorized into two fundamental components: the real part (ϵ') and the imaginary part (ϵ''). The real part (ϵ') signifies a material's capacity to store electrical energy through an internal electric field, whereas the imaginary part (ϵ'') indicates dielectric losses resulting from energy dissipation within the material when exposed to a fluctuating electric field.

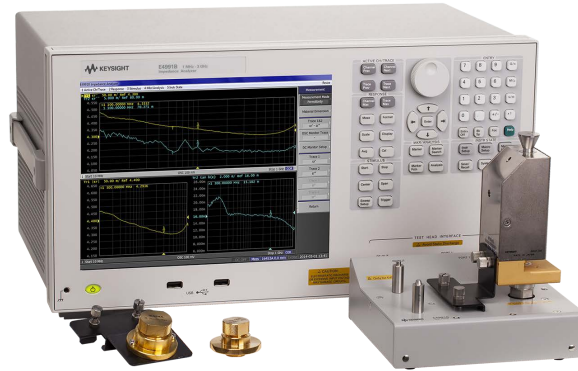


Figure 3.4. Measurement setup to determine the permittivity parameter [13].

Fig 3.5 shows the relative permittivity components of a noise suppression sheet measured using a parallel conducting plates fixture, connected to a material analyzer equipment. As expected, the magnetic properties are more relevant than the electric for magnetic absorbers.

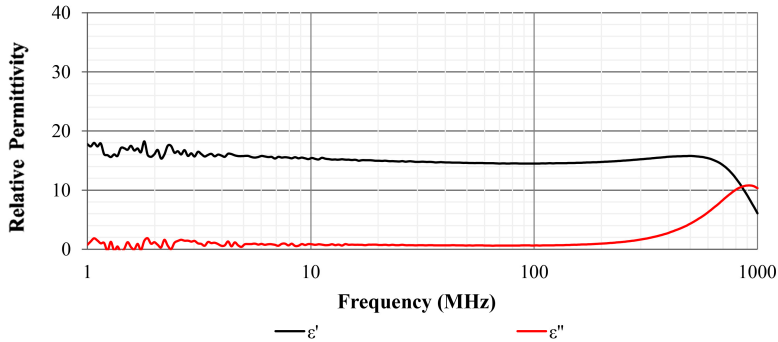


Figure 3.5. Relative permittivity representation of a noise suppression sheet.

3.2 Scientific conference article I: Performance characterization

Title: Characterization of electromagnetic noise suppression sheet for aerospace applications.

Authors: Adrián Suárez, Jorge Victoria, Antonio Alcarria, José Torres.

Published in: 2016 ESA Workshop on Aerospace EMC (Aerospace EMC) Proceedings, IEEE, Valencia, Spain.

DOI: 10.1109/AeroEMC.2016.7504546

Description: The ESA Workshop on Aerospace EMC (Aerospace EMC) is an international conference with a high scientific level supported by the IEEE EMC Society. It is an annual conference that promotes EMC research, innovation and international cooperation. The submitted contributions are subjected to the peer review process to assess the quality of the manuscript before it is published in the IEEE Xplore database, one of the most comprehensive interdisciplinary engineering databases in the world.

Synopsis:

In the first contribution, the main methods of characterization of electromagnetic absorbers are implemented, and the results obtained with different materials and thicknesses are analyzed. Electromagnetic absorbers are characterized by their electromagnetic permeability, but their effect on a specific application depends largely on their dimensions, geometry, and the properties of the noise source. This article presents three characterization methods aimed at evaluating the behavior of absorbers in different applications, considering various parameters. Multiple samples with different characteristics are analyzed, assessing their ability to address EMI issues in transmission lines, resonant cavities, and magnetic coupling between nearby circuits or components.

Using the transmission line method, the absorbent sample is placed on a PCB with a conductive line designed to maintain a constant impedance of 50 ohms over a wide frequency range. The attenuation produced by the absorber between the two ends of the line is measured using a network analyzer, characterizing its effect as a low-pass filter. When measuring samples with different thicknesses and materials, it is observed that the filtering effect increases with thickness and permeability value. Increasing the thickness also results in a reduction in the filter's cutoff frequency.

Placing the samples in front of a reflective material at the termination through a coaxial line allows us to measure their absorption capacity by measuring the reflected energy with the network analyzer equipment. This measurement enables the evaluation of the usefulness of different materials and thicknesses in reducing or eliminating electromagnetic resonances produced in an electronic device due to multiple reflections

inside the device generated by its own operation. The obtained measurements show an increase in absorption with thickness and a shift in the absorption peak towards lower frequencies.

To evaluate the magnetic shielding of the absorbers to prevent the creation of EMI through coupling between the noise source and its victim, this situation is simulated in our experimental design. Two low-impedance antennas are designed, with one serving as the emitter (connected to the output of the network analyzer) and the other as the receiver (connected to the input). They are placed in parallel at a fixed distance, and the absorber sample is introduced between them to measure the decoupling capacity. The results show a direct dependence on the permeability and thickness of the samples.

With the different implemented measurement systems, the ideal material can be selected for each application based on critical frequencies and their energy levels. The results provide information on the thickness effect and are consistent with permeability measurements.

CHARACTERIZATION OF ELECTROMAGNETIC NOISE SUPPRESSION SHEET FOR AEROSPACE APPLICATIONS

A. Suarez⁽¹⁾, J. Victoria⁽¹⁾, A. Alcarria⁽¹⁾, J. Torres⁽¹⁾

⁽¹⁾ Communications and Digital Systems Design Group – University of Valencia, Av. Universitat s/n, 46100 Burjassot, Valencia (SPAIN), Email: adrian.suarez@uv.es

ABSTRACT

Electromagnetic noise suppression sheets based on absorber materials can be an interesting solution to reduce or suppress noise emissions at a high-frequency region that may cause complex EMI problems. These materials usually are characterized by their permeability but their performance also depend on other factors such as dimension, geometry, thickness or noise source kind. Three experimental methods are proposed in order to characterize absorber sheets in different kind of applications taking into account the last factors. These setups make it possible to test several samples with different characteristics and to analyse the absorption capacity in applications with transmission line problems, cavity resonance and coupling between electronic circuits placed one on top of the other.

1. INTRODUCTION

Electromagnetic Interference (EMI) has become a serious problem since it can arise anywhere in electronic circuits with unpredictable and damaging effects. This issue has grown in recent years due to a number of factors including the increase in the devices' frequency, the high integration in electronic systems and the size and thickness reduction of the Printed Circuit Boards (PCBs).

The most common means of solving electromagnetic noise problems is to shield the system with conductive materials such as: shielded enclosure, foil tape or conductive gasket. Nevertheless, a large number of electronic devices have a lot of parts that operate at high-frequency which can generate harmonic noise emissions at several GHz. These kinds of emissions may cause complex EMI problems that cannot be removed with grounding techniques and simple shielding. In order to avoid these issues, an electromagnetic noise suppression material based on a sheet-type absorbing material can be used to suppress the unwanted high-frequency components [1].

The previously exposed solution consists of a composite material with magnetic particles embedded in a polymer and their internal properties are defined by permeability complex parameter [2]. This parameter is characteristic of the composition of the sheet. Nevertheless, it could result difficult to estimate the absorber material performance because it depends on several factors such

as the distance between the noise source and the absorber material, sheet thickness, size and geometry. Thus, in basic systems the attenuation of a certain electromagnetic noise suppression material may be estimated [3]. However, in order to study its response in a complex electronic system, it might obtain a real approach through some experimental characterization methods. In specific applications, it could be more interesting to measure the absorbing capacity through experimental setups that make it possible to analyse the material performance by comparing several sheets that provide different behaviour. Thereby, several experimental test can be implemented to characterize the absorber material according to the shape, dimensions and thickness.

This paper gathers the most important experimental methods to characterize electromagnetic noise suppression materials. These methods simulate problems based on: transmission lines, cavity resonance and inter-decoupling. A description of these setups and experimental results will be shown in order to determine which material provides the best performance to reduce electromagnetic noise problems depending on the application.

2. CHARACTERIZATION AND PROPERTIES

One of the most important parameter that describes the material's capacity to absorb electromagnetic noise is the permeability (μ). The losses of the magnetic flux can be quantified by separating it into its complex form due to the real component provides the reflection or inductive part and the imaginary component the accounts for losses or absorption part [4] [5].

As regards the permeability parameter, that relates the magnetic flux density to the magnetic field in a defined medium, the parameter μ' defines the magnetic flux that the material is able to reflect and μ'' describes the material effectiveness to absorb the magnetic noise. The behaviour of these parameters depend on the material composition and the frequency. There are materials that can offer a flat attenuation response in a large frequency range and others are able to provide a higher attenuation level but in a less frequency range. Along the same lines, there are materials capable of maintain the same μ'' in a huge frequency range and others can provide a higher magnetic losses but in a

narrower frequency range. Therefore, it is very important to know in which frequency appear the noise and its amplitude. With this data it is possible to establish a balance between reflection and magnetic losses depending on the application and the kind of electromagnetic noise. Experimental methods described in this contribution make it possible to analyse how the correct selection of a specific noise suppression sheet can solve or reduce EMC problems in an electronic design.

Fig. 1 shows the complex permeability of some noise suppression sheets with different performances. These data have been obtained by looking up the datasheets of the WE-FAS EMI Flexible Absorber Sheets products range produced by Würth Elektronik. Fig. 1(a) shows a balance between μ' value and frequency due to, the materials that offer the maximum value set to decreasing before. As regards the μ'' parameters, it is extended up hundreds of megahertz and several gigahertz. As shown in Fig. 1, the maximum magnetic losses value is provided by the WE-FAS 344 material due to it offers a significantly increase at 9 MHz and reaches the peak value around 200 MHz. It is important to highlight the WE-FAS 334 material tendency due to it has the steepest rising edge in 20 MHz and an almost flat response in the frequency range of 40-200 MHz.

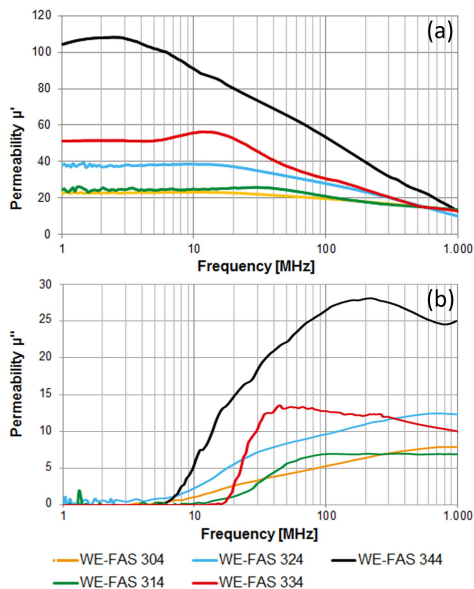


Figure 1. Permeability of noise suppression materials.

This kind of dielectro-magnetic composite material is based on a ferrite powder which is mainly composed of iron. It is also formed by a lesser amount of other elements such as aluminium and silicon. In order to hold

the ferrite powder, a polymer that provides flexibility and consistency to the sheet is used. The performance of these materials depends on the amount of each element of the composite, the ferrite grains size, distribution and position. The design of these parameters allows the material to attenuate or absorb electromagnetic noise of a certain range of frequencies.

In addition, these materials are able to attenuate the electrical field and, as a result, they provide an effective solution to reduce high-frequency EMI problems.

3. MEASURING METHODS

Three experimental methods for measuring the electromagnetic noise suppression sheet characteristics will be described in this part. Those procedures are set aside for characterizing the noise suppression sheets performance in various kind of applications by trying with several sheets with different composition, thickness or size.

3.1. Microstrip Line Method

A standard method [6] based on a microstrip line (MSL) test fixture can be used to evaluate the attenuation of conducting current noise in a PCB or noise path when the noise suppression sheet is installed. Thereby, the MSL is employed as a transmission line which provides the noise that will be measured to know the sample absorption capability. Hence, this test fixture simulates a noise source inside an electronic circuit and with this method it is possible to determine the transmission attenuation power ratio (R_{tp}).

The standard manufactured MSL employed in this procedure consists of a PCB where the strip conductor is printed and two SMA type connectors are connected in both ends. The MSL is composed of polytetrafluoroethylene (PTFE) dielectric PCB material (length = 100 mm, width = 50 mm, thickness 1.6 mm), a copper strip conductor (length = 54.4 mm, width = 4.4 mm, thickness 0.018 mm) and a copper ground plane located in the bottom (length = 100 mm, width = 50 mm, thickness 0.018 mm). The SMA connectors are installed on the opposite side of the MSL and they are connected with the end of the MSL through two vias.

Absorbing ratio can be obtained by comparing the transmission line power ratio before and after installing the noise suppression sample on the test fixture. A sample of the same PCB has been used to evaluate the material characteristics. In order to carry out the measurements, each end of a network analyser coaxial cables are connected to each SMA test fixture ports, as shown in Fig. 2. The network analyser have to be configured to operate as signal source and signal receiver to start the measurement procedure.

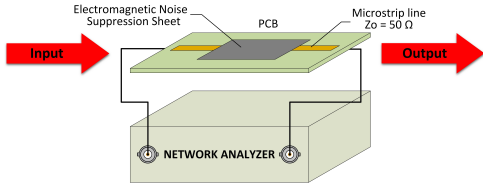


Figure 2. Microstrip Line Measurement System.

A main of determining the absorption material capability is through measuring and saving S_{11} and S_{21} data as a reference. These parameters could be renamed as S_{11R} and S_{21R} , respectively. Subsequently, the sample (length = 100 mm, width = 50 mm) is placed on the MSL, covering completely the test fixture, and the S_{11} and S_{21} parameters are measuring and saving anew. Finally, these last parameters are recalled as S_{11M} and S_{21M} , respectively. Once both measurements have been done, it is possible to calculate the R_p value by using the Eq. 1. The calculated value shows attenuation noise ratio due to the test sample.

$$R_{tp} = -10 \lg \left(\frac{10 \frac{S_{21M}}{10}}{1 - 10 \frac{S_{11M}}{10}} \right) \text{ (dB)} \quad (1)$$

This method makes it possible to evaluate the performance of the noise suppression sheets in systems with transmission line issues through an experimental procedure. In this way, it is possible to try several sheets with different composition or thickness in order to obtain the maximum transmission attenuation power ratio in a specific application. This kind of problems can appear in high-frequency data buses where there are some digital signals switching at some megahertz or gigahertz that can produce conducted noise in their lines. An interesting solution in this sort of application is to place a noise suppression sheet on the data bus as shown in Fig. 3. It acts as a low-pass filter absorbing or attenuating high-frequency conducted noise.

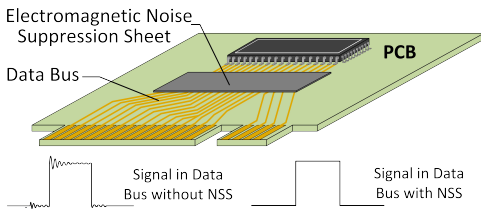


Figure 3. Transmission Line Application.

3.2. Coaxial Line Method

An electronic circuit placed inside of a shielded enclosure can generate cavity resonance at certain frequencies when the cover is closed due to the can size and characteristics. A means of reducing these issues is to place an absorber sheet inside the enclosure to attenuate or suppress the cavity resonance and avoid internal reflections. In order to evaluate this material in this kind of application, an experimental measurement system based on a coaxial line can be used. In this procedure, one terminal of the coaxial line is shorted with a metallic surface, and the reflected energy inside it is measured with a network analyser is shown in Fig. 4.

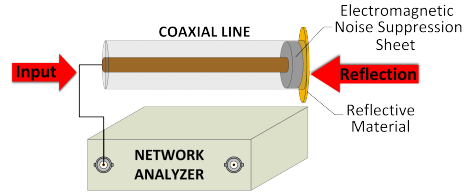


Figure 4. Coaxial Line Measurement Procedure.

In order to characterize the absorption capacity of different compositions and/or thicknesses, it is necessary to repeat the process setting the absorber material attached over the reflector and compare the results. This experiment is known as 39 D Coaxial Line Method [7] due to a coaxial line with a diameter of 39 mm is used for measurement complex permittivity and permeability of the sample under test. The evaluation of noise suppression materials in this experiment is carried out by measuring and saving the reflection parameter S_{21} in the coaxial line without ferrite material. This parameter is used as a reference and it is renamed as S_{21R} . Next, the sample is placed before the reflection material and the same parameter is measured renaming it as S_{21M} . Both measurements determine the absorption ratio S_{21AR} of the noise suppression sample by using the Eq. 2.

$$S_{11AR} = \frac{S_{11M}}{S_{11R}} \quad (2)$$

Coaxial line experimental method provides a means of studying the noise suppression material capability to solve problems in system with cavity resonance. Cavity resonance is a problem which can appear when an electronic circuit is placed inside a metal can. The resonance inside the enclosure it is usually caused by noisy circuits and it may cause interference problems or even generate a system malfunction. Considering this, after evaluating some noise suppression materials with several compositions and sheet thickness it is possible to choose the sheet with the best performance to filter the

resonance frequency. In this kind of application a sheet is placed under the cover of the metal enclosure to absorb the electromagnetic noise as illustrates Fig. 5.

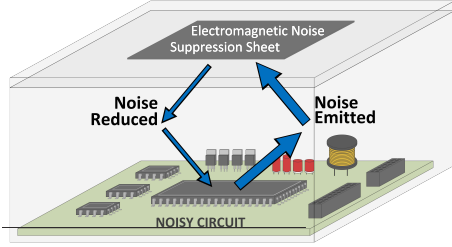


Figure 5. Coaxial Line Application.

3.3. Inter-decoupling Method

Another experimental method to consider is the inter-decoupling due to this measuring makes it possible to evaluate noise suppression materials in applications in which there are electromagnetic interferences between two circuits or PCBs placed one above the other. The magnetic sheets absorption capacity for reducing or suppressing the coupling can be analysed by employing a pair of loop antennas. Thereby, both loop antennas simulate a coupling system being that, one is used as noise source and the other one as receiver or victim. The loop antennas employed to carry on this experiment have been designed and implemented in a PCB following the recommended instructions described in the standard [6]. The option chosen is the shielded multi-layer antenna with slit with which it is possible to measure in the 0.1 – 3 GHz frequency range. This electromagnetic interference situation is often observed when there is a noisy electronic component or circuit placed in a PCB that can affect to the nearby elements.

The absorption effect is determined through arranging the pair of loop antennas in the same plane one above the other measuring the coupling between them. This value is taken as a reference and it is compared to the coupling measured with a noise suppression sheet set perpendicular to both antennas between them, as shown in Fig. 6. Subsequently, a network analyser is configured as signal source and signal receiver and each connector is connected to each loop antenna.

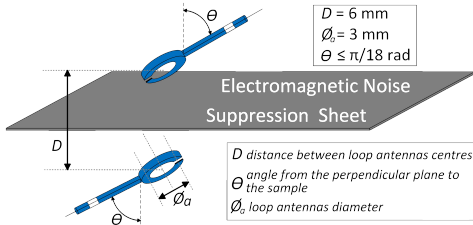


Figure 6. Inter-decoupling Measurement Procedure.

The absorbing material capacity to lead to a part of magnetic flux is determined by the electromagnetic material loss and it can be observed by trying with several sheets with different composites, sizes and thickness. Considering this procedure, inter-decoupling ratio (R_{de}) can be obtained by comparing the measures obtained with sample placed with the reference. As already mentioned previously, the reference value is measured with both loop antennas aligned in the same plane and following the indicated distances as shown in Fig. 6. The acquired S_{11} and S_{21} data are saved and renamed as S_{11R} and S_{21R} , respectively. Following on from this procedure, the noise suppression sample (length = 100 mm, width = 50 mm) is placed between the antennas and the S_{11} and S_{21} parameters are measuring and saving anew, recalling them as S_{11M} and S_{21M} , respectively. The R_{de} value is calculated by the Eq. 3 and it compares the transmission characteristics with and without the sample.

$$R_{de} = S_{21R} - S_{21M} \quad (dB) \quad (3)$$

Inter-decoupling is a common issue in electronic systems based on a rack which holds some PCBs or devices with space limits that contain electronic circuits placed one on top of the other. An interesting solution which can reduce the unintentional coupling in this kind of systems is focus on filtering the electromagnetic interferences by placing the noise suppression sheet on the noise source or protecting the interfered part as shown in Fig. 7.

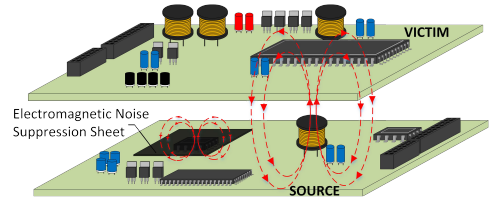


Figure 7. Inter-decoupling Application.

4. RESULTS AND DISCUSSION

The results presented in this part, correspond to the analysis of the acquired data by trying different materials of the WE-FAS EMI range which have been measured with the setups described above. The family that provides the best behaviour will be also shown as a function of the sheet thickness. Considering this, it is possible to evaluate the noise suppression materials performance according to their composition and thickness.

4.1. Microstrip Line Method

Fig. 8(a) illustrates the absorption rate measured by trying some absorbers with the same size (length = 100

mm, width = 50 mm), thickness (0.3mm) and different composition in the MSL method. It is important to highlight the 33403 material tendency being that it shows a huge absorption capacity since 1 GHz compared with the rest materials. It continues decreasing linearly and it provides an attenuation around -35 dB at 3 GHz. This sheet have this performance due to it has been designed in order to be employed in RFID applications. For this reason, the composition of this sheet, based on a special rubber material with ferrite powder, has been designed to provide a high-attenuation at high-frequencies with the objective of ensuring the correct communication in the frequency range of 13.56 MHz.

Regarding to Fig. 8(b), shows the return losses or absorption rate according to the different 304 sheet thicknesses. Thereby, this experimental setup allows to demonstrate that there is quite clear connection between absorption capacity and material thickness since the larger the thickness, the higher the attenuation is.

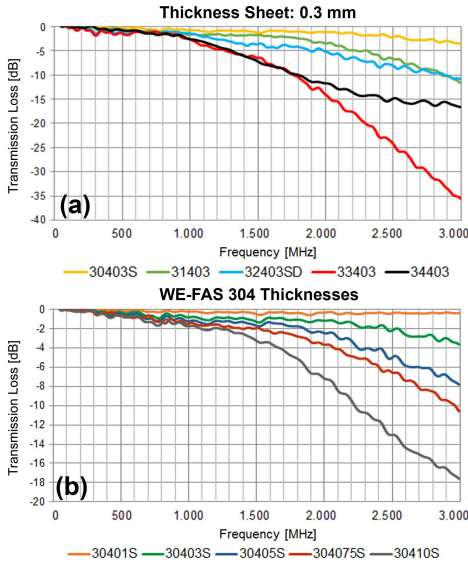


Figure 8. Transmission Loss depending on the material characteristics (a) and as a function of the sheet thickness (b).

4.2. Coaxial Line Method

The reflection attenuation measured with the experimental coaxial line method is shown in Fig. 9. As can be seen in Fig. 9(a), several noise suppression sheets with the same size and thickness (0.3 mm) but with different amounts of ferrite powder has been tried. As it is in the case of MSL method, 33403 material provides the higher losses at high frequencies. It is worth

noting the 34403 material attenuates more the frequency range up to 1.1 GHz offering a different performance from the rest.

Fig. 9(b) shows that the 30410S sheet, as a result of its larger thickness (1 mm), provides the higher absorption capacity up to 2.3 GHz and at higher frequencies the sheet 304075S, with a lower thickness (0.75 mm), is able to filter more amount of electromagnetic noise. It demonstrates that with a same size and thickness, by modifying the internal material composition, it is possible to focus on the attenuation in a certain frequency range.

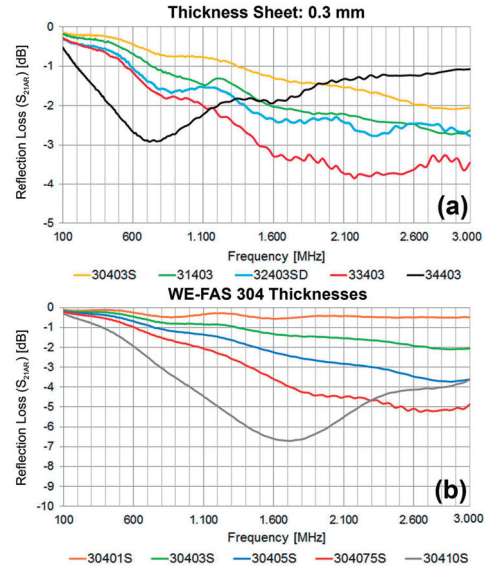


Figure 9. Reflection Loss depending on the material characteristics (a) and as a function of the sheet thickness (b).

4.3. Inter-decoupling Method

Fig. 10(a) illustrates the absorption rate measured by trying some absorbers between the pair of loop antennas following the described procedure. The 34403 material offer the higher attenuation in the frequency range up to 450 MHz if it is compared with the rest of the rage materials with the same thickness (0.3 mm) and dimensions. Nevertheless, other materials as 30403 could provide a greater attenuation in frequencies higher to 550 MHz.

In terms of thickness the 32410 (1 mm) sheet offers the maximum attenuation over the whole frequency range measured as can be seen in Fig. 10(b). Practically, it is possible to observe a proportional relation between thickness and attenuation considering that the thinner

the thickness, the lower the attenuation is. However, it is also worth noting that as frequency increases the 30403, 31403 and 32403 traces are nearer. It is because of their internal material composition is very similar if it is compared to 33403 and 34403.

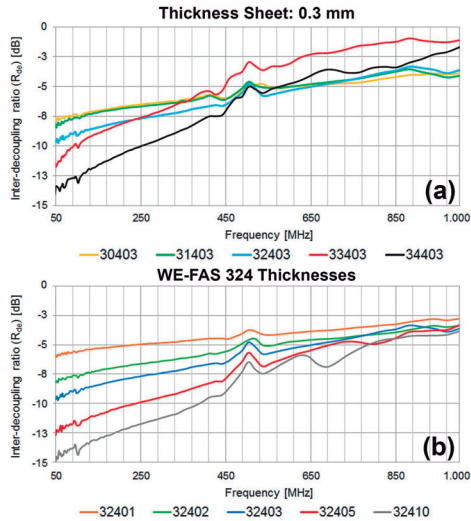


Figure 10. Inter-decoupling ratio depending on the material characteristics (a) and as a function of the sheet thickness (b).

5. CONCLUSIONS

Electromagnetic noise suppression sheets can solve a variety of EMI problems in different kinds of applications. Three of the most important experimental methods have been described and related to common real problems that can appear in electronic systems. Thereby, absorber materials can be characterized in order to be employed in applications with data buses affected by conducted problems, electronic circuits located inside an enclosure with malfunctions due to a cavity resonance and electromagnetic interference between components placed in the same circuit or between PCBs held in a rack.

It can be deduced from the results that there is a balance between frequency range and attenuation ratio due to the material that usually provides the maximum attenuation is able to maintain it only in a certain range of frequency. Moreover, the dependence on the attenuation ratio with the sheet thickness have been checked in the three methods.

In summary, absorber sheets can provide a lot of advantages and these experimental procedures make it possible to try different kind of compositions and sizes. Furthermore, it is possible to evaluate between several

sheet thicknesses, sizes and shapes to choose the best solution to obtain the best performance, depending on the device space limits. Therefore, these materials can provide an innovative solution without modifying or redesigning the electronic circuit or product.

6. REFERENCES

- 1 Yoshida, S., Ono, H., Ando, S., Tsuda, F., Ito, T., Shimada, Y., Yamaguchi, M., Arai, K., Ohnuma, S. & Masumoto, T. (2001). High-frequency noise suppression in downsized circuits using magnetic granular films. *IEEE Trans. Magn.* **37**(4), 2401–2403.
- 2 Yoshida, S., Ono, H., Ando, S., Yamaguchi, M., & Shimada, Y. (2003). Control of magnetic loss profile for RF noise suppression sheets. *IEEE Int. Symp. EMC*. Istanbul, Turkey, pp962–965.
- 3 Kim, S. (2012). Numerical analysis on power absorption by Fe₃O₄ thin films for conduction noise in Microstrip line. *IEEE Trans. Magn.* **48**(11), 3490–3493.
- 4 Sharma, A., Rahman, N., Obol, M., & Afsar, M. (2010). Precise characterization and design of composite absorbers for wideband microwave applications. *Microwave Conference (EuMC), 2010 European*. Paris, France, pp160–163.
- 5 Brander, T., Gerfer, A., Rall, B., & Zenkner, H. (2010). *Trilogy of Magnetics: Design Guide for EMI filter design, SMP & RF circuits*, Swiridoff Verlag, Künzelsau, Germany, pp30–32.
- 6 IEC 62333-2, Part 2: Noise suppression sheet for digital devices and equipment - Part 2: Measuring methods.
- 7 Shimada, K., Ishizuka, K., & Tokuda, M. (2006). A study of RF absorber for anechoic chambers used in the frequency range for power line communication system. *PIERS Online*, **2**(5), 538–543.

3.3 Scientific conference article II: Field distribution in complex circuits

Title: Characterization of Flexible Absorber Sheets with an EMC Scanner System.

Authors: Adrián Suárez, Jorge Victoria, Antonio Alcarria, José Torres, Pedro A. Martínez, Jesús Soret, Julio Martos, Raimundo García-Olcina, Víctor Martínez, Ismael Mialdea.

Published in: SAAEI 2017 Proceedings, Valencia, Spain

Description: Annual Seminar on Automation, Industrial Electronics and Instrumentation (SAAEI) is a conference with a high scientific level. It is an annual conference reference for the exchange of experiences in the power electronics environment. It is focused on the topics of Power Electronics, System Control, Instrumentation and its Technological and Didactic Applications. The submitted contributions are subjected to the peer review process to assess the quality of the manuscript before it is published.

Synopsis:

In this article presented at the "Annual Seminar on Automation, Industrial Electronics, and Instrumentation (SAAEI)" in 2017, we designed an experiment to analyze the effect of magnetic absorbers on reducing EMI at the PCB level.

We designed a circuit that generates high-frequency interference and laid out the traces to maximize radiation. We used measurement equipment based on a near-field probe array (EMScan), connected to a network analyzer, which allows us to measure the magnetic field distribution at each frequency.

In the results, we observed that magnetic absorbers are capable of significantly reducing the magnetic field within a certain range of frequencies. This capability can be useful for addressing EMI issues at the PCB level without the need for circuit redesign or component modification, which represents a significant benefit for designers during the certification stage of their devices.

The utility of EMScan is also demonstrated, both for locating critical areas of the PCB and for evaluating the impact of corrective measures applied, such as in this case, shielding using magnetic absorption sheets.

Characterization of Flexible Absorber Sheets with an EMC Scanner System

A. Suárez¹, J. Victoria¹, A. Alcarria¹, J. Torres¹, P.A. Martínez¹, J. Soret¹, J. Martos¹, R. García-Olcina¹, V. Martínez¹, I. Mialdea¹.

¹*Cátedra EMC Würth Elektronik – DSDC Group – University of Valencia, Spain*

Abstract— The use of high-frequency switching and low-voltage signals along with the reduction of electronic designs size has become a major problem in terms of Electromagnetic Compatibility (EMC). A solution to reduce or suppress these kinds of emissions that may cause complex EMI problems is based on flexible absorber. Thereby, in order to evaluate the performance of this product, it is introduced a new EMC and EMI diagnostic and testing tool in this contribution: EMSCAN EHX. This is a scanner which achieves quick tests and a real-time view of the radiated emissions, making easy to find out EMI problems and test different solutions. This can be carried out on the lab-bench without resorting to an anechoic chamber or large antennas. Therefore, flexible absorber sheets are evaluated through measuring with the EMSCAN the ability that they have to attenuate electromagnetic noise.

Index Terms— EMC Scanner, Electromagnetic shielding, Electromagnetic wave absorption, Flexible absorber sheet, Magnetic shielding, Permeability.

I. INTRODUCTION

ELECTROMAGNETIC Interference (EMI) has become a serious difficulty since it can arise anywhere in electronic circuits with unpredictable and damaging effects. This problem has grown in recent years due to a number of factors including an increase in the frequency of devices, the high integration in electronic systems, the use of low voltage signals and the size and thickness reduction of the Printed Circuit Boards (PCBs). To avoid those problems pre-compliance testing is a fundamental part of the designing process to identify the radiations source.

The most common means of solving electromagnetic noise problems is to shield the system or device with conductive materials such as: shielded enclosure, foil tape or conductive gasket. Nevertheless, recent electronic devices have a lot of parts that operate at hundreds of MHz and several GHz which can generate harmonic noise emissions at a high-frequency region. These kinds of emissions may cause complex EMI problems that cannot be removed with simple shielding. An innovative shielding technique to solve EMI problem is making use of Flexible Absorber Sheets (FAS) based on a dielectric-magnetic composite material formed by a polymer

filled with ferrite powder. These materials can be used to suppress those unwanted high-frequency components [1] thanks to they have a greater permeability to magnetic fields (H) than the air around them. Therefore, an absorber sheet can concentrate the magnetic field lines and, by strategic placement of it, it is possible to concentrate this magnetic flux and influencing the intensity and shape of that field.

The main property that allows these magnetic materials to influence the magnetic field in its environment is the relative permeability (μ_r) [2]. This parameter is characteristic of the composition of the sheet, although it could result difficult to estimate the absorber material performance in attenuation terms due to it depends on several factors such as: gap between the sheet and the noise source, sheet thickness, kind of adhesive size and geometry. Thus, in basic systems the attenuation of a certain electromagnetic noise suppression material may be estimated [3] whereas, in a complex electronic system, it might obtain a real approach through an experimental characterization technique. In certain applications, it could be more interesting to measure the absorbing capacity through a measurement setup. This can make it possible to analyze the material performance by comparing several sheets that provide different behavior.

Thereby, in this contribution, FAS absorbing ability to attenuate electromagnetic noise is measured through using an EMC Scanner. Therefore, this scanner makes it possible to analyze and compare the magnetic behavior of an electronic circuit. This allow the designer to place the absorber material in the area with EMI problems and evaluate its performance, checking at the same time if the problem has been solved or attenuated.

II. FLEXIBLE ABSORBER SHEETS PROPERTIES

One of the most important parameter that describes the material's capacity to absorb electromagnetic noise is the relative permeability. It relates the magnetic flux density to the magnetic field in a defined medium. It can be expressed in its complex form by using (1) to be analyzed better.

$$\mu_r = \mu' - j\mu'' \quad (1)$$

The parameter μ' defines the magnetic flux that the material is able to reflect and μ'' describes the material effectiveness to

absorb the magnetic noise. The behavior of these parameters depend on the material composition and the frequency. There are materials that can offer a flat attenuation response in a large frequency range and others are able to provide a higher attenuation level but in a less frequency range. Along the same lines, there are materials capable of maintain the same μ'' in a huge frequency range and others can provide a higher magnetic loss but in a narrower frequency range. Therefore, it is very important to identify in which frequency appear the electromagnetic noise and its amplitude. By that means, with this data it is possible to establish a balance between reflection and magnetic losses depending on the kind of electromagnetic noise.

Fig. 1 shows the complex permeability of absorber materials with different performances. These data have been obtained by looking up the datasheets of the WE-FAS EMI Flexible Absorber Sheets products range manufactured by Würth Elektronik. As can be observed, there is a balance between μ' value and frequency due to, the materials that offer the maximum value set to decreasing before. As regards the μ'' parameters, it is extended up hundreds of megahertz and several gigahertz. High μ' materials are utilized in order to maximize magnetic flux control with minimum losses whereas materials with high μ'' are useful and utilized when dealing with noise, such as in noise filters.

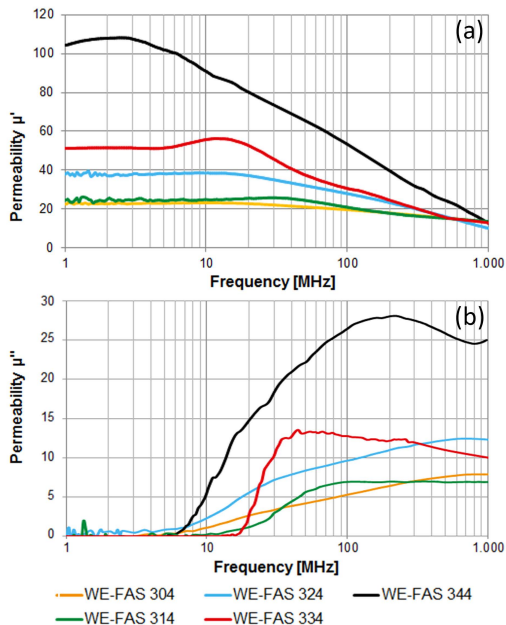


Fig. 1. Permeability of different Flexible Absorber Sheet composition.

As shown in Fig. 1, the maximum magnetic losses value is provided by the WE-FAS 344 material due to it offers a significantly increase at 9 MHz and reaches the peak value

around 200 MHz. It is important to highlight the WE-FAS 334 material tendency due to it has the steepest rising edge in 20 MHz and an almost flat response in the frequency range of 40-200 MHz.

The correct selection of the material is then paramount to the suitability of the material in the application specific frequency with the aim of achieving the desired effect of filtering or flux control.

III. MEASUREMENT SETUP AND DESCRIPTION

The setup developed for the data analysis [4] is shown in Fig. 2. It is composed by the EMSCAN EHX Scanner which is connected by a compact adaptor to the external trigger and the RF connector of the spectrum analyzer. This adaptor is also connected by USB to a computer which is responsible for running the EMxpert software where the data is analyzed and showed.

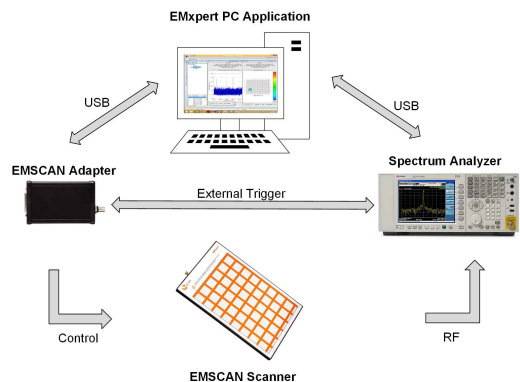


Fig. 2. Diagram of the measurement setup.

The Device Under Test (DUT) is placed on the matrix of the EMSCAN EHX Scanner and the layout of the DUT can be placed on the software in order to have a virtual reference on the radiation map that the software generates [5].

A. EMSCAN

The principal equipment for these measurements is the EMSCAN EHX. This device is capable of providing unique pre- and post- EMC compliance testing in real time. The using of this equipment allows the designer to analyze and compare design iterations.

The scanner is a passive device that couples the very-near-field emissions received from the DUT. The measurements of these coupled fields are carried out with the spectrum analyzer and the adaptor synchronizes it with the scanner. Then, the EMxpert software knows the insertion loss of each probe of the matrix that composes the scanner across the frequency range. It applies the compensation for the internal losses derived from the scanner and the antenna factor compensation to obtain the display of an accurate H-field data through the

interpolation between probes [6]. This means that scanner delivers repeatable and reliable results that may pinpoint in less than a second the cause of a design EMI failure.

The EHX scanner model utilized in this measurement setup, consists of 2436 loops into 1218 magnetic wide band near field probes (H-field) that operate between 150 kHz and 8 GHz [7]. Each row and column of the EHX corresponds to an individual Near Field Probe (NFP) that is spaced every 7.5 mm in array distribution providing an effective resolution of 3.75 mm. The effective scan area is about 31.6 cm x 21.18 cm and the measurement sensitivity goes from -130 dBm to 35 dBm, depending of the spectrum analyzer used.

Therefore, EMSCAN makes it possible to analyze and compare the magnetic behavior of an electronic circuit allowing the designer to place the absorber material in the area with EMI problems and evaluate its performance, checking at the same time if the problem has been solved or attenuated.

B. Electromagnetic Noise PCB Generator

In order to characterize the effectiveness of several FAS, an electromagnetic noise source capable of generate enough radiated emissions has been designed.

This noise source has been implemented in a PCB which is based on the NB3N5573 oscillator integrated circuit (IC) that acts as a crystal frequency multiplier and is powered by 3.3 V [8]. The input fundamental parallel mode crystal resonator is a 27 MHz crystal and the IC can generate a selectable output frequency which multiply by 1, 2, 4 or 8 the input frequency.

After the output of the NB3N5573, there are connected two noisy paths based on a long spiral track and a long serpentine track that work as EMI antennas. The layout of the Electromagnetic Noise Generator circuit is shown in Fig. 3. The output of the oscillator circuit is connected to one of two noisy path based on a long spiral track and a long serpentine track with the aim of they work like EMI antennas as shown in Fig. 3.

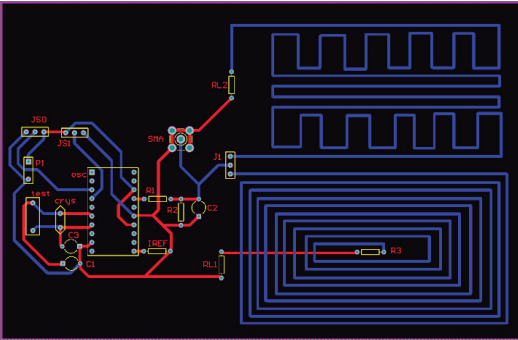


Fig. 3. Layout of the electromagnetic noise generator PCB.

IV. RESULTS

The results presented in this part, correspond to the analysis of the acquired data by trying different materials of the WE-FAS EMI range which have been measured with the setup described above. The family that provides the best behavior will be also shown as a function of the sheet thickness. Considering this, it is possible to evaluate the absorber material performance according to their composition and thickness.

Thereby, absorption ability of each absorbing sheet can be analyzed by trying to place different flexible ferrites with several thicknesses and compositions. Subsequently, the radiation measured is compared with the value obtained without setting any shielding between the EMSCAN and the EMI antennas.

A. Spiral Antenna

The first case study is the EMI source based on the spiral antenna. Fig. 4 shows the reference of radiated emissions measured in that area before placing any absorber material.

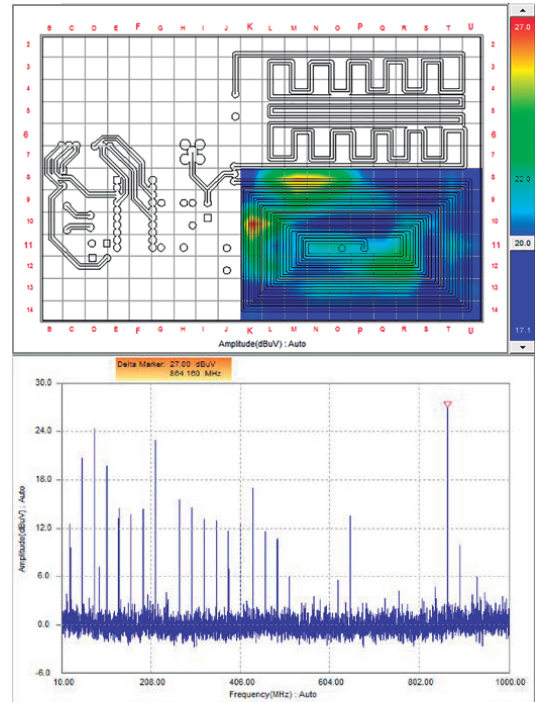


Fig. 4. Radiated emissions reference the spiral antenna. Spatial radiated emissions diagram (above) and frequency spectral (bellow).

As can be observed in the spatial diagram, the maximum value of radiated emissions measured in the spiral antenna area is 27 dBuV. The frequency spectral graph locates the maximum peak at 864 MHz and also shows important peaks over the entire 1 GHz bandwidth.

Subsequently, the spatial radiation diagrams of the WE-FAS 324 absorber material are shown in Fig. 5 to analyze the performance of the same material composition depending on the sheet thickness. This product is available in three different thicknesses: 0.1 mm, 0.5 mm and 1.0 mm. From the Fig. 5 radiation spatial diagrams it is evidenced the effect of placing absorber sheets with a greater thickness and it is also proved their ability to attenuate electromagnetic noise. In the case of 0.1 mm sheet, the maximum peak is decreased 2,4 dBuV, as to the sheet of 0.5 mm, the noise has been attenuated 3,5 dBuV and the sheet with 1.0 mm thickness has reduced the radiation 5,6 dBuV with respect the reference without any shielding.

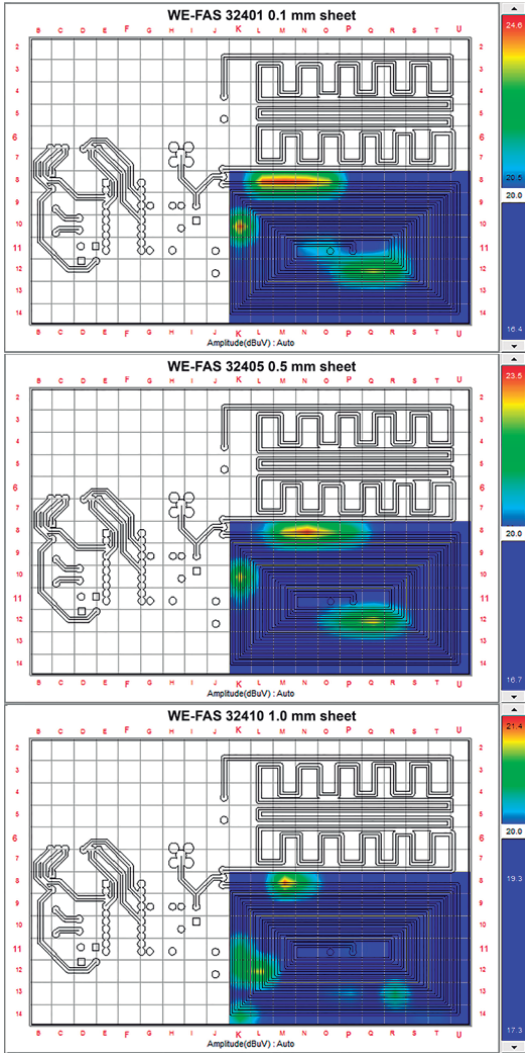


Fig. 5. Radiated emissions measured in the spiral antenna after placing WE-FAS 324 flexible absorber sheets with different thickness.

This comparison can also be carried out analyzing the attenuation ability of several materials with the same thickness but with different composition. Thus, 30403, 31403, 32403, 33403 and 34403 absorber sheets are compared in Table 1 by showing their maximum radiation peak and the attenuation value.

Material	Maximum Radiation Peak with Shielding (dBuV)	Attenuation Value (dBuV)
30403	25.3	1.7
31403	25.1	1.9
32403	24.3	2.7
33403	23.4	3.6
34403	23.0	4.0

B. Serpentine Antenna

With regard to the results obtained with the serpentine EMI source, Fig. 6 shows the reference of radiated emissions measured in that area before placing any absorber material.

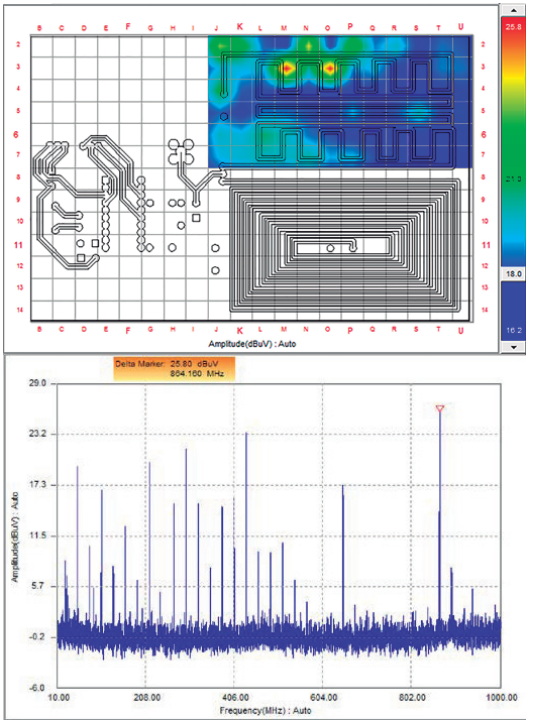


Fig. 6. Radiated emissions reference the serpentine antenna. Spatial radiated emissions diagram (above) and frequency spectral (bellow).

As shown in Fig. 6, the maximum value of radiated emissions measured in the serpentine antenna area is 25,8 dBuV. The frequency spectral graph locates the maximum peak at 864 MHz and also shows important peaks over the

entire 1 GHz bandwidth. The same sheets which have been employed in the spiral antenna are used in this case to evaluate the absorber material performance depending on the thickness: 32401 (0.1 mm), 32405 (0.5 mm) and 32410 (1.0 mm). This comparison is shown in Fig. 7.

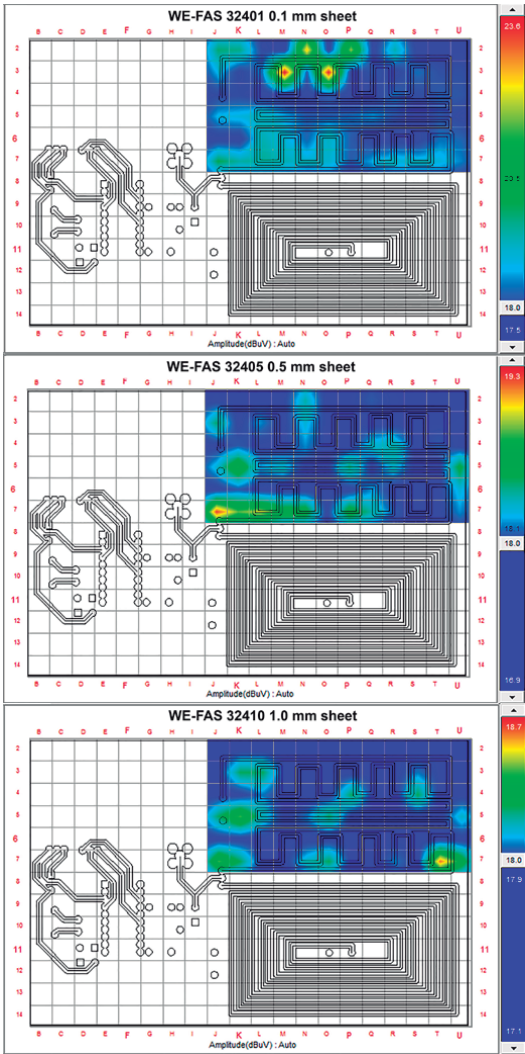


Fig. 7. Radiated emissions measured in the serpentine antenna after placing WE-FAS 324 flexible absorber sheets with different thickness.

Fig. 7 radiation spatial diagrams showed the effect of placing absorber sheets with different thickness and their capability to reduce EMI. In the case of 0.1 mm sheet, the maximum peak is attenuated 2,2 dBuV, as to the sheet of 0.5 mm, the noise has been reduced 6,5 dBuV and the sheet with 1.0 mm thickness has decreased the radiation 7,1 dBuV, compared with the reference maximum peak without any absorber sheet.

This comparison can also be carried out analyzing the attenuation ability of several materials with the same thickness but with different composition. Thus, 30403, 31403, 32403, 33403 and 34403 absorber sheets are compared in Table 2 by comparing their maximum radiation peak and the attenuation value. According to the permeability graph, the analysis of these results shows that a material with higher absorption parameter such as 344 is able to attenuate more the electromagnetic noise than another material with lower losses. It can be observed if 34403 sheet is compared with the rest.

Material	Maximum Radiation Peak with Shielding (dBuV)	Attenuation Value (dBuV)
30403	21,2	4.6
31403	21,1	4.7
32403	19,8	6.0
33403	20,8	5.0
34403	18,3	7.5

V. CONCLUSION

In summary, flexible absorber sheets provide an innovative shielding solution due to a variety of EMI complex problems can be reduced without modifying or redesigning the electronic circuit or product. As detailed above, permeability property defines the response of this kind of materials, however, to obtain a response in terms of attenuation an EMC scanner can provide more useful information to evaluate the sheets performance taking into account other factors such as thickness, size, shape and geometry.

Thereby, the measures carried out with the EMC scanner has shown in both spiral and serpentine antennas that the larger the thickness sheet, the higher the attenuation is. Nevertheless, there is no a proportional ratio considering that when the thickness sheet doubles the attenuation not always is reduced in the same proportion.

With regard to the material composition, the EMC scanner allow the designer to evaluate several sheets and decide which absorber material is suitable to solve or reduce the radiation problems.

Therefore, absorber sheets provide a lot of advantages and an EMC scanner is a great tool to evaluate the performance of them and to know how this material is able to improve the behavior of a certain application.

ACKNOWLEDGMENT

Authors thank Würth Elektronik eiSos the information and materials provided about Flexible Absorber Sheets WE-FAS to carry out this contribution.

REFERENCES

[1] S. Yoshida, H. Ono, S. Ando, F. Tsuda, T. Ito, Y. Shimada, M. Yamaguchi, K. Arai, S. Ohnuma, and T. Masumoto, "High-frequency noise suppression in downsized circuits using magnetic granular films, *IEEE Trans. Magn.*, vol. 37, no. 4, pp. 2401–2403, Jul. 2001.

- [2] S. Yoshida, H. Ono, S. Ando, M. Yamaguchi, Y. Shimada, "Control of magnetic loss profile for RF noise suppression sheets", *IEEE Int. Symp. EMC*, vol. 2, pp. 962-965, May 2003.
- [3] S. S. Kim, "Numerical analysis on power absorption by Fe₃O₄ thin films for conduction noise in Microstrip line", *IEEE Trans. Magn.*, vol. 48, no. 11, pp. 3490-3493, Nov. 2012.
- [4] C. Caudron "How to Diagnose Board-Level Design Issues Using Very-Near-Field Measurements", *EMSCAN EMxpert Application Note*, Jun. 2014.
- [5] Z. Ji, Y. Tengfei, A. Xiaohui, "Analyse and research of radiated emission on PCBs", *Int. Conf. Electronics, Communications and Control (ICECC)*, pp. 727-730, 2011.
- [6] EMSCAN, "Understanding Compensation", *EMSCAN EHX Technical bulletin* #7, Nov. 2011.
- [7] EMSCAN, "Real-time EMC and EMI diagnostic tool: Test ultra-high speed (> 2 GHz) PCBs in real-time on your lab-bench", *EMSCAN EHX Datasheet*, Feb. 2017.
- [8] ON Semiconductor, "3.3 V, Crystal to 25 MHz, 100 MHz, 125 MHz and 200 MHz Dual HCSL Clock Generator", *NB3N5573 Datasheet*, Rev. 11, Mar. 2017.

3.4 Summary

Magnetic absorber materials are defined by their electromagnetic characteristics, including permeability, permittivity, and resistivity. However, more than these properties alone are needed to offer sufficient insight to comprehend and forecast the effectiveness of absorber sheets across various EMI applications such as filtering, decoupling, and absorption. Hence, we conducted measurements through various setups. Ultimately, we evaluated the shielding effect of magnetic absorber sheets on an electronic noisy circuit by employing a matrix of magnetic probes connected to a spectrum analyzer. The measurement techniques outlined in this chapter serve as the experimental groundwork of the Ph.D. thesis.

Chapter 4. MODELLING AND SIMULATION

OF MAGNETIC ABSORBER SHEETS

Simulation models are created based on Finite Elements Methodology (FEM). The measurement setups are also simulated, and the results of the simulation and measurement are compared for the validation of the models. Finally, the validated models are used to solve critical EMI challenges that are covered mainly by MAS: optimization of NFC communication systems and countermeasure of EMI produced by metallic planes.

4.1 Simulation Model Design

Utilizing the measured resistivity, magnetic permeability, and tangent magnetic loss, we developed models for magnetic absorber sheets using an electromagnetic analysis simulator (ANSYS HFSS). The precision of these models is validated by comparing the S parameters obtained from the Finite Element Method (FEM) simulation model with experimental data [14].

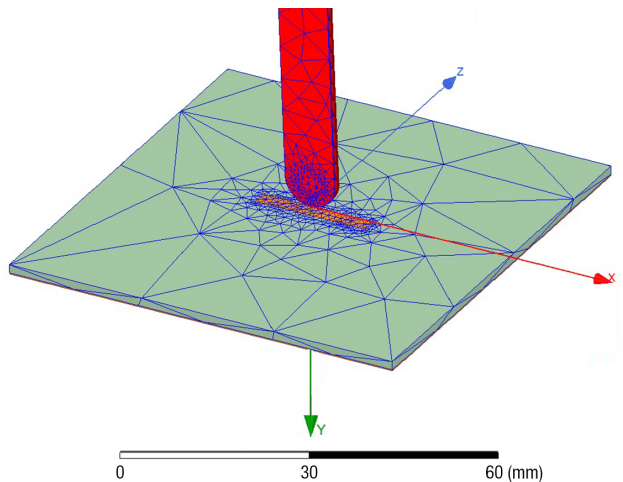


Figure 4.1. FEM simulation model for the measurement setup.

The use of simulation for electromagnetic absorption sheets serves several crucial purposes in the context of this research:

- Facilitate a cost-effective analysis of MAS performance without the necessity of physical prototypes, resulting in time and resource savings during the product development phase.
- Provide a predictive understanding of MAS behavior in specific scenarios, aiding in anticipating potential issues and making informed decisions during the design phase.
- Identify optimal parameters such as material composition, thickness, size, and shape of MAS to achieve the desired level of EMI reduction.
- Validate MAS effectiveness under diverse conditions, reducing the need for extensive physical testing, particularly in the early stages of product development.
- Assist in selecting appropriate materials for MAS by allowing us to analyze electromagnetic performance, ensuring optimal shielding without interfering with communication signals.
- Optimize noise suppression sheets for specific frequency ranges used in NFC or RFID applications, critical for effective communication in the radio-frequency spectrum.
- Prevent detuning in NFC or RFID systems due to nearby conductive surfaces or materials by evaluating the impact of different noise suppression sheet configurations through simulations.

Address space constraints in NFC or RFID applications by using simulations to optimize the thickness, size, and shape of MAS. This ensures effective shielding without excessive space, cost, and weight.

4.2 Scientific article I: Modelling an FSFS

Title: Improving the efficiency of NFC systems through optimizing the Sintered Ferrite Sheet thickness selection.

Authors: Jorge Victoria, Adrián Suárez, Pedro A. Martínez, Antonio Alcarria, Alexander Gerfer, José Torres.

Published in: IEEE Transactions on Electromagnetic Compatibility, vol. 62, no. 4, p. 1504 - 1514 (2020).

DOI: 10.1109/TEM.2020.3003800

Impact factor (2020): JCR: 2.006; SJR: 0.655

Quartile (2020): JCR: Q3 (category: Engineering, Electrical & Electronic)
SJR: Q1 (category: Electrical and Electronic Engineering)

Citations: 8 (WoS, accessed on March 2024).

Description: IEEE Transactions on Electromagnetic Compatibility (ISSN 1558-187X) is an international peer-reviewed journal supported by the EMC Society and publishes original and significant contributions related to all disciplines of electromagnetic compatibility (EMC) and relevant methods to predict, assess, and prevent electromagnetic interference (EMI) and increase device/product immunity. The impact factor, quartile, JIF percentile, and rank information have been obtained from Journal Citation Reports (JCR) and Scimago Journal Rank (SJR) databases according to the publication year (2020). The citations have been consulted in the Web of Science database.

Synopsis:

This article examines the use of magnetic absorbers, specifically sintered ferrite sheets, to enhance the efficiency of Near Field Communication systems. NFC communication systems operate on the principle of magnetic induction between the transmitting and receiving antennas. The presence of electrically conductive surfaces in proximity can interfere to the extent of disrupting their proper functioning. The magnetic field generated by the transmitter can induce a current in a metallic plane (Eddy current), generating a magnetic field in the opposite direction. This alteration affects the magnitude of the magnetic field, the maximum communication distance, and the resonance frequency adjustment at which the transmitter and receiver communicate (13.56 MHz for NFC).

Flexible sintered ferrite sheets, positioned between the antenna and the conductor plane, can prevent these electromagnetic interferences by redirecting the magnetic flux. FSFS prevents the flux from penetrating the plane and the effect of the eddy currents. It

is important for the selected FSFS to exhibit high permeability (μ') and low losses (μ'') at 13.56 MHz to avoid reducing the flux.

In this study, we analyze the performance of FSFS in compensating for the effect of a conductor plane on an NFC antenna based on its thickness, ensuring that the antenna's communication frequency remains unaltered and communication stays tuned. To achieve this, we design an NFC antenna on a printed circuit board, to which we can add different thicknesses of FSFS, an aluminum sheet at a controlled distance, or a battery to simulate a real-world scenario.

A network analyzer allows us to measure the original resonance frequency of the antenna, its value when the conductive sheet is added, and the insertion of FSFS. Using a measurement setup based on the EMScan magnetic probe array and a spectrum analyzer, we observe the magnetic field distribution and the effect produced by different combinations of conductor planes with FSFS.

By simulating the antenna and using material models, we can obtain both the resonance frequency and the magnitude and distribution of the magnetic field. The results are compared with those obtained experimentally.

This work allows us to conclude that FSFS can solve interference problems caused by metallic planes in NFC systems, emphasizing the critical importance of selecting the appropriate thickness to ensure optimal communication. The finite element-based simulations and the models generated in this study prove to be highly useful and precise for this purpose.

Improving the Efficiency of NFC Systems Through Optimizing the Sintered Ferrite Sheet Thickness Selection

Jorge Victoria, *Member, IEEE*, Adrian Suarez , *Member, IEEE*, Pedro A. Martinez, *Member, IEEE*, Antonio Alcarria, *Member, IEEE*, Alexander Gerfer, and Jose Torres , *Senior Member, IEEE*

Abstract—The reduction of embedded portable devices involves a magnetic field interference problem when it integrates near field communication (NFC) due to the presence of conductive surfaces, such as ground planes, batteries, or metallic enclosures. Flexible sintered ferrite sheets (FSFS) represent an interesting shielding solution to prevent electromagnetic interferences problems related to NFC, thanks to their ability to control the magnetic flux. The characterization of FSFS effectiveness is analyzed as a function of the sheet thickness in this contribution. This is performed with the aim of determining which is the optimum thickness value to retune an NFC antenna to its original operation frequency value (13.56 MHz) when it is affected by a near conductive surface. A finite element method simulation model is designed and corroborated with the experimental results to evaluate the performance of different FSFS thicknesses in terms of resonant frequency shift, magnetic field strength, and communication distance. An electromagnetic scanner is also used to determine the ability of the best FSFS thickness to shield an NFC transmitter antenna when a battery is set under it, emulating a usual problem. The results obtained show that the magnetic field strength is significantly attenuated and the communication distance is highly shorted. Therefore, besides selecting a material that provides high reflection and low losses at 13.56 MHz, thickness must be considered to ensure the greatest communication effectiveness. Consequently, the use of a wrong FSFS thickness could lead to shifting the resonance frequency to lower values than expected, detuning the communication.

Index Terms—Eddy currents, electromagnetic compatibility (EMC), ferrite films, magnetic shielding, near field communication (NFC), permeability, thickness control.

I. INTRODUCTION

TRADITIONAL shielding techniques usually have been focused on controlling electromagnetic interferences (EMI) using spatial separation between the noise source and the victim

circuit or the orthogonalization of them [1]. Another common shielding mechanism refers to a metallic barrier or casing that electromagnetically separates the sensitive circuit from an electromagnetic (EM) source [2]. Nevertheless, these techniques cannot always be used when dealing with electromagnetic compatibility (EMC) problems due to a strong intentional EM source that has to be integrated into a device. The continuous implementation of new advanced functionalities and the miniaturization of electronic devices for embedded systems has become a serious difficulty in terms of intrasystem compatibility. This evolution usually involves higher component integration, printed circuit board (PCB) size and thickness reduction, and the miniaturization of the device housing [3]. These design principles are often used to achieve a device with better performance and features; however, they increase the likelihood of generating complex EMI problems, especially in those that integrate near magnetic field coupling, such as near field communication (NFC) [4].

In the last ten years, NFC has become an independent field that brings together elements from several areas such as RF technology and EMC requirements, telecommunications, semiconductor technology, data protection and cryptography, manufacturing process, and other related areas. The rise of NFC is due to its versatility to be used in traditional applications, such as accessing control, identification, or payment. This technology provides an added value to traditional devices that nowadays can communicate with a smartphone or tablet [5], [6]. The forms of NFC signals in terms of appearances and amplitudes are described in the international standards ISO 18092 (NFC IP-1) and ISO 21481 (NFC IP2), which are extensively based on the contactless proximity chip-card standards ISO 14443 A and B to explain the communication protocols for the air interface and the modes of communication. NFC can support different communications modes, depending on which device (initiator or target) generates the EM field at the communication frequency (13.56 MHz). In the case of passive communication mode, the NFC transmitter (initiator) generates the EM field to send the commands and, when an NFC receiver device (target) is present in the field generated, it sends the answers using load modulation. In accordance with NFC standards ISO 18092 and 14443 A, the minimum value of field that needs to be provided by an initiator in order to guarantee the communication with an NFC target device is 1.5 A/m. Concerning the bandwidth of

Manuscript received December 14, 2019; revised April 15, 2020; accepted June 14, 2020. Date of publication July 14, 2020; date of current version August 13, 2020. This work was supported by the University of Valencia and EMC experts of Würth Elektronik eiSos. This article was presented in part at the 2019 IEEE International Symposium on EMC and SIPI in New Orleans, LA, July 2019. (*Corresponding author: Adrian Suarez.*)

Jorge Victoria, Antonio Alcarria, and Alexander Gerfer are with the Würth Elektronik eiSos, 74638 Waldenburg, Germany (e-mail: orge.victoria@we-online.de; antonio.alcarria@we-online.de; alexandr.gerfer@we-online.de).

Adrian Suarez, Pedro A. Martinez, and Jose Torres are with the Department of Electronic Engineering University of Valencia, 46010 Valencia, Spain (e-mail: adrian.suarez@uv.es; pedro.a.martinez@uv.es; jose.torres@uv.es).

Color versions of one or more of the figures in this article are available online at <https://ieeexplore.ieee.org>.

Digital Object Identifier 10.1109/TEMC.2020.3003800

0018-9375 © 2020 IEEE. Personal use is permitted, but republication/redistribution requires IEEE permission. See <https://www.ieee.org/publications/rights/index.html> for more information.

NFC, the value of 1.356 MHz is widely used around the resonant or carrier frequency when this is defined at 13.56 MHz, using typically a bit rate of 106 kbit/s [5], [6].

Thereby, NFC faces the challenge of the environmental problems arising from the EM field generated by the antennas and how to prevent them. These problems are generally related to environments hostile to EM field propagation, EMC pollution, and the effects of the casing, metal parts or the presence of the battery [5]. The proximity effects of conductive elements on the performance of an NFC antenna can be found in [7]–[11], where is reported that the presence of metallic parts shifts the resonant frequency f_r of the loop antenna and generate stray fields. Consequently, the field effectiveness is attenuated and the communication distance is reduced. The analysis of the attenuation ratio produced by several conductive elements placed at different distances is shown in [12], [13]. This is due to the magnetic flux provided by the transmitter antenna blocked by the metallic components, inducing eddy currents that reduce the inductance of the loop antenna significantly [14]. Some of the drawbacks of this situation are the possibility of heating the device and the need for increasing the supply power and thus the energy consumption to provide the same level of emitted field. This is critical in embedded portable electronic devices such as wearables, smartphones, or tablets due to the waste of battery that is produced [15].

Thereby, the management of the magnetic near field is considered a difficult problem to solve and the integration of an NFC transmitter system into an electronic design requires the use of shielding solutions based on materials able to ensure the magnetic coupling communication [16]. Additionally, the other electronic parts can be sensitive to the surrounding electromagnetic environment generated by the NFC antenna; thus, it is very important to control EM fields for preventing nearby circuits from unwanted electromagnetic interactions. Therefore, some research contributions report that the most effective method to avoid the performance degradation of the NFC loop antenna due to eddy currents is the insertion of magnetic shielding that provides high relative permeability between this and the conductive surface [6], [12], [17]–[21]. Thus, the use of a flexible sintered ferrite sheet (FSFS) represents a shielding solution to manage the magnetic flux generated by the NFC antenna, improving the communication efficiency through increasing the antenna inductance and avoiding undesired magnetic interference couplings. These sheets make it possible to concentrate the magnetic field only where it is needed, protecting the surroundings and increasing the reliability and the distance range of data communications due to their materials properties. Additionally, FSFS represents a shielding solution with great versatility in terms of mechanical properties that can provide a lightweight solution with high flexibility [22]–[24].

This contribution focuses on analyzing the effectiveness of a high-permeability ferrite sintered sheet to determine which sheet thickness provides the best performance to retune an NFC antenna to its original operation frequency value (13.56 MHz) when it is affected by a near conductive surface. Consequently, a simulation model has been designed and compared to the measurements obtained from an experimental setup with the

objective of evaluating the performance of different ferrite sheet thicknesses. The accuracy of the study is validated though comparing S parameters provided by the FEM simulation model and experimentally through a network analyzer equipment. Thereby, computed results show an evaluation of different FSFS thicknesses versus the EM field emitted by the NFC antenna and the detection distance resultant to communicate with other NFC devices. An EM scanner is also used to determine the ability of the FSFS to shield an NFC transmitter antenna when a conductive element such as a battery is placed under it. The rest of this article is organized as follows. First, Section II explains the reduction of antenna inductance, considering the eddy currents phenomena, and describes the features of the evaluated FSFS material. Section III contains the definition of the simulation model and the experimental measurement setup, whereas Section IV shows the results obtained from both sources. Subsequently, Section V analyzes and discusses the performance of the FSFS material in terms of the sheet thickness, evaluating the error produced in the resonant frequency, the intensity of the EM field emitted, and the communication distance. Finally, the main conclusions of the research are summarized in Section VI.

II. SHIELDING MECHANISM: MAGNETIC FLUX MANAGEMENT

A. Eddy Currents

An NFC communication based on passive communication mode needs that the NFC tag receives a minimum magnetic field level H_{\min} to be powered by the NFC transmitter device. The magnetic flux generated by the transmitter antenna passes through the turns of the receiver loop antenna considering communication in free space. This magnetic flux should induce enough current in the receiver antenna to enable its activation and the sending of the information to the NFC reader device. Nevertheless, when a conductive plane is located under the communication area, the magnetic field lines produce eddy currents, which, according to Lenz's law, generates an opposite stray H in phase opposition to the intended primary H .

The diagram that is shown in Fig. 1 represents the main H-fields that appear in NFC communication when a conductive plane is introduced. Thereby, it is possible to observe how the performance of the magnetic coupling is reduced due to the increase of the losses caused by the conductive surface. The total magnetic flux coupled into the receiver coil is determined by adding the intended primary magnetic flux generated by the NFC transmitter antenna (blue lines) and the secondary stray secondary magnetic field (red lines) that traverses the metal element generating eddy currents. As the diagram shows, the secondary field is opposite to the primary, resulting in an efficiency reduction of the communication distance. The undesired secondary field is produced by the eddy currents induced by the primary field within the conductive surface. Eddy currents are loops of electrical current induced within conductors by a changing magnetic field in the conductor according to the Faraday's law. Besides causing power losses in the communication, eddy currents flowing through the resistance of the conductive surface are dissipated as heat, which could result in the warming of the device.

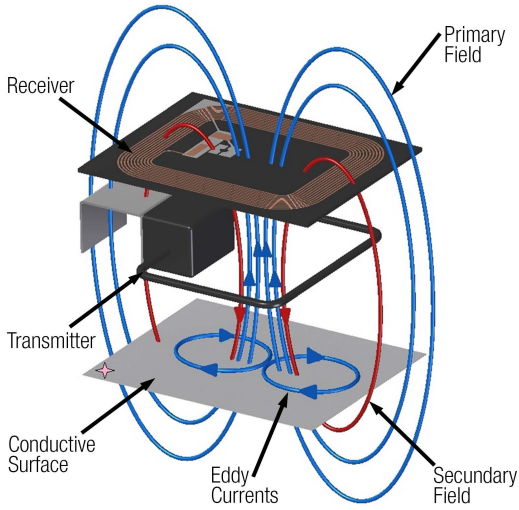


Fig. 1. Diagram of the stray effects caused by placing a conductive surface close to the NFC communication area without shielding.

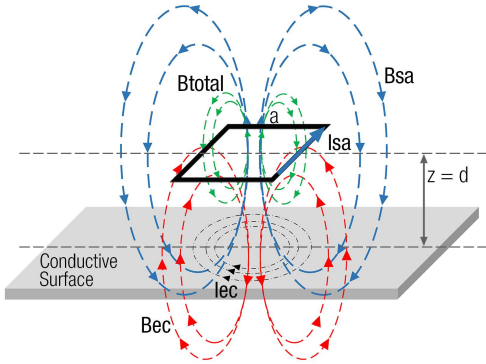


Fig. 2. Approximation model for a coil antenna affected by a conductive surface based on Biot Savart's law.

The stray H produced by the conductive surface is characterized in [8] and [25] as a virtual antenna to describe a mathematical model, assuming that it has the same characteristics as the original antenna through which flows an equal current with opposite value. This model is based on Biot Savart's law, considering two magnetic flux densities B as shown in Fig. 2: the magnetic flux density B_{sa} (blue field lines) due to the loop antenna and the magnetic flux density B_{ec} (red field lines) produced by eddy currents induced in the conductive surface. These components can be estimated by considering the transmitter device as a square antenna of side a , located at the point z (located in the orthogonal direction by taking as a reference the center of the square loop), carrying a current I_{sa} that induces an

eddy current I_{ec} in the conductive surface located at a distance d parallel to the antenna. This induced current I_{ec} generates a magnetic flux leakage that degrades extremely the total magnetic field by the NFC transmitter when the distance d is minimum.

Hence, the total magnitude of magnetic flux density B_{total} (green field lines) is defined as the sum of both components and can be represented as [27]

$$B_{total} = B_{sa} + B_{ec} \quad (1)$$

where

$$B_{sa} = \frac{\mu I_{sa}}{2\pi R^2} \frac{a^2}{\sqrt{z^2 + a^2/2}} \quad (2)$$

$$B_{ec} = -\frac{\mu I_{ec}}{2\pi \left(\sqrt{(z-d)^2 + a^2/2} \right)^2} \frac{a^2}{\sqrt{(z-d)^2 + a^2/2}}. \quad (3)$$

It can be known from (3) that the stray magnetic field decreases with the distance; consequently, the worst case occurs when the transmitter antenna and the conductive surface are joined and d is negligible.

The deterioration of the total magnetic field H turns into a reduction of the magnetic flux Φ generated by the NFC transmitter. From the point of view of the inductance of the antenna L_a , it can be deduced that it is reduced due to the presence of the conductive plane since it is proportional to the magnetic flux Φ and therefore to the magnetic field H . Hence, it can be known from (4) that the inductance L_a is directly connected to the magnetic field H , the number of loops N , permeability of the medium μ , the area of the antenna A , and inverse to the current I

$$L_a = \frac{H\mu NA}{I}. \quad (4)$$

Subsequently to the decrease of the inductance, the communication frequency is detuned because the antenna and the matching circuit are unbalanced. As a result, the resonant frequency f_r that corresponds to the operating frequency of the NFC system is shifted. Depending on the tolerance of the NFC system, this modification in the NFC transmitter frequency could reduce the effectiveness of the communication. Therefore, the center frequency shifting could lead to the loss of information or even prevent the communication between NFC devices by the mismatch of the emitter and receiver antennas as [10] reports in terms of the success of reading depending on the percentage of center frequency shift. The resonant frequency f_r can be calculated by using Thomson's equation (5), considering the capacitor C connected in parallel with the inductance of the antenna L_a

$$f_r = \frac{1}{2\pi\sqrt{L_a C}}. \quad (5)$$

B. Flexible Sintered Ferrite Sheet Characterization

FSFS is composed of precracked thin ferrite plates placed between a layer of adhesive tape and a PET cover layer. This layer configuration is meant to provide protection, high surface resistivity, and isolation from top to bottom sides. Moreover,

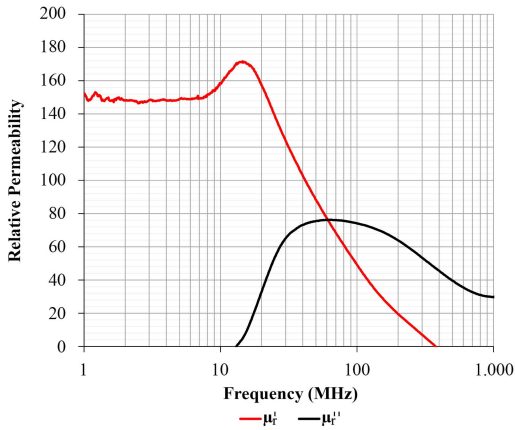


Fig. 3. Relative Permeability of flexible sintered ferrite sheet analyzed.

this shielding solution has to provide high permeability and low losses at the NFC communication frequency. Ni-Zn ferrite compositions provide these last features that combined with dopants such as Co_2O_3 and Bi_2O_3 can help to reduce the sintering temperature and, consequently, improving their magnetic properties [28]. The FSFS preparation is carried out via a solid-state reaction synthesis that is based on a conventional ceramic technique [29]. The raw materials Fe_2O_3 , NiO , CuO , and ZnO are wet mixed in deionized water by a ball mill. Once the powder is dried, it is calcined and, subsequently, the oxide mixtures can be doped with Co_2O_3 and Bi_2O_3 by ball milling. After drying again, the mixtures are granulated by using a binder and pressed to form thin flakes that, finally, are sintered in air at 1000°C [30].

The ferrite plates that form a ferrite sheet define its magnetic properties and the frequency at which it provides great effectiveness. The material used in this research is based on a Ni-Cu-Zn composition that provides an initial permeability $\mu_i = 150$. Although this is an interesting parameter for evaluating if the material is useful for NFC applications, the relative permeability μ_r is the parameter that provides more information about the magnetic properties of a certain material at a certain frequency point. This is defined through the permeability complex parameter, separating it into its complex form components. The real component μ'_r represents the inductance ability of the material to concentrate and redirect the magnetic flux; otherwise, the imaginary component μ''_r quantifies the losses or effectiveness to absorb the magnetic noise [31]. In the low-frequency region, a magnetic sheet usually provides low losses and a significant steady value of inductive component that starts to decay from some megahertz depending on its internal composition and manufacturing process [32]. Concretely, the FSFS analyzed in this work provides a high value of the inductive component (≈ 170) and a low value of the losses component (≈ 2.5) at the NFC communication frequency (13.56 MHz). Fig. 3 represents the relative permeability profiles of the FSFS composition analyzed

split into real and imaginary components. The results were obtained with the Keysight E4991A Material Analyzer, together with the 16454A Magnetic Material Test Fixture. This fixture is based on cavity resonance and single-turn inductor theories and allows for measuring the magnetic properties of a material. The sample under test must have a toroidal shape in order to be able to fit inside the fixture so that a toroidal core is manufactured with the material of each absorber composition. This toroidal sample has an outer diameter of 20 mm, 8 mm of inner diameter, and the thickness is 1 mm. When the sample is placed inside the fixture, an ideal single-turn inductor with no flux leakage is formed. Therefore, the internal software of the equipment calculates automatically the permeability from the inductance value of the sample [32]. Thereby, it is possible to obtain direct complex permeability readouts, considering that the 16454A has a tolerance of 10% according to the accuracy of the test fixture to characterize a sample with the described dimensions. As can be observed, the material reaches μ'_r the maximum value at 13.56 MHz while maintaining a low μ''_r , avoiding causing losses to the communication signal. Note that μ''_r is negligible in the low-frequency region whereas it is increased from the communication frequency, providing shielding against high-frequency EMI. Consequently, this ferrite sheet is able to redirect and concentrate the magnetic flux, improving the performance of the NFC system. The μ'_r of the sample decreased from approximately 15 through 400 MHz. The reactive component, μ''_r , starts to increase from zero, reaching the maximum point with a value of 76 at 75.4 MHz.

Besides providing a permeability behavior that improves the performance of the transmission, it is important to ensure that the FSFS provides a high surface resistance value ($R_S = 1\ \Omega$) since the power loss caused by eddy currents is significant in those materials with very low resistivity. A metal casing or a lithium battery represents one of these materials; thus, the ferrite sheet placed between the conductive element and the NFC antenna has to ensure to isolate this by means of reducing its conductivity. Fig. 4 shows the diagram of an NFC system with a conductive surface close to the transmitter antenna. Contrary to the situation shown in Fig. 1, in this case, the FSFS shields the communication area avoiding that eddy currents induced in the conductive surface could produce an opposite magnetic flux.

III. CHARACTERIZATION SETUP

A. NFC Antenna Design

An NFC antenna model has been designed to carry out the characterization of different FSFS thicknesses. This design has been implemented in a PCB with two layers that hold the six-turn loop antenna and the matching circuit associated components. The PCB loop antenna has been manufactured with TG135 FR4 substrate material, selecting 1.55 mm of substrate thickness and 35 micrometers of copper thickness. The traces of the loop are 0.8 mm in width and the spacing between them is 0.6 mm. Fig. 5 represents the dimensions of the proposed NFC antenna.

An aluminum sheet employed as the conductive surface to be placed under the NFC antenna is $75 \times 65\ \text{mm}$ and it has a thickness of 1.6 mm. It is noteworthy that this metal sheet

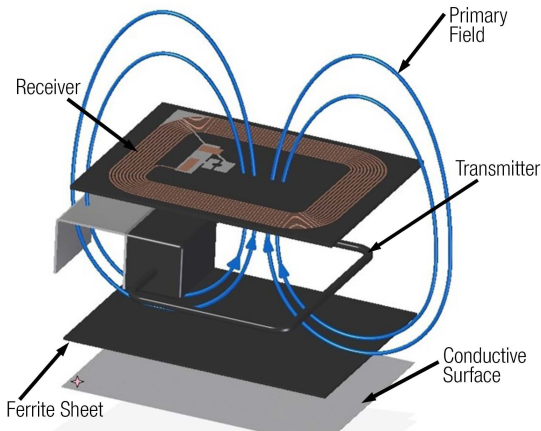


Fig. 4. Diagram of magnetic field produced when a conductive surface is close to the NFC communication area with shielding.

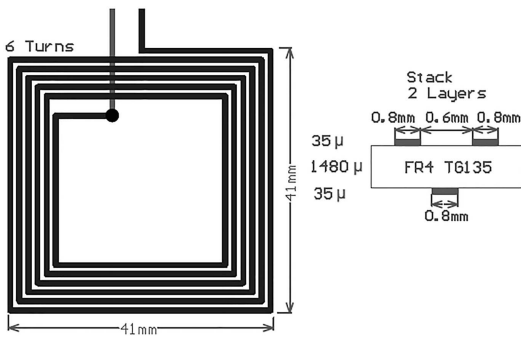


Fig. 5. Structure and dimensions of the proposed NFC antenna.

emulates a metal casing, a metal shielding, or a battery that can be located close to the NFC antenna. According to the PCB and the metal sheet, the flexible sintered ferrite sheets evaluated are 60×60 mm and they have a thickness from 0.14 to 0.50 mm in order to cover the loop antenna and its surroundings. Thereby, the FSFS is placed on top of the metal sheet and under the NFC antenna, shielding the communication area.

B. Simulation Model

The shielding performance of different FSFS thickness and the relation between the efficiency of NFC communication and the magnetic field strength is specifically examined through an electromagnetic analysis simulator (ANSYS HFSS). The proposed simulation model is shown in Fig. 6. It is formed by the loop antenna and the aluminum sheet described in Section III-A. The FSFS described in Section II-B is introduced between them with the aim of evaluating its effectiveness to prevent the degradation effects caused by the presence of the metal sheet.

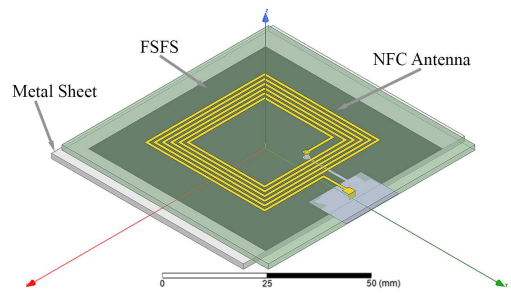


Fig. 6. NFC antenna simulation model.

The metal sheet has been placed at a fixed distance of 0.5 mm from the PCB model in order to ensure that the influence of the distance variation was negligible. Note that the impedance matching circuit has not been modified and the same values have been used. This simulation model makes it possible to evaluate the antenna in a free environment, with the influence of the metal sheet and when it is shielded with the FSFS.

This simulation model makes it possible to determine the resonant frequency of the NFC antenna evaluating different cases: free space (ideal case), introducing the aluminum sheet under the antenna at 0.5 mm and placing the FSFS shielding under the antenna protecting the communication area. This parameter will be analyzed through the S_{11} parameter. The magnetic field strength H produced by the antenna influenced by the aluminum sheet and the different FSFS is also studied to analyze how it is distributed. Derived from these simulation results it is possible to determine the maximum distance at which an NFC tag can be detected in the different cases and knowing which FSFS thickness provides the best performance to ensure retuning the NFC antenna at the communication frequency. The minimum magnetic field strength H_{\min} necessary to activate a passive NFC tag considered in this research is 1.5 A/m as is described in the ISO/IEC 14443 standard.

C. Experimental Measurement Setups

The experimental measurements are focused on determining the return loss (S_{11} parameter) and the distribution of the magnetic field strength H through a very-near field scanner. The S_{11} parameter is measured taking into account the same dimensions and distribution of the simulation model to verify the accuracy between both results. These measurements have been carried out considering these scenarios.

- 1) NFC antenna in the free space (reference scenario).
- 2) NFC antenna with an aluminum sheet placed under it at a distance of 0.5 mm (unshielded test scenario).
- 3) Placing the FSFS between the NFC antenna and the aluminum sheet (shielded test scenario).

The FSFS thicknesses that have been evaluated are 0.14, 0.3, 0.4, and 0.5 mm. These measurements will make it possible to conclude if the simulation results correlate with the experimental ones. The distribution of the magnetic field is measured with

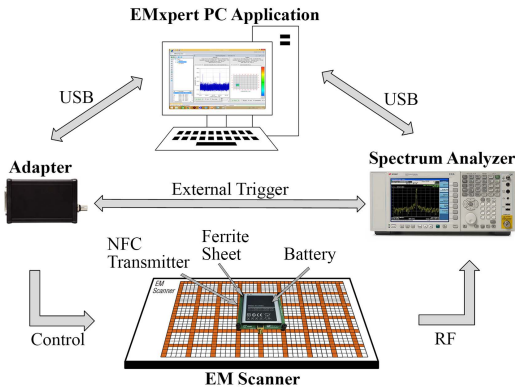


Fig. 7. NFC antenna simulation model.

an EM scanner. This system is a passive device that couples the very-near-field emissions received from a device under test (DUT). Subsequently, the scanner would represent the receiver antenna in the NFC communication. The measurements of these coupled fields are carried out with a spectrum analyzer that is synchronized with the scanner. The software used (EMxpert) compensates the insertion loss of each probe of the matrix that composes the scanner throughout the frequency range analyzed in order to display an accurate H -field value. Each cell of the EM scanner corresponds to an individual near field probe (NFP) and it is spaced 7.5 mm in array distribution, providing an effective resolution of 3.75 mm [33]. The measurements obtained from the EM scanner are represented through the frequency spectrum and the spatial magnetic radiation diagram. The measurements of these coupled fields are carried out with a spectrum analyzer that is synchronized with the scanner as is shown in Fig. 7.

The characterization is performed by placing the NFC antenna on the selected area of the EM scanner in order to measure the signal emitted in the scenarios 1 and 2. A third measure will be taken with the FSFS inserted between the metallic sheet and the NFC antenna to evaluate the performance of this shielding solution (scenario 3). The last measurement corresponds to the placement of a Li-ion battery instead of the aluminum sheet in order to evaluate other specific usual problem [34]. Fig. 8 shows the orientation of the NFC antenna, the position of the FSFS placed under it and how the conductive element is set.

IV. RESULTS AND DISCUSSION

The first part of this section is focused on verifying the simulation model by comparing its results with the experimental measurements. Thereby, the S_{11} parameter obtained from the simulation model is compared to the experimental return loss provided by the network analyzer equipment. Fig. 9 shows the experimental measurements (solid traces) and simulation data (dashed traces) of the S_{11} parameter by considering the NFC antenna without disturbances (red traces), the NFC antenna with the aluminum sheet placed under it (black traces), and adding a

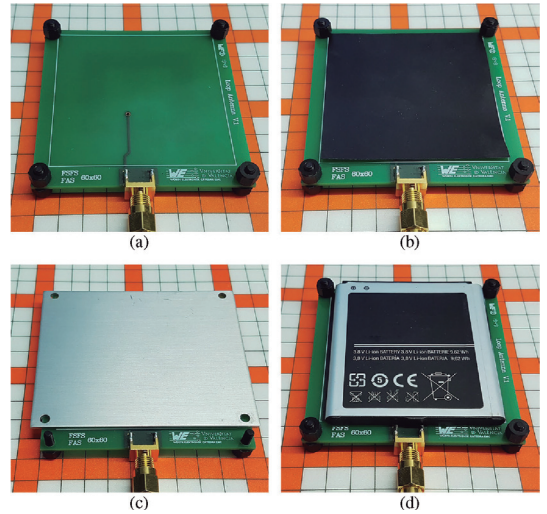


Fig. 8. Measurement setup to evaluate the performance of the FSFS in NFC systems. (a) NFC antenna (scenario 1). (b) NFC antenna placing the FSFS before placing the conductive element (scenario 3). (c) NFC antenna with the aluminum sheet placed under it (scenario 2). (d) NFC antenna with a battery placed under it (scenario 2).

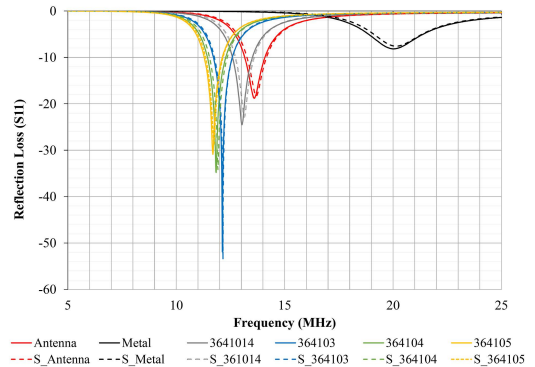


Fig. 9. Variation of the return loss (S_{11} parameter) depending on the FSFS thickness. Comparison between the simulated and experimental results.

FSFS with different thicknesses between the NFC antenna and the metal (grey traces correspond to 0.14 mm, blue traces to 0.3 mm, green traces to 0.4 mm, and yellow traces to 0.5 mm). From the results obtained, it is possible to verify that the simulated and measured results are a good match and, consequently, the data derived from the simulation model can be considered. Regarding the reflection loss determined, the resonant frequency of the antenna is shifted from 13.6 to 20.2 MHz (a relative error of 48.8%) when the aluminum sheet is under the NFC antenna. This error is decreased when the FSFS is introduced between them, being 3.6%, 11.0%, 12.7%, and 14.0% for the FSFS thickness of 0.14, 0.3, 0.4, and 0.5 mm, respectively. This results in a

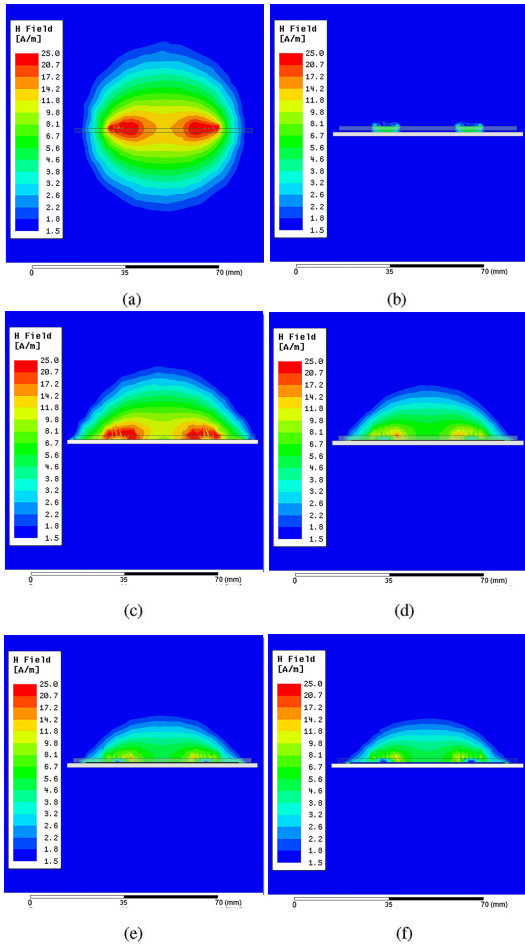


Fig. 10. Variation of the magnetic field strength H generated by the NFC antenna, considering different situations. (a) Antenna in the free space. (b) Antenna with metal. (c) Antenna with 0.14 mm FSFS and metal. (d) Antenna with 0.3 mm FSFS and metal. (e) Antenna with 0.4 mm FSFS and metal. (f) Antenna with 0.5 mm FSFS and metal.

reduction of the f_r as the FSFS thickness increases since the thickest samples introduce more inductance than needed in the NFC antenna and shift the f_r value to lower values than the desired (lower to 13.56 MHz).

The simulation model makes it possible to analyze the performance of the different FSFS thicknesses in terms of the magnetic field distribution. Fig. 10 represents the magnetic field strength generated by the NFC antenna, considering the same cases studied before. The minimum value has been set to 1.5 A/m since this is the minimum field to power an NFC passive tag defined by the standard. Thereby, the dark blue color represents the area where it is not possible to communicate with an NFC passive tag. When the antenna is considered in the free space, the magnetic

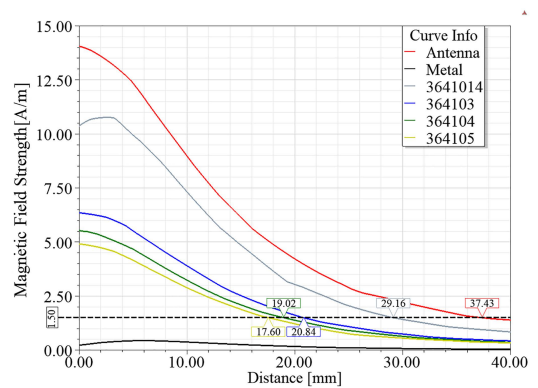


Fig. 11. Magnetic field strength H as a function of the distance in the z -axis direction, considering different situations: antenna in the free space, antenna with metal, and antenna shielded with metal.

field is distributed similarly both over and under the NFC antenna (see Fig. 10(a)), whereas when the aluminum sheet is introduced, the magnetic field is significantly attenuated in both sides (see Fig. 10(b)). When the FSFS with the lower thickness (0.14 mm) is set under the antenna, it is possible to observe how a significant part of the field is recovered in the upper area (see Fig. 10(c)). This situation is also shown in the other cases where the FSFS of higher thickness is placed; however, the thicker the FSFS thickness, the lower the magnetic field provided by the antenna (see Fig. 10(c)–(f)).

As has been explained above, the attenuation of the magnetic field generated by the NFC antenna results in a shorter communication area. This fact is shown in Fig. 11 where the magnetic field strength is represented as a function of the distance in the orthogonal direction (z -axis direction). Thereby, it is possible to determine which is the maximum distance for each case study, taking as a reference 1.5 A/m. The NFC antenna in the free space provides the largest distance, whereas the worst case is represented when the metal sheet is placed without shielding the antenna. By comparing the responses of the NFC antenna with the FSFS shielding it, it is verified that the thinner sheet yields the best performance because the 0.14 mm FSFS sample can recover better the f_r to its original value (reference scenario) than the thicker ones. The FSFS with the lower thickness (0.14 mm) allows detecting an NFC tag up to 29.16 mm; this is 8.27 mm shorter than the antenna in the free space but 8.32, 10.14, and 11.56 mm larger than the 0.3, 0.4, and 0.5 mm ferrite sheets samples, respectively.

The simulation model designed makes it possible to evaluate thinner FSFS thicknesses to obtain an optimized solution to retune with higher accuracy the shift of the resonant frequency and, consequently, the attenuation of the magnetic field and the communication distance. Several FSFS with thicknesses from 0.05 to 0.08 mm have been computed to evaluate the sheet thickness with greater performance to tune the NFC antenna to 13.56 MHz. Fig. 12 shows that these thinner sheets tune

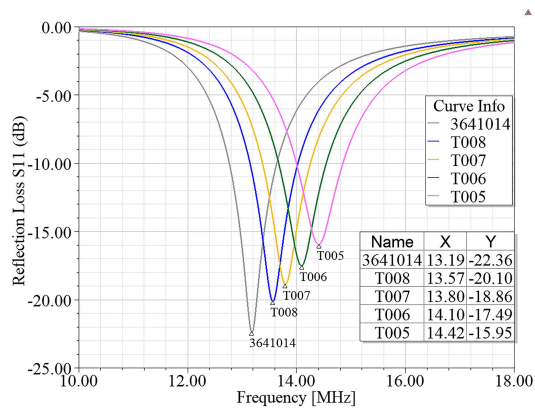


Fig. 12. Variation of the return loss (S_{11} parameter) depending on the FSFS thickness. Simulation of optimized FSFS thickness.

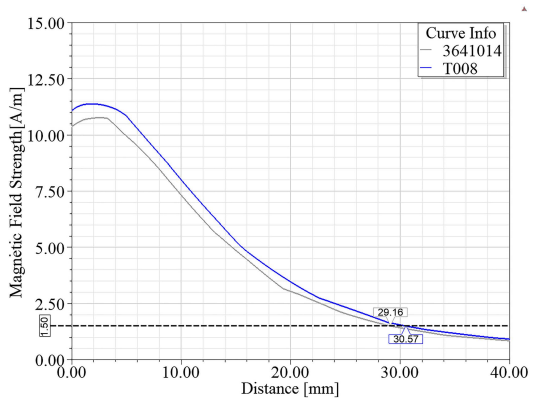


Fig. 14. Magnetic field strength H as the distance in the z -axis direction is increased, comparing the best real FSFS thickness to the most optimized FSFS thickness computed.

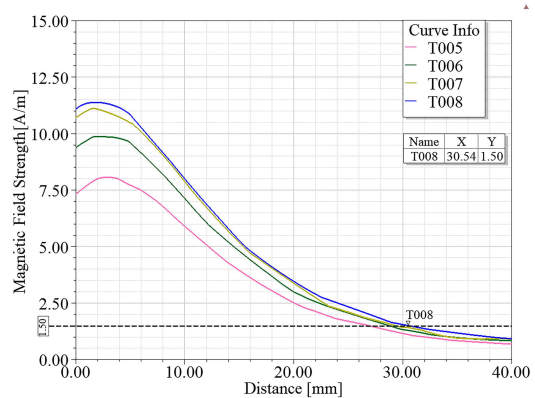


Fig. 13. Variation of the return loss (S_{11} parameter) depending on the FSFS thickness. Simulation of optimized FSFS thickness.

better the antenna than the 0.14 mm sheet. The optimum FSFS thickness corresponds to T008 (0.08 mm) since it is able to set the resonant frequency at 13.57 MHz. Another fact to highlight is the response of the T005 and T006 FSFS since their traces show that if the FSFS does not contain a minimum amount of shielding, it is not possible to solve completely the problems caused by this specific metal sheet.

Fig. 13 shows the comparison of the computed FSFS thicknesses in terms of the magnetic field as a function of the distance (z -axis direction). According to the reflection loss parameter, the T008 FSFS provides the maximum communication distance (30.54 mm).

The T008 optimum FSFS thickness is compared to the real FSFS 3641014 sheet in Fig. 14 in order to evaluate, in terms of distance, which is the deviation between the real solution and the optimum FSFS thickness obtained by simulation. The computed improves to the real solution in 1.41 mm; therefore in

those applications that do not need a high-resolution distance, this difference could be considered negligible.

As has been explained above, the study is focused on analyzing the effects of an aluminum sheet under the NFC antenna. However, the negative effects that this situation generates in the performance of the communication are very similar when a Li-ion battery is placed under it. This degradation effect has been analyzed with an EM scanner. Therefore, it is possible to measure and analyze the power transmitted by the NFC antenna before and after placing the battery close to it. Once the attenuation caused by the battery is determined, the 0.14 mm FSFS is placed under the antenna to evaluate its ability to manage the magnetic flux and preserving the originally transmitted signal without reducing the communication performance. Fig. 15 shows the four spatial magnetic radiation diagrams obtained after studying the three described scenarios. Note that the results shown correspond to the signal acquired by the near field probe matrix of the EM scanner that has been computed by the Spectrum Analyzer. Thus, the measurements are represented in terms of relative values (dBuV) of H -field emitted by the NFC antenna. The signal emitted by the NFC antenna (reference scenario) and its distribution is shown in Fig. 15(a), whose maximum power measured is 112.0 dBuV. When the aluminum sheet is set under the NFC antenna (see Fig. 15(c)), the signal emitted is reduced to 98.1 dBuV, attenuating the signal 13.9 dB. If the battery is placed under the NFC antenna (see Fig. 15(d)), the results obtained show that the emitted signal is highly degraded, providing similar results than the aluminum sheet. In these two cases (unshielded scenario), the predominance of dark blue and light green in the spatial diagram shows the reduction of communication effectiveness. Thereby, this scenario results in degradation or even a loss of the communication, since the power transmitted from the NFC transmitter to the receiver device may not be enough to carry out its activation. The result of placing the FSFS between the NFC antenna and the battery is shown in Fig. 15(b). This diagram (shielded scenario) shows that the

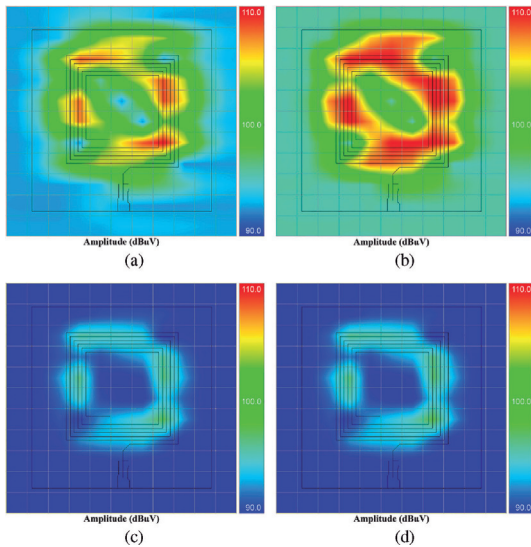


Fig. 15. Spatial radiated emissions diagram measured with the EM scanner. (a) NFC antenna (scenario 1). (b) NFC antenna placing the FSFS between the battery and itself (scenario 3). (c) NFC antenna with the aluminum sheet placed under it (scenario 2). (d) NFC antenna with a battery placed under it (scenario 2).

power measured has been increased up to 115.5 dBuV when the FSFS is introduced to shield the NFC antenna from the battery. The introduction of the FSFS results in amplifying 3.5 dB the emitted signal if it is compared to the signal reference without shielding. In this case, the distribution of the spatial radiation diagram shows how the power distributed in the NFC antenna area is redder than the reference measurement. If the value obtained from the shielded scenario is also compared to the unshielded scenario (Fig. 15(d)), it is possible to observe that the signal has amplified by 17.4 dB and, thus, the value of the reference scenario has been recovered.

V. CONCLUSION

The performance of different high permeability FSFS thicknesses has been evaluated to reduce EMI problems caused by near conductive surfaces that lead to shifting the NFC communication frequency. Besides selecting a material with the proper relative permeability at 13.56 MHz, it is necessary to consider the FSFS thickness to optimize the communication effectiveness.

The results obtained from reflection loss allow verifying that the simulated and experimental results are a good match and, consequently, the data derived from the simulation model can be considered as an accurate approach. Both sources of information show that the presence of the aluminum sheet shifts significantly the resonant frequency to higher frequencies. When the different FSFS are introduced between the metal and the NFC antenna, the resonant frequency is reduced. Nevertheless, large FSFS thicknesses (from 0.3 to 0.5 mm) provide a higher

inductance than the NFC antenna in the free space, avoiding the reestablishment of the communication frequency to the original value. The thinner FSFS (0.14 mm thickness) provides the best performance compared to larger FSFS thicknesses since it is able to retune the communication frequency reducing the relative error caused by the metal sheet from 48.8% to 3.6%.

This conclusion is also verified from the point of view of the magnetic field strength and distance range. When the 0.14 mm FSFS is set under the antenna, a significant part of the field is recovered in the upper area. This situation is also shown in the cases where the FSFS has a higher thickness; however the thicker the FSFS thickness, the lower the magnetic field provided by the antenna. Therefore, the largest communication distance is obtained with the thinner material (0.14 mm), providing a range of at least 30% greater than thicker sheets. The simulation model makes it possible to determine that the optimum FSFS thickness value that allows retuning the antenna to 13.56 MHz corresponds to 0.08 mm.

The experimental measurement setup implemented with the EM scanner allows emulating a real NFC communication system. The signal measured in the EM scanner that represents the NFC tag shows that the 0.14 mm FSFS thickness can shield the NFC antenna when a conductive surface (the aluminum sheet or the battery) is set under it.

Consequently, the right selection of the FSFS thickness is essential to prevent EMI problems related to NFC. The presence of a conductive surface can detune the communication, likewise, the use of a wrong FSFS thickness could lead to shifting the resonant frequency to lower values than expected.

ACKNOWLEDGMENT

The research has been carried out through the funds of the University of Valencia and it is not part of the financing of any national or international project. This manuscript follows the research line of the in-progress PhD of the first author Jorge Victoria and it is supported as well as researchers from the University of Valencia and EMC experts of Würth Elektronik eiSos.

REFERENCES

- [1] E. F. Vance and W. Graf, "The role of shielding in interference control," *IEEE Trans. Electromagn. Compat.*, vol. 30, no. 3, pp. 294–297, Aug. 1988.
- [2] S. Cruciani, T. Campi, F. Maradei, and M. Feliziani, "Active shielding design for wireless power transfer systems," *IEEE Trans. Electromagn. Compat.*, vol. 61, no. 6, pp. 1–8, Oct. 2019.
- [3] S. Piersanti *et al.*, "Near-field shielding performances of EMI noise suppression absorbers" *IEEE Trans. Electromagn. Compat.*, vol. 59, no. 2, pp. 654–661, Apr. 2017.
- [4] M. H. Nisanci, F. de Paulis, D. Di Febo, and A. Orlandi, "Synthesis of composite materials with conductive aligned cylindrical inclusions," in *Proc. Progr. Electromagn. Res. Symp.*, Kuala Lumpur, Malaysia, 2012, pp. 27–30.
- [5] D. Paret, *Antenna Designs for NFC Devices*, 1st ed., Hoboken, NJ, USA: John Wiley & Sons, 2016.
- [6] K. Finkenzeller, *RFID Handbook: Fundamentals and Applications in Contactless Smart Cards and Identification*, 3rd ed., Hoboken, NJ, USA: Wiley, 2010.
- [7] X. Qing and Z. N. Chen, "Proximity effects of metallic environments on high frequency RFID reader antenna: Study and applications," *IEEE Trans. Antennas Propag.*, vol. 55, no. 11, pp. 3105–3111, Nov. 2007.

- [8] A. I. Petriariu *et al.*, "Design of an high frequency RFID multi-loop antenna for applications in metallic environments," *Adv. Electr. Comput. Eng.*, vol. 18, no. 2, pp. 35–41, 2018.
- [9] B. Lee, B. Kim, and S. Yang, "Enhanced loop structure of NFC antenna for mobile handset applications," *Int. J. Antennas Propag.*, vol. 2014, pp. 1–6, Apr. 2014.
- [10] A. I. Petriariu *et al.*, "Influence of different types of metal plates on a high frequency RFID loop antenna: Study and design," *Adv. Electr. Comput. Eng.*, vol. 9, no. 2, 2009, pp. 3–8, Dec. 2019.
- [11] M. Periyasamy and R. Dhanasekaran, "Assessment and analysis of performance of 13.56 MHz passive RFID in metal and liquid environment," in *Proc. Int. Conf. Commun. Signal Process.*, Melmaruvathur, India, 2014, pp. 1122–1125.
- [12] J. Zhu, Y. Ban, C. Sim, and G. Wu, "NFC antenna with nonuniform meandering line and partial coverage ferrite sheet for metal cover smartphone applications," *IEEE Trans. Antennas Propag.*, vol. 65, no. 6, pp. 2827–2835, Jun. 2017.
- [13] J. Zhu, Y. Ban, R. Xu, C. Sim, J. Guo, and Z. Yu, "Miniaturized dual-loop NFC antenna with a very small slot clearance for metal-cover smartphone applications," *IEEE Trans. Antennas Propag.*, vol. 66, no. 3, pp. 1553–1558, Mar. 2018.
- [14] T. Brander, A. Gerfer, B. Rall, and H. Zenkner, *Trilogy of Magnetics: Design Guide for EMI Filter Design SMPs & RF Circuits*, 5th ed., Waldenburg, Germany: Würth Elektronik, 2018.
- [15] B. Lee, B. Kim, F. J. Harackiewicz, B. Mun, and H. Lee, "NFC antenna design for low-permeability ferromagnetic material," *IEEE Antennas Wireless Propag. Lett.*, vol. 13, no. 1, pp. 59–62, Jan. 2014.
- [16] V. Coskun, K. Ok, and B. Ozdenizci, *Near Field Communication (NFC): From Theory to Practice*, 1st ed. Hoboken, NJ, USA: John Wiley & Sons, 2012.
- [17] M. Gebhart, R. Neubauer, M. Stark, and D. Warnez, "Design of 13.56 MHz smartcard stickers with ferrite for payment and authentication," in *Proc. 3rd Int. Workshop Near Field Commun.*, Hagenberg, Austria, 2011, pp. 59–64.
- [18] S. S. Lau, "Practical design of 13.56 MHz near field communication (NFC) and radio frequency identification (RFID) antenna using ferrite sheet on metallic surface by network analyzer," in *Proc. IEEE Int. Conf. Ind. Eng. Eng. Manage.*, Singapore, 2015, pp. 1362–1366.
- [19] S. Wielandt, D. Mercy, N. Stevens, L. De Strycker, and J. Goemaere, "Evaluation of shielding materials for low frequency RFID systems," in *Proc. Int. Symp. Electromagn. Compat.*, Rome, Italy, 2012, pp. 1–5.
- [20] P. Lathiya and J. Wang, "Effects of the sintering temperature on RF complex permeability of NiCuCoZn ferrites for near-field communication applications," *IEEE Trans. Magn.*, vol. 55, no. 2, pp. 1–4, Feb. 2019.
- [21] C. Stergiou, E. Eleftheriou, and V. Zaspalis, "Enhancement of the near-field UHF RFID with ferrite substrates," *IEEE Trans. Magn.*, vol. 48, no. 4, pp. 1497–1500, Apr. 2012.
- [22] M. Y. Koledintseva, J. L. Drewniak, R. E. DuBroff, K. N. Rozanov, and B. Archambeault, "Modeling of shielding composite materials and structures for microwave frequencies," *Progr. Electromagn. Res. B*, vol. 15, pp. 197–215, 2009.
- [23] M. H. Nisanci, F. de Paulis, D. Di Febo, and A. Orlandi, "Sensitivity analysis of electromagnetic transmission, reflection and absorption coefficients for biphasic composite structures," in *Proc. Int. Symp. Electromagn. Compat.*, Gothenburg, Sweden, 2014, pp. 438–443.
- [24] W. Pachler *et al.*, "A silver inkjet printed ferrite NFC antenna," in *Proc. Loughborough Antennas Propag. Conf.*, Loughborough, UK, 2014, pp. 95–99.
- [25] I. Lee, N. Kim, I. Cho and I. Hong, "Design of a patterned soft magnetic structure to reduce magnetic flux leakage of magnetic induction wireless power transfer systems," *IEEE Trans. Electromagn. Compat.*, vol. 59, no. 6, pp. 1856–1863, Dec. 2017.
- [26] Y. Yashima, H. Omori, T. Morizane, N. Kimura, and M. Nakaoka, "Leakage magnetic field reduction from wireless power transfer system embedding new eddy current-based shielding method," in *Proc. Int. Conf. Electr. Drives Power Electron.*, Tatranska Lomnica, Slovak Republic, 2015, pp. 241–245.
- [27] S. D. Young, and R. A. Freedman, *University Physics with Modern Physics*. San Francisco, CA, USA: Pearson, 2004.
- [28] P. Lathiya and J. Wang, "Effects of the sintering temperature on RF complex permeability of NiCuCoZn ferrites for near-field communication applications," *IEEE Trans. Magn.*, vol. 55, no. 2, pp. 1–4, Feb. 2019.
- [29] X. Wu, S. Yan, W. Liu, Z. Feng, Y. Chen, and V. G. Harris, "Influence of particle size on the magnetic spectrum of NiCuZn ferrites for electromagnetic shielding applications," *J. Magn. Magn. Mater.*, vol. 401, pp. 1093–1096, Mar. 2016.
- [30] Y. Yang, H. Zhang and J. Li, "Effects of sintering temperature on microstructure and magnetic properties of NiCuZn ferrites for NFC application," in *Proc. 19th Int. Conf. Electron. Packag. Technol.*, Shanghai, China, 2018, pp. 928–932.
- [31] A. Suarez *et al.*, "Effectiveness assessment of a nanocrystalline sleeve ferrite core compared with ceramic cores for reducing conducted EMI," *Electronics*, vol. 8, no. 7, pp. 1–21, Jul. 2019.
- [32] J. Victoria *et al.*, "Transmission attenuation power ratio analysis of flexible electromagnetic absorber sheets combined with a metal layer," *Materials*, vol. 11, no. 9, pp. 1–14, Sep. 2018.
- [33] Z. Ji, Y. Tengfei and Z. Xiaohui, "Analyse and research of radiated emission on PCBs," in *Proc. Int. Conf. Electron., Commun. Control*, Ningbo, China, 2011, pp. 727–730.
- [34] J. Victoria *et al.*, "Study of a novel high permeability ferrite sheet intended for near field communication systems," in *Proc. IEEE Int. Symp. Electromagn. Compat., Signal Power Integrity*, New Orleans, LA, USA, 2019, pp. 78–83.



Jorge Victoria (Member, IEEE) received the Laurea degree in electrical engineering, in 2005 from the University of Valencia, Valencia, Spain, where he is currently working toward the Industrial Ph.D. degree. From 2006 to 2012, he worked as EMC and Project Manager for Electromedical Devices with the research institute in Biomechanics of Valencia (IBV). Since 2013, he has been a Division Manager for EMC Shielding Materials at Würth Elektronik eiSos. Since 2014, he has been a Co-Director of the EMC Catedra University of Valencia-Würth Elektronik eiSos. His research interests include the advanced characterization of shielding materials to manage EMI interferences, specifically those based on magnetic sheets, such as sintered ferrite sheets or noise suppression absorbers.



Adrian Suarez (Member, IEEE) was born in Valencia, Spain, in 1990. He received the B.S. and M.S. degrees in electronics engineering in 2013 from the University of Valencia, Valencia, Spain, where he is currently working toward the Ph.D. degree. From 2013 to 2015.

He was a Research Assistant with the Design of Communication and Digital Systems Research Group, University of Valencia. Since 2015, he has been a Research Assistant with EMC Catedra University of Valencia-Würth Elektronik eiSos, Electronics Engineering Department, University of Valencia. Since 2017, he has been an Adjunct Professor with the Electronics Engineering Department, University of Valencia. He collaborated in the IEEE EMC Society through the Technical Committee 4 for EMI control. His research interests include the advanced characterization of shielding materials and the study of cable filtering materials based on conventional ceramics and nanocrystalline compositions.



Pedro A. Martinez (Member, IEEE) was born in Valencia, Spain, in 1978. He received the B.S. and M.S. degrees in electronics engineering, in 2012 from the University of Valencia, Valencia, Spain, where he is currently working toward the Ph.D. degree.

From 2012 to 2016, he was a Research Assistant with the Design of Communication and Digital Systems Research Group, University of Valencia. Since 2016, he has been a Research Assistant with EMC Catedra University of Valencia-Würth Elektronik eiSos, Electronics Engineering Department, University of Valencia. Since 2018, he has been an Adjunct Professor with the Electronics Engineering Department, University of Valencia. He collaborated with the IEEE EMC Society through the Technical Committee 4 for EMI control. His research interests include the advanced characterization of shielding materials and the study of cable filtering materials based on conventional ceramics and nanocrystalline compositions.



Antonio Alcarria (Member, IEEE) was born in Cuenca, Spain, in 1992. He received the B.S. and M.S. degrees in electronics and telecommunications engineering from the University of Valencia, Valencia, Spain, in 2017.

Since 2015, he has been specialized in the Research, Design and Development on the field of the Electromagnetic Compatibility working with EMC Catedra University of Valencia-Würth Elektronik eiSos, a collaboration researching between Würth Elektronik and the University of Valencia. In November 2017, he also joined the main headquarter of Würth Elektronik in Waldenburg as EMC Product Manager combining his main job in the company with the research in the EMC Catedra University of Valencia-Würth Elektronik eiSos. His research interests include the advanced characterization of shielding materials to manage EMI interferences, specifically those based on magnetic sheets such as sintered ferrite sheets or noise suppression absorbers.



Alexander Gerfer was born in 1965. He received the Dipl.-Ing. degree in electrical engineering from the Technical University of Cologne, Cologne, Germany.

He worked in the field of research and development for precision measuring instruments following his training as a Radio and Television Technician. He published numerous application circuits and construction guidelines from the field of consumer electronics. He worked in electronic component distribution. Since 1997, he has been the Head of R&D Department, Würth Elektronik eiSos. He is one of the authors of the *Trilogy of Magnetics: Design Guide for EMI Filter Design, SMP & RF Circuits* book. He collaborated with the Board of Directors of the Power Sources Manufacturers Association (PSMA). His research interests include the characterization of EMC filtering components and new design approaches for optimizing the design of magnetic components.



Jose Torres (Senior Member, IEEE) received the B.S. and M.S. degrees, in 2000 and Ph.D. degree, in 2005 from the University of Valencia, Valencia, Spain, all in electronics engineering.

From 2013 to 2015, he was a Research Assistant with the Design of Communication and Digital Systems Research Group, University of Valencia. Since 2015, he has been a Research Assistant with EMC Catedra University of Valencia-Würth Elektronik eiSos, Electronics Engineering Department, University of Valencia. Since 2005, he has been an Associate Professor with the Electronics Engineering Department, University of Valencia. He has been part of more than 20 national and international projects as a Researcher and Coordinator. He is the co-author of more than 30 scientific papers and reviewer of several IEEE journals. He collaborated with the Spanish Association of Telecommunications Engineers and is Co-Director of the EMC Catedra University of Valencia-Würth Elektronik eiSos. His research interests include signal integrity design, FPGA-based read-out systems for high-energy physics and IoT system development, and EMI management in embedded systems.

4.3 Scientific conference article III: Modelling an NSS

Title: Design approach for high efficiency NFC systems with magnetic shielding materials.

Authors: Jorge Victoria, Pedro A Martínez, Adrián Suárez, Antonio Alcarria, Sebastián Mirasol, José Torres.

Published in: 2020 International Symposium on Electromagnetic Compatibility - EMC EUROPE, IEEE. Rome, Italy.

DOI: 10.1109/EMCEUROPE48519.2020.9245861

Description: The International Symposium on Electromagnetic Compatibility - EMC EUROPE is an international conference with a high scientific level supported by IEEE and the EMC Society. It is an annual conference that promotes EMC research, innovation and international cooperation. The submitted contributions are subjected to the peer review process to assess the quality of the manuscript before it is published in the IEEE Xplore database, one of the most comprehensive interdisciplinary engineering databases in the world.

Synopsis:

In this contribution presented at the 2020 EMC Europe conference, we analyze the use of ferrite-polymer composite sheets, known as Noise Suppression Sheets, for solving issues related to the presence of metals in non-magnetically shielded NFC systems.

Ferrite sheets exhibit high permeability, which can sometimes lead to excessive inductance in antennas, resulting in a mismatch in the resonance frequency (13.56 MHz). The NSS studied here, with low permeability ($\mu_r = 25$) at the communication frequency, allows us to precisely adjust the necessary inductance to strengthen the system without affecting communication.

To achieve this, we evaluate different thicknesses placed between the NFC antenna and the metal plane. We analyze the equivalent circuit and resonance frequency in each situation. The results are based on measurements with the Smith chart and simulations using the models developed in this thesis. From these findings, we conclude that the presence of a metal surface shifts the resonance frequency, hindering system communication. However, a properly dimensioned NSS allows us to restore the frequency to its ideal value. The usefulness of both Smith chart measurements and simulations with the created models is demonstrated in the design phase.

Design approach for high efficiency NFC systems with magnetic shielding materials

Jorge Victoria
Product Management
Würth Elektronik eiSos
Waldenburg, Germany
jorge.victoria@we-online.de

Pedro A. Martinez
Department of Electronic Engineering
University of Valencia
Valencia, Spain
pedro.a.martinez@uv.es

Adrian Suarez
Department of Electronic Engineering
University of Valencia
Valencia, Spain
adrian.suarez@uv.es

Antonio Alcarria
Product Management
Würth Elektronik eiSos
Waldenburg, Germany
antonio.alcarria@we-online.de

Sebastian Mirasol
Product Management
Würth Elektronik eiSos
Waldenburg, Germany
sebastian.mirasolmenacho@we-online.de

Jose Torres
Department of Electronic Engineering
University of Valencia
Valencia, Spain
jose.torres@uv.es

Abstract—The performance of a Near Field Communication (NFC) antenna may be diminished when it is placed close to any conductive surface such as a metallic case or a battery. This degradation is caused due to the stray magnetic field created by the eddy currents induced on the surface, which is opposite to the intended field generated by the NFC antenna. One of the first solutions that come to mind to designers when facing this problem is the use of high permeability magnetic shielding based on sintered ferrite sheets. This is a good approach but something that is not generally taken into account is that these materials introduce an additional inductance to the NFC antenna. If the permeability of the material is too high (respecting the necessary value for solving the problem), this additional inductance results in shifting the resonance frequency to lower values than the desired (13.56 MHz). Thereby this contribution focuses on the analysis of a ferrite-polymer composite magnetic shielding that provides lower relative permeability ($\mu_r = 25$) at the communication frequency. This approach is more effective against the presence of a metallic element when there is a gap of some millimeters between the conductive surface and the NFC antenna. Therefore, different thicknesses of the same ferrite-polymer material are evaluated and the effect of introducing this kind of shielding between the conductive surface and the NFC antenna is analyzed from the standpoint of the loop antenna equivalent circuit. The results presented are based on the Smith Chart measurement as well as a simulation model that corroborates the results obtained experimentally.

Keywords—Magnetic shielding, ferrite-polymer composite, near field communication (NFC), antenna equivalent circuit, board-level-shielding (BLS), thickness control

I. INTRODUCTION

The intrasystem electromagnetic interferences (EMI) have been traditionally controlled by basic techniques such as the physical separation of source and victim circuits, changing their orientation or enclosing one of them in a metallic case to ensure the shielding [1]. Nevertheless, the ongoing trend to miniaturize electronic devices with the aim of providing more advanced functionalities involves the use of embedded systems with high-frequency operations, the integration of communication circuits, the reduction of the device housing and thus the reduction of PCB size and thickness that leads to a higher component integration [2]. These design restrictions make it impossible to use basic shielding techniques so that the use of magnetic shielding. Specifically, this solution is very effective to reduce EMI problems produced when an NFC antenna is embedded onto a system where are near a

conductive surfaces such as battery packs, ground planes or metallic elements. The placement of an NFC antenna close to one of this kind of elements result in a high reduction of the communication range or may prevent the communication. This is caused by the eddy currents induced on the conductive element that generates a stray magnetic field opposite to the intended one, resulting in the reduction of the total field [A3]. It has been verified that the influence of the kind of high conductivity metallic surface on the performance of the antenna can be considered negligible. However, it is quite significant the distance from the conductive element to the NFC antenna, since a significant shift of the communication frequency is produced when it is shorter than 40 mm [A4]. The use of high permeability magnetic shielding based on sintered ferrite sheets ($\mu_r \approx 200$) is, generally, the solution used by designers to prevent this kind of EMI problem. However, in those designs where there is a gap between the conductive surface and the NFC antenna, the use of a high-permeability sintered ferrite sheet could result in shifting the resonance frequency to a lower value than desired. The effect of the sintered ferrite can be controlled by reducing the sheet thickness, although this is not always possible due to it is complicated manufacturing sheets with a thickness lower to 0.05 mm.

Considering this fact, in this contribution, we analyze the effectiveness of another magnetic shielding solution based on a ferrite-polymer composite (also known as absorber or noise suppression sheet) taking advantage of it provides lower relative permeability ($\mu_r = 25$) than sintered ferrites at the communication frequency (13.56 MHz) [5]. This feature is interesting since other solutions such as sintered ferrite sheets that provide higher permeability could provide high inductance than needed, resulting in a reduction of communication effectiveness. Therefore, the effect of having a conductive surface located under an NFC loop antenna with a gap of 0.5 mm between them is analyzed from the point of view of the equivalent circuit. This is an important factor since the designer determines the components that implement the matching circuit of the antenna from considering the equivalent circuit of the loop antenna with the objective of achieving a resonant circuit that operates at a certain communication frequency (f_{op}). The presence of a conductive surface close to the NFC antenna modifies the values of the components that represent its equivalent circuit. This changes the value of the antenna self-resonance frequency (f_{sr}), and,

thus, its Q factor, resulting in performance deterioration of the communication [6].

Consequently, the implications of introducing a ferrite-polymer material between the conductive surface and the NFC antenna are analyzed from the point of view of the loop antenna equivalent circuit. Different thicknesses of the same ferrite-polymer material are evaluated and the results obtained through experimental and simulation procedures are studied with the aim of determining how these components can help to restore the antenna circuit and ensure the efficiency of the communication.

II. FERRITE-POLYMER COMPOSITE CHARACTERIZATION

The host matrix of ferrite-polymer composites is based on a silicon rubber matrix with embedded inclusions. These inclusions are basically iron particles in form of flakes prepared by the mechanical forging of spherical iron powders while using an attrition mill. When the size of the inclusions and the spatial periods are tiny compared with the wavelength of the electromagnetic field generated by the noise source, the composite materials can be considered as homogeneous materials [7], [8]. Hence, this kind of material can be characterized through the geometrical and physical properties of the inclusions, the host medium, and the orientation of the inclusions regarding the host matrix. From the standpoint of the magnetic properties, the material used in this research provides an initial permeability $\mu_i = 25$ since with higher initial permeability materials it was not possible to retune the NFC antenna to the original operation frequency. The selection of the right material has been carried out by evaluating the relative permeability parameter because of this parameter allow the designer to know the effectiveness of that material to solve this EMI problem. Thereby, it is interesting to analyze the material in terms of the complex relative permeability that separates the μ_r into the real and imaginary components. The real component μ_r' represents the inductance ability of the material to concentrate and redirect the magnetic flux, otherwise the imaginary component μ_r'' quantifies the losses or effectiveness to absorb the magnetic noise [9].

Even though this kind of shielding solution is often applied for solving problems related to absorb high-frequency EMI [10], by selecting a ferrite-polymer composite with the right μ_r behavior it can be used to improve the performance of NFC communications. Therefore, this magnetic shielding solution should provide a steady and high value of inductance (μ_r') as well as present low losses (μ_r'') in the low-frequency region and particularly at 13.56 MHz, since this is the NFC communication frequency. Particularly, the ferrite-polymer studied in this work meet these features because, as shown in Fig. 1 by means of the complex relative permeability representation, the inductance trace presents a steady value of 25 at the same time that the losses can be considered negligible up to about 17 MHz, preventing to cause undesirable losses to the communication signal. The permeability data is obtained with an E4991A Material Analyzer together with the 16454A Magnetic Material Text Fixture. This fixture is based on cavity resonance and single-turn inductor theories and allows for measuring the magnetic properties of a material. The sample under test must have a toroidal shape in order to be able to fit inside the fixture, so that a toroidal core is manufactured with the material of each absorber composition. The toroidal sample has an outer diameter of 20 mm, 8 mm of inner diameter, and the thickness is 1 mm [7].

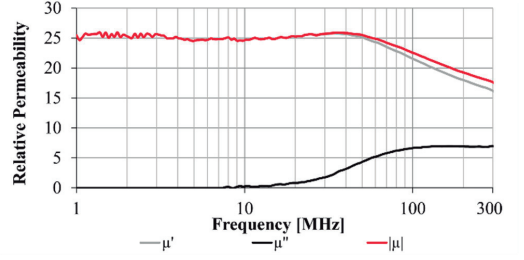


Fig. 1. Relative permeability of ferrite-polymer composite sheet analyzed. performance.

From the analysis of the response of the material, it is possible to conclude that it meets the design requirements to shield an NFC communication system against the presence of disturbance elements such as conductive surfaces since it is able to redirect and concentrate the magnetic flux.

III. NFC LOOP ANTENNA EQUIVALENT CIRCUIT

The NFC antenna designed to characterize the effectiveness of the ferrite-polymer material performance to ensure the NFC communication is implemented by means of a two-layer PCB that contains the six-turn loop antenna and the footprints to set the matching circuit associated components printed on the top layer. The PCB loop antenna is based on FR4 substrate material that presents a substrate thickness of 1.48 mm and the copper thickness is 35 micrometers. The loop has dimensions of 41 mm \times 41 mm with a spacing between traces of 0.6 mm and a trace width of 0.8 mm. Fig. 2 shows the top layer view of the PCB that holds the described NFC loop antenna. Thereby, a 60 mm \times 60 mm ferrite-polymer sheet can be pasted on the bottom layer covering the antenna area. The conductive surface is going to be represented by an aluminum sheet that has a thickness of 1.6 mm is placed under the PCB (in the bottom side) at a distance of 0.5 mm in order to emulate the effect of a metal casing, a metal shielding or a battery that can be located close to the NFC antenna.

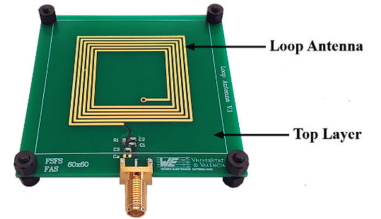


Fig. 2. Top layer view of NFC loop antenna implemented to characterize the ferrite-polymer composite performance.

Besides determining the performance of the shielding solution through an experimental evaluation, a simulation model that integrates the NFC antenna, the metal sheet and the ferrite-polymer sheet has been designed to be characterized with an electromagnetic analysis simulator (ANSYS HFSS). The simulation model emulates the experimental setup described to corroborate the results obtained. It is formed by the loop antenna described above and an aluminum sheet that is placed on this at a distance of 0.5 cm. The magnetic permeability and tangent magnetic loss are the main parameters introduced to characterize the ferrite-polymer sheet model.

From the Smith Chart, it is possible to determine the equivalent circuit of the loop antenna described above through a Network Analyzer equipment. The Smith Chart allows determining the self-resonance frequency (f_{sr}) at which the loop antenna (without introducing the matching circuit) produces the resonance. The f_{sr} is determined at the point of the Smith Chart where the reactance is cancelled, leaving only the real term. The value of the f_{sr} depends on the intrinsic components of the loop antenna. These components are the inductance of the antenna (L_a) and the resistance that is in series (R_s) with L_a that generally are measured at 1 MHz, as well as the resistance that appears in parallel (R_p) that corresponds to the real term measured at the f_{sr} and the parallel capacitance (C_a). Fig. 3(a) shows the components forming the equivalent circuit of the loop antenna and its topology and Fig. 3(b) the reduced equivalent circuit that we are going to use to compare the results obtained.

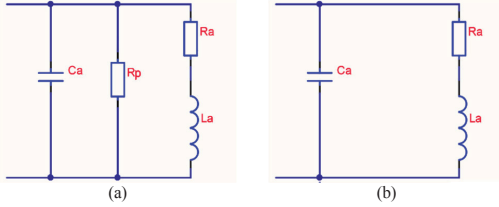


Fig. 3. Equivalent circuit of the NFC loop antenna. (a) Equivalent circuit extended. (b) Reduced equivalent circuit.

Fig. 4 shows the measured Smith Chart of the NFC loop antenna without the presence of any conductive surface and without placing any shielding solution. Marker 3 shows that $f_{sr} = 50.2$ MHz and $R_p = 18.72$ k Ω . Marker 1 provides the value of the inductance and series resistance at 1 MHz, being $R_s = 0.42$ Ω . From this measurement it is also possible to obtain the value of the inductance, being $L_a = 2.05$ μ H at 1 MHz.

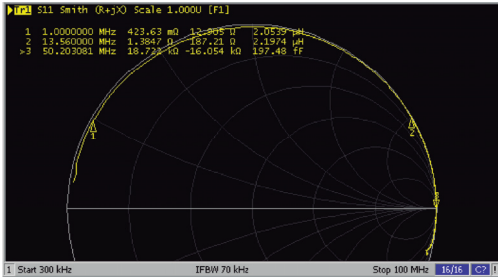


Fig. 4. Experimentally measured Smith Chart of the loop antenna without any conductive surface and without placing any shielding.

Likewise, the Smith Chart of the loop antenna is computed with the simulation model with the aim of checking the experimentally acquired data. Hence, the simulated Smith Chart is shown in Fig. 5. Note that the obtained values are normalized so that the values have to be multiplied by the port impedance (50 Ω). Consequently, marker 1 (m1) shows that $R_s = 0.64$ Ω at 1 MHz and marker 3 (m3) that $f_{sr} = 48.99$ MHz and $R_p = 18.00$ k Ω at f_{sr} .

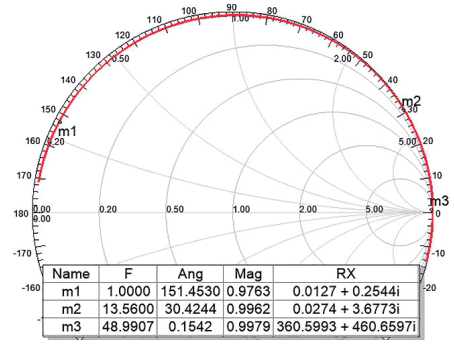


Fig. 5. Simulated Smith Chart of the loop antenna without any conductive surface and without placing any shielding.

The simulated Smith Chart does not provide the value of the inductance so that it is obtained through representing L_a . The simulated inductance of the NFC antenna compared with the experimentally measured is represented in Fig. 6.

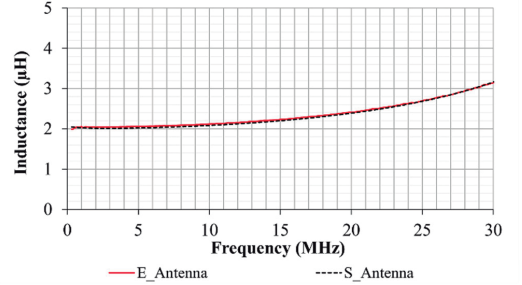


Fig. 6. Simulated and experimentally measured NFC antenna inductance.

By comparing both simulation and experimentally measured data it is possible to verify that the values of the equivalent circuit components match.

Subsequently, from loop antenna data obtained from Smith Chart, it can be calculated the value of the reduced equivalent circuit and transform it to the reduced one as shown in Fig 4(a) and Fig. 4(b), respectively. The capacitance C_a is calculated from the f_{sr} and the simulated and experimental inductance L_a by:

$$f_{sr} = \frac{1}{2\pi\sqrt{L_a C_a}} \quad (1)$$

therefore, C_a is given by:

$$C_a = \frac{1}{(2\pi f_{sr})^2 L_a} \quad (2)$$

The value of R_a is determined by the sum of the series resistance R_s and R_p . This last value has to be considered at the operation frequency of 13.56 MHz so that it has to be transformed by considering f_{sr} , f_{op} , and R_p at f_{op} ($R_{p(fop)}$) [11]. This conversion is shown in (4) and the determination of R_a is carried out by (3):

$$R_a = R_s + \frac{(2\pi f_{op} L_a)^2}{R_{p(fop)}} \quad (3)$$

where $R_{p(fop)}$ is given by:

$$R_p(f_{op}) = \frac{R_p(f_{sr})}{\sqrt{f_{op}/f_{sr}}} \quad (4)$$

Table I summarizes parameters obtained from the Smith Chart simulated and measured experimentally as well as the results calculated from (2), (3) and (4).

TABLE I. VALUES OF THE LOOP ANTENNA EQUIVALENT CIRCUIT COMPONENTS

Component	Unit	Experimental	Simulated
f_r	MHz	50.20	48.99
$R_s @ 1 \text{ MHz}$	Ω	0.42	0.64
$L_a @ 1 \text{ MHz}$	μF	2.05	2.03
$R_p @ f_r$	$k\Omega$	18.72	18.00
f_{op}	MHz	13.56	13.56
C_a	pF	4.89	5.22
$R_p @ f_{op}$	$k\Omega$	36.00	34.20
R_a	Ω	1.27	1.51

From the simulated and experimental values presented in Table I, the reduced equivalent circuit of the NFC loop antenna can be defined. Fig. 7 illustrates how the most important component that is the inductance L_a is practically equal in both cases and the resistance and capacitance of the antenna are quite similar.

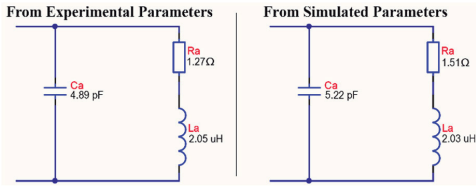


Fig. 7. Comparison between equivalent circuits of the NFC loop antenna obtained experimentally and from the simulation model.

IV. INFLUENCE OF THE METAL AND FERRITE-POLYMER ON THE NFC LOOP ANTENNA

As explained above, the effect of introducing an aluminum under the NFC antenna, 0.5 cm from the bottom side of the PCB, is analyzed. Thereby, we are emulating the effect of having a conductive surface close to the NFC communication area. The ferrite-polymer sheet will be placed on the bottom side of the PCB, between the NFC loop antenna and metal sheet. Fig. 8(a) shows the experimental setup used to emulate this situation and Fig. 8 (b) the setup designed in the simulation model.

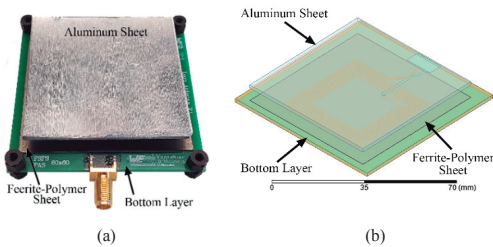


Fig. 8. NFC antenna with an aluminum sheet placed under it at a distance of 0.5 mm and placing the ferrite-polymer shielding solution between them. (a) Experimental setup. (b) Simulation model.

With the help of a Network Analyzer, S_{11} parameter of the NFC antenna with the original matching circuit set has been

studied. The goal with this step is to analyze the disturbance to the S_{11} produced by the metal sheet when it is placed close to the antenna. Moreover, different ferrite-polymer sheets with the same composition but with different thicknesses (0.1 mm, 0.2 mm and 0.3 mm) have been evaluated to determine which sheet is able to retune the NFC antenna to the original f_{op} value provided by this antenna and cancelling, at the same time, the influence of the metal sheet. Thereby, Fig. 9 shows how the aluminum sheet shifts the f_{op} to a higher value (15.25 MHz) caused by the capacitive effect introduced. This detuning may lead to prevent the NFC communication. When the shielding is placed, it is possible to observe how the f_{op} is moved to lower frequencies. In particular, the ferrite-polymer with a thickness of 0.1 mm, 0.2 mm and 0.3 mm are able to shift the f_{op} to 14.26 MHz, 13.51 MHz, and 13.23 MHz, respectively. Consequently, the ferrite-polymer with a sheet thickness of 0.2 mm is the best solution to solve the influence of the metal sheet located at 0.5 cm, considering the composition analyzed in this contribution ($\mu_r = 25$).

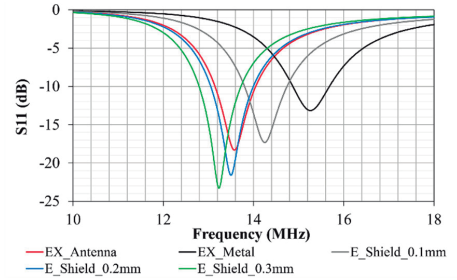


Fig. 9. Variation of the return loss (S_{11} parameter) depending on the ferrite-polymer sheet thickness that is shielding the NFC antenna against the metal.

Simulated and experimentally measured inductances are represented in Fig. 10. In this graph, it is possible to observe the effect of introducing the aluminum sheet from the point of view of the inductance of the antenna. Thereby, the metal reduces significantly the L_a (black traces), whereas the placement of the ferrite-polymer increases it (grey traces). When the ferrite-polymer is introduced between the NFC antenna and the metal sheet, the inductance achieved is quite similar to the original trace.

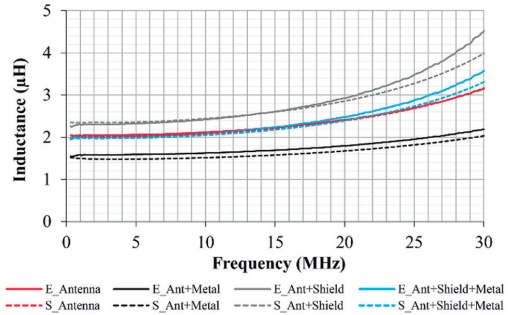


Fig. 10. Simulated and experimentally measured inductance when the metal, ferrite-polymer and the combination of both is analyzed.

V. RESULTS AND DISCUSSION

The results presented in this part, correspond to the evaluation of the ferrite-polymer composite with a thickness of 0.2 mm to retune an NFC antenna affected by the influence

of an aluminum sheet. Thereby, it could be evaluated the performance of a low permeability magnetic sheet to solve EMI problems caused by the eddy currents generated in the conductive surface.

The first study case is the measurement and simulation of the NFC antenna with the aluminum sheet located at 0.5 cm under the antenna without placing any shielding solution between them. The equivalent circuit considering the influence of the metal is carried out in the same way that has been done in the case of the NFC antenna without any disturbance. Thus, the experimentally measured and simulate Smith Charts are shown in Fig. 11.

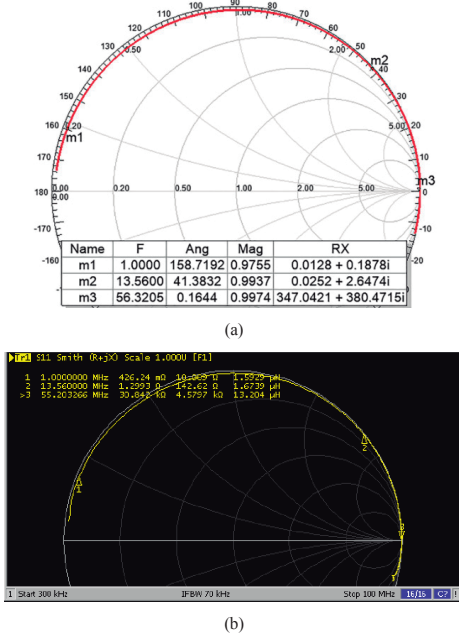


Fig. 11. Smith Chart of the NFC loop antenna influenced by the aluminum sheet and without placing any shielding. (a) Simulated results. (b) Experimentally measured.

Table II summarizes the values determined through the simulated model and experimentally measured. From the results obtained it is possible to determine that the influence of the aluminum sheet reduces the inductance L_a of the NFC antenna about 0.5 uH if it is compared to the original values of the antenna presented in Table I. This reduction of L_a leads to the shift of the f_{sr} to higher frequency values than the originally designed when the matching circuit is introduced, reducing or even preventing the NFC communication.

TABLE II. VALUES OF THE LOOP ANTENNA EQUIVALENT CIRCUIT COMPONENTS (INFLUENCED BY THE METAL SHEET)

Component	Unit	Experimental	Simulated
f_{sr}	MHz	55.70	56.30
$R_s @ 1 \text{ MHz}$	Ω	0.45	0.64
$L_a @ 1 \text{ MHz}$	μF	1.59	1.50
$R_p @ f_{sr}$	k Ω	30.90	17.40
f_{op}	MHz	13.56	13.56
C_a	pF	5.13	5.33
$R_p @ f_{op}$	k Ω	62.60	35.40

Component	Unit	Experimental	Simulated
R_a	Ω	7.42	1.10

From the simulated and experimental values presented in Table II, the reduced equivalent circuit of the NFC loop antenna when is influenced by the aluminum sheet can be determined. Fig. 12 illustrates how the most important component that is the inductance L_a is practically equal in both cases and the resistance and capacitance of the antenna are very similar.

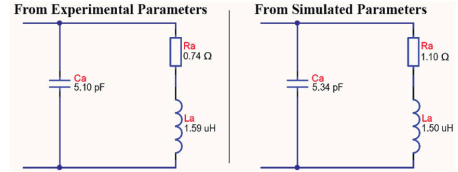


Fig. 12. Comparison between equivalent circuits of the NFC loop antenna influenced by an aluminum sheet obtained experimentally and from the simulated model.

The second study case corresponds to the measurement and simulation by shielding the NFC antenna with the ferrite-polymer sheet (0.2 mm thickness) against the aluminum sheet located at 0.5 cm under the antenna. The equivalent circuit considering the influence of the metal is carried out in the same way that has been done in the last cases. Thus, the experimentally measured and simulate Smith Charts are shown in Fig. 13.

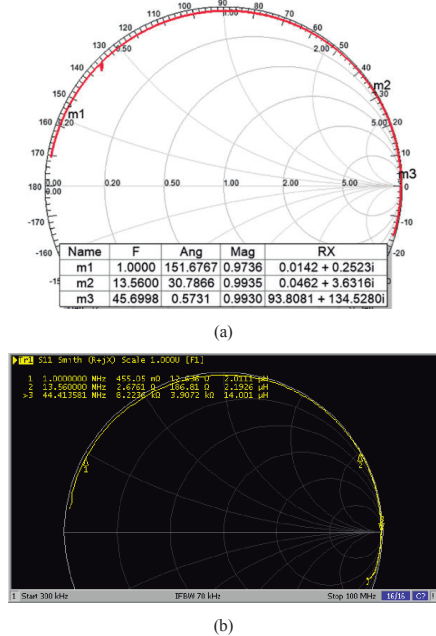


Fig. 13. Smith Chart of the loop antenna shielded with the ferrite-polymer sheet (0.2 mm thickness) against the conductive surface. (a) Simulated results. (b) Experimentally measured.

Table III summarizes the values determined through the simulated model and experimentally measured. By comparing the results of Table III with those shown in Table I it is possible to determine that the influence of the aluminum sheet

has been shielded by means of the ferrite-polymer sheet, recovering the value of L_a to a quite similar value than the measured in the original NFC antenna without the influence of the conductive surface. This increase of L_a leads to the shift of the f_{sr} to lower frequency values than the originally designed when the matching circuit is introduced, retuning the NFC communication.

TABLE III. VALUES OF THE LOOP ANTENNA EQUIVALENT CIRCUIT COMPONENTS (WITH METAL SHEET AND FERRITE-POLYMER)

Component	Unit	Experimental	Simulated
f_{sr}	MHz	44.40	47.50
$R_s @ 1 \text{ MHz}$	Ω	0.46	0.71
$L_a @ 1 \text{ MHz}$	μF	2.01	2.01
$R_p @ f_{sr}$	$k\Omega$	8.22	4.69
f_{op}	MHz	13.56	13.56
C_a	pF	6.39	6.02
$R_p @ f_{op}$	$k\Omega$	14.90	8.61
R_a	Ω	2.43	4.13

From the simulated and experimental values presented in Table III, it can be determined the reduced equivalent circuit of the NFC loop antenna when it is shielded against the influence of the aluminum sheet. Fig. 14 illustrates how the most important component that is the inductance L_a is practically equal in both cases and the resistance and capacitance of the antenna are quite similar.

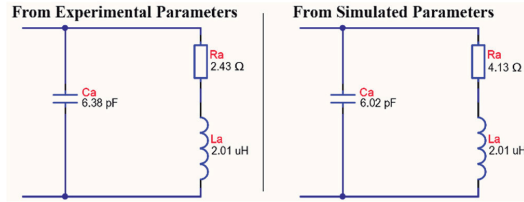


Fig. 14. Comparison between equivalent circuits of the NFC loop antenna with the ferrite-polymer sheet shielding the effect of the aluminum sheet obtained experimentally and from the simulation model.

This match between the equivalent circuits obtained from the original antenna and the shielded antenna near to the metal sheet can be observed from the standpoint of the S_{11} parameter. Fig. 15 shows a comparison of the S_{11} parameters experimentally measured (solid traces) and simulated (dashed traces), considering the cases analyzed in this contribution: NFC antenna, the antenna affected by the aluminum sheet at 0.5 cm and the antenna shielded with the ferrite-polymer against the presence of the aluminum sheet.

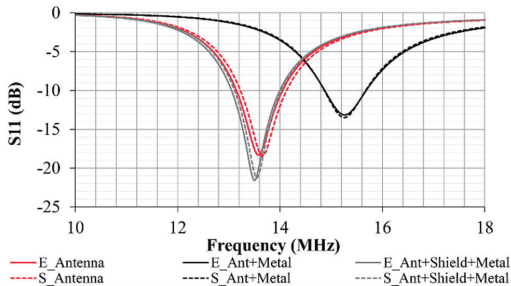


Fig. 15. Comparison between S_{11} parameters to determine the value of the communication frequency before and after shielding the NFC antenna against the aluminum sheet effect.

VI. CONCLUSIONS

Considering the results, it is clearly demonstrated that the presence of a conductive surface near to the NFC antenna leads to modify the intrinsic components of the loop antenna and, thus, making unusable the original matching circuit designed for communicating at 13.56 MHz. The capacitance introduced in the system by the metal sheet shifts the working frequency to higher values, affecting the NFC communication. The solution proposed for this EMI problem, a low permeability ferrite-polymer composite sheet, has been analyzed to evaluate its real effectiveness in shielding the NFC antenna and ensuring its original and correct behavior.

Thereby, with the results obtained from the evaluation of the equivalent circuits for the NFC system considering the original antenna, the influence of an aluminum sheet and the NFC antenna shielded it has been expounded and verified that this shielding solution is able to recover significantly the original behavior of the antenna. Both equivalent circuits for the original NFC antenna and the shielded NFC antenna show quite similar component values and behavior. Hence, the introduction of the ferrite-polymer composite sheet under the NFC antenna results in solving the detuning of the NFC communication system caused by the metal plane without the having to redesign the original matching circuit.

REFERENCES

- [1] E. F. Vance and W. Graf, "The role of shielding in interference control," *IEEE T ELECTROMAGN C*, vol. 30, no. 3, pp. 294–297, Aug. 1988, 10.1109/15.3308.
- [2] S. Piersanti et al., "Near-field shielding performances of EMI noise suppression absorbers," *IEEE T ELECTROMAGN C*, vol. 59, no. 2, Apr., pp. 654–661, 2017.
- [3] J. Victoria et al., "Study of a Novel High Permeability Ferrite Sheet Intended for Near Field Communication Systems," in *2019 IEEE International Symposium on Electromagnetic Compatibility, Signal & Power Integrity (EMC+SIPI)*, New Orleans, LA, USA, 2019, pp. 78–83, 10.1109/ISEMC.2019.8825260.
- [4] A. I. Petrariu et al., "Influence of Different Types of Metal Plates on a High Frequency RFID Loop Antenna: Study and Design," *Advances in Electrical and Computer Eng.*, vol. 9, no. 2, 2009, pp. 3–8. Dec. 2019.
- [5] B. Lee, B. Kim, F. J. Harackiewicz, B. Mun and H. Lee, "NFC Antenna Design for Low-Permeability Ferromagnetic Material," in *IEEE Antennas and Wireless Propagation Letters*, vol. 13, pp. 59–62, 2014.
- [6] K. Finkenzeller, *RFID Handbook: Fundamentals and Applications in Contactless Smart Cards and Identification*, 3rd ed., John Wiley & Sons, Inc., Hoboken, NJ, USA, 2010.
- [7] J. Victoria, A. Suarez, J. Torres, P. Martinez, A. Alcarria, J. Martos, R. Garcia-Olcina, J. Soret, S. Muetsch, and A. Gerfer, "Transmission Attenuation Power Ratio Analysis of Flexible Electromagnetic Absorber Sheets Combined with a Metal Layer," *Materials*, vol. 11, no. 9, p. 1612–1626, Sep. 2018.
- [8] G. Lovat, P. Burghignoli and S. Celozzi, "Shielding Properties of a Wire-Medium Screen," in *IEEE T ELECTROMAGN C*, vol. 50, no. 1, pp. 80–88, Feb. 2008.
- [9] A. Suarez et al., "Effectiveness Assessment of a Nanocrystalline Sleeve Ferrite Core Compared with Ceramic Cores for Reducing Conducted EMI," *Electronics*, vol. 8, no. 7, pp. 1–21, Jul. 2019, doi.org/10.3390/electronics8070800.
- [10] A. Suarez, J. Victoria, A. Alcarria and J. Torres, "Characterization of electromagnetic noise suppression sheet for aerospace applications," *2016 ESA Workshop on Aerospace EMC*, Spain, 2016, pp. 1–6.
- [11] S. S. Lau, "Practical design of 13.56MHz Near Field Communication (NFC) and Radio Frequency Identification (RFID) antenna using ferrite sheet on metallic surface by Network Analyzer," *2015 IEEE International Conference on Industrial Engineering and Engineering Management (IEEM)*, Singapore, 2015, pp. 1362–1366.

4.4 Summary

In this chapter, we created simulation models of absorber sheets and used them to solve EMI challenges. The results have shown significant accuracy in terms of selecting the right material and thickness, and the designed solutions have been successfully implemented. We also combined our simulated data with the Smith chart, an essential tool in RF and microwave engineering commonly used in designing antennas, filters, amplifiers, and other RF circuits.

Chapter 5. DESIGN OF A HYBRID SHEET FOR ELECTROMAGNETIC SHIELDING AT THE PRINTED CIRCUIT LEVEL

This chapter covers the study of different compositions for a hybrid sheet for electromagnetic shielding at the printed circuit level (BLS). Using the measurement systems defined and implemented in Chapter 3 and the models created and validated in Chapter 4, different combinations of MAS and metal sheets are evaluated. The use of such a combination allows the BLS to be on a broad frequency range without affecting useful low-frequency signals. Adding an electrically isolated adhesive layer, this hybrid solution can be used directly on the PCB without the need for redesign.

5.1 Hybrid shielding sheet design

The ongoing trend toward the miniaturization of electronic devices, aimed at enhancing functionalities and performance, presents a recurrent challenge in detecting and mitigating electromagnetic interference. The resulting design constraints often complicate the application of conventional EMI shielding techniques, necessitating innovative solutions. Consequently, board-level shielding solutions are widely adopted in PCB applications to reduce intra-system EMI from integrated circuits (ICs) and enhance the overall immunity of electronic devices.

BLS is commonly achieved through the utilization of metallic shielded enclosures covering critical areas. However, numerous electronic devices featuring multiple high-frequency components operating at several gigahertz can generate harmonic noise emissions. These emissions pose complex EMI challenges that extend beyond the efficacy of traditional grounding techniques and simple shielding methods.

This chapter delves into the analysis of a magnetic absorber sheet in combination with a metal layer as a board-level shield solution. This hybrid approach is anticipated to yield higher shielding effectiveness compared to using only a magnetic sheet. The combination leverages the magnetic material's absorbing properties and metal loss mechanisms,

including reflection and eddy current losses. Notably, the hybrid structure offers a significant advantage in that it does not necessitate the redesign of electronics; it can be easily applied over the EMI source. This involves combining magnetic material with varying thicknesses with metal layers.

The simulation models, previously created and validated in Chapter 4, will play a pivotal role in exploring diverse material compositions, thicknesses, and configurations before embarking on the production of physical prototypes. Additionally, simulations will enable the anticipation of the behavior of the noise suppression sheet in intricate electromagnetic environments. This understanding is particularly valuable in scenarios where measurements may be complicated or costly.

5.2 Scientific article II: Material properties definition

Title: Transmission Attenuation Power Ratio Analysis of Flexible Electromagnetic Absorber Sheets Combined with a Metal Layer.

Authors: Jorge Victoria, Adrián Suárez, José Torres, Pedro A. Martínez, Antonio Alcarria, Julio Martos, Raimundo García-Olcina, Jesús Soret, Steffen Muetsch, Alexander Gerfer.

Published in Materials (MDPI), vol. 11, no. 2, p. 174 (2018).

DOI: 10.3390/ma11020174

Impact factor (2018): JCR: 2.972; SJR: 0.686

Quartile (2018): JCR: Q2 (category: Materials Science, Multidisciplinary)
SJR: Q2 (category: Materials Science)

Citations: 13 (WoS, accessed on March 2024).

Description: Materials (ISSN 1996-1944; CODEN: MATEG9) is a peer-reviewed, open access journal of materials science and engineering published semimonthly online by MDPI. The Portuguese Materials Society (SPM), Spanish Materials Society (SOCIEMAT) and Manufacturing Engineering Society (MES) are affiliated with Materials. The impact factor, quartile and rank information have been obtained from Journal Citation Reports (JCR) and Scimago Journal Rank (SJR) databases according to the publication year (2020). The citations have been consulted in the Web of Science database.

Synopsis:

In this article, we propose combining a magnetic absorbent sheet with a metal sheet to enhance the effect of EMI elimination on a transmission line.

We employ an experimental design based on the IEC 62333-2 standard [14]. Our circuit simulates a transmission line between ports 1 and 2 of our network analyzer. By

applying an absorbent sheet to the line, we quantify the attenuation produced at different frequencies using parameters S_{21} (energy transmitted from port 1 to port 2) and S_{11} (energy reflected to port 1 due to the discontinuity in the transmission line caused by the introduction of the absorbent). This attenuation exhibits a low-pass filter profile that enables EMI reduction at high frequencies.

We combine different materials and thicknesses of both absorbent and metal to analyze their effect on the magnitude and frequency distribution of the obtained attenuation.

Adding a metal layer parallel to both the line and the circuit ground plane poses the risk of signal radiation due to capacitive coupling or magnetic fields generated by eddy currents in the metal.





To measure reradiation, we implement a new experimental design. We add a near-field probe directly placed on the metal layer and connect it to port 2 of the vector network analyzer (VNA). We terminate our transmission line with a $50\ \Omega$ load and measure transmission S_{21} , which, in this case, represents the portion of energy transmitted by port 1 that is radiated to the magnetic field probe connected to port 2 for each frequency.

The results demonstrate that the combination of absorbent with metal offers a more significant attenuation and frequency range than the original absorbent alone. In cases where the absorbent's permeability is very high, and the thickness is greater, this effect is reduced because the electromagnetic field reaching the metal layer is lower.

It is also confirmed that both copper and aluminum offer similar results and that no significant reradiation effects occur in any case.

Article

Transmission Attenuation Power Ratio Analysis of Flexible Electromagnetic Absorber Sheets Combined with a Metal Layer

Jorge Victoria ^{1,2}, Adrian Suarez ^{1,*} , Jose Torres ¹, Pedro A. Martinez ¹, Antonio Alcarria ^{1,2}, Julio Martos ¹ , Raimundo Garcia-Olcina ¹ , Jesus Soret ¹ , Steffen Muetsch ² and Alexander Gerfer ²

¹ Department of Electronic Engineering, University of Valencia, 46100 Burjassot, Spain; Jorge.Victoria@we-online.de (J.V.); Jose.Torres@uv.es (J.T.); Pedro.A.Martinez@uv.es (P.A.M.); Antonio.Alcarria@we-online.de (A.A.); Julio.Martos@uv.es (J.M.); Raimundo.Garcia@uv.es (R.G.-O.); Jesus.Soret@uv.es (J.S.)

² Würth Elektronik eiSos GmbH & Co. KG, 74638 Waldenburg, Germany; Steffen.Muetsch@we-online.de (S.M.); Alexander.Gerfer@we-online.de (A.G.)

* Correspondence: adrian.suarez@uv.es; Tel.: +34-963-544-146

Received: 27 July 2018; Accepted: 3 September 2018; Published: 4 September 2018



Abstract: Electromagnetic noise absorber sheets have become a solution for solving complex electromagnetic interference (EMI) problems due to their high magnetic losses. This contribution is focused on characterizing a novel structure that is based on an absorber film with a metal layer attached on its top side. Two different absorber compositions were combined with Al and Cu metal layers in order to study the improvement on the performance of these structures, depending on the complex permeability, absorber film thickness, and type of metal. The transmission attenuation power ratio of the absorber films is analyzed and compared to the performance of absorber and metal structures. The measurement procedure is carried out attaching the films into a microstrip line that has been designed based on IEC standard (IEC 62333-2). This test fixture is employed as a transmission line to simulate a general noise path. The performance of absorber composites to filter electromagnetic noise is evaluated through analyzing S_{21} and S_{11} parameters. This is carried out with the aim of finding out in which conditions the absorption loss is improved when a metal layer is attached. In addition, the possible re-radiation effect, due to the magnetic field that is generated by the eddy currents induced in the metal layer, is examined.

Keywords: flexible electromagnetic absorber sheet; complex permeability; magnetic materials; electromagnetic interference; power absorption; microstrip line; insertion loss

1. Introduction

Electronic devices continually integrate more complex and more advanced functionalities. This involves the use of increasing operating frequencies, the miniaturization of the electronic design and high component integration, printed circuit board (PCB) size and thickness reduction, and using signals of very low voltage amplitude [1]. These design principles are often used to achieve a device with better performance and features; nevertheless, they increase the likelihood of generating complex electromagnetic interference (EMI) problems. The electronics can be sensitive to the surrounding electromagnetic environment, and it can also act as noise source, thus, it is very important to manage electromagnetic noise for avoiding unwanted electromagnetic interactions with nearby systems. Furthermore, at gigahertz (GHz) frequencies, semiconductor elements and PCB tracks radiate electromagnetic noise [2,3]. Therefore, the ability to control complex EMI problems either by

eliminating or by reducing them is in high demand [4]. Consequently, electromagnetic shielding is one of the main concerns for electronic engineers, designing enclosures or devices that contain complex electronic systems [5].

Generally, the most common means of solving electromagnetic noise problems is to shield the system using a conductive shielded enclosure, foil tape, or conductive gasket. However, sometimes conductive shielding is not suitable due to size or weight restrictions and, thus, complex EMI problems cannot be resolved with conductive shielding techniques [6,7].

In this way, the use of noise suppression sheets (NSS) or flexible absorber sheets (FAS) has gained more interest in the solution of complex EMI problems because they are able to provide a lightweight solution with high flexibility and greater electromagnetic shielding than conductive shields [8,9]. These magnetic shielding materials have many advantages because they can be adapted to achieve complex shapes and are easily assembled with adhesive to a certain component or surface. Therefore, FAS represent a magnetic shielding solution with a great versatility in terms of mechanical properties.

Electromagnetic absorber materials are based on composite structures, usually a polymer host matrix with ferromagnetic metal flakes embedded [5,10,11]. Absorbing materials can be defined as a class of material with a specific ability to absorb and convert electromagnetic noise into heat. These types of amorphous magnetic thin films are classified in the categories of metamaterials, because they are able to provide electromagnetic properties that cannot be met by conventional homogeneous materials [1,12,13]. The capability that magnetic thin films present to reduce EMI is determined by its absorption loss and this depends on many factors, such as material parameters, frequency and sample dimensions [14,15]. Equation (1) [16,17] shows the influence of each last factor in order to determine the insertion loss (A), that is, the effectiveness of a certain shielding to filter electromagnetic noise. Thereby, the insertion loss depends on the relative permeability (μ_r) and conductivity (σ_r) defined by the material composition, frequency (f), and the shield thickness (t):

$$A = 0.132t\sqrt{f\mu_r\sigma_r} \text{ dB} \quad (1)$$

In this equation, the absorption loss or insertion loss A is expressed in decibel, t in millimeters, f in Hertz, and μ_r and σ_r are dimensionless parameters.

Many extensive studies on high frequency absorption properties of various materials have been carried out to look into how the parameters that interact in Equation (1) contributes to reduce the unwanted electromagnetic field. In fact, much attention has been paid in previous studies to analyze the conduction noise attenuation of magnetic thin films on transmission lines due to the different dominant factors, including: magnetic loss due to ferromagnetic resonance [3,18], dielectric loss provided for space charge polarization in the composites [19,20], and ohmic loss in electrically conductive sheets [21,22]. In particular, this contribution is focused on emulating electromagnetic conduction noise and evaluating two absorber sheets with the same thickness, shape, and size, but with different compositions. The main parameter studied is the transmission attenuation power ratio (R_{tp}), since it is center on determining the attenuation of conducting current noise along electromagnetic noise paths achieve by the installation of a FAS by only measuring the S parameters. Thereby, R_{tp} is used to characterize magnetic sheets and allow for obtaining the FAS attenuation ratio without needing to find out the material parameters and the thickness of the shield as occurs in the absorption loss general expression (Equation (1)). One of the sheets provides a higher magnetic loss value than the other in order to characterize how this difference could modify the performance of these FAS when a metal layer is placed on its top surface. The advantage of this multilayer shield structure mostly resides in the increase of the absorption loss due to the losses that were introduced by the metal layer. In this way, the metal layer can filter the unwanted electromagnetic field that is not absorbed by the magnetic film. This structure could extend the working bandwidth of these materials and obtain a greater attenuation than each of these materials could provide individually.

Thereby, different metals are combined with the two different FAS compositions with the aim of analyzing the effect of introducing a conductive plane on the absorber structure. There, the first

shield, a high conductivity material, such as copper or aluminum, can provide a better reflection loss at higher frequencies than magnetic materials, whereas a magnetic film is a high-permeability material, which provides the maximum absorption loss at lower frequencies.

Because of the metal layers features, the re-radiation parameter is characterized to verify that the electromagnetic noise concentrated in its own metal layer does not generate an additional electromagnetic field that could act as an artificial noise source. Taking all of these issues into consideration, the R_{tp} of different material combinations is determined and analyzed.

2. Materials and Methods

2.1. FAS Characterization

The flexible absorber sheet's host matrix is based on a silicone rubber matrix and the inclusions embedded are iron particles in form of flakes prepared by the mechanical forging of spherical iron powders while using an attrition mill. When the size of the inclusions and the spatial periods are tiny compared with the wavelength of the electromagnetic field generated by the noise source, the composite materials can be considered as homogeneous materials [23,24]. Hence, this kind of material can be characterized through the geometrical and physical properties of the inclusions, the host medium, and the orientation of the inclusions regarding the host matrix. In addition to these characteristics, there are other properties that define the electromagnetic behavior: the volume fractions of the host material and inclusions, orientation and alignment of inclusions, statistical distribution of the parameters of inclusions, distance and contact between the inclusions, and the frequency dependence of constitutive parameters of the host material and inclusions [25,26].

Table 1 defines the characteristics of absorber sheets with 0.3 mm thickness in order to compare both compositions, although in the next section more sheet thicknesses will be employed in order to provide a wider material characterization.

Table 1. Comparison of magnetic properties for 3441 and 304 magnetic films.

Parameters	3441	304
Thickness (mm)	0.3	0.3
Size (mm)	50×100	50×100
Surface resistivity (Ω/sq)	1×10^6	1×10^9
Density (g/cm^3)	3.9	3.5
Relaxation frequ. (GHz)	0.163	2.185
Initial permeability	200	25

Figure 1 shows four micrographs of the samples, which were obtained with the S-4800 (Hitachi, Tokyo, Japan) scanning electron microscopy (SEM). The (a) and (b) photographs have been taken over the top surface of each material and they show the inclusions distributed into the host matrix. By comparing both images, it is possible to observe that 3441 material has a higher density of flakes, since it is difficult to distinguish gaps between them. On the other hand, 304 material shows a similar distribution, but in this case, the gaps between iron flakes can be identified because the density of this composition is lower. These gaps represent the polymer that joins the flakes. The in-plane orientation state of the flake in the FAS and the alignment of the inclusions regarding the host matrix can be observed in (c) and (d) micrographs, which show the FAS cross-section. These captions show how 3441 material has been manufactured to be more densely packed than 304 material. Thus, 3441 material integrates a higher number of flakes in the same sheet thickness, suggesting that this difference in its internal structure might be one of the most important factors why 3441 provides higher magnetic losses.

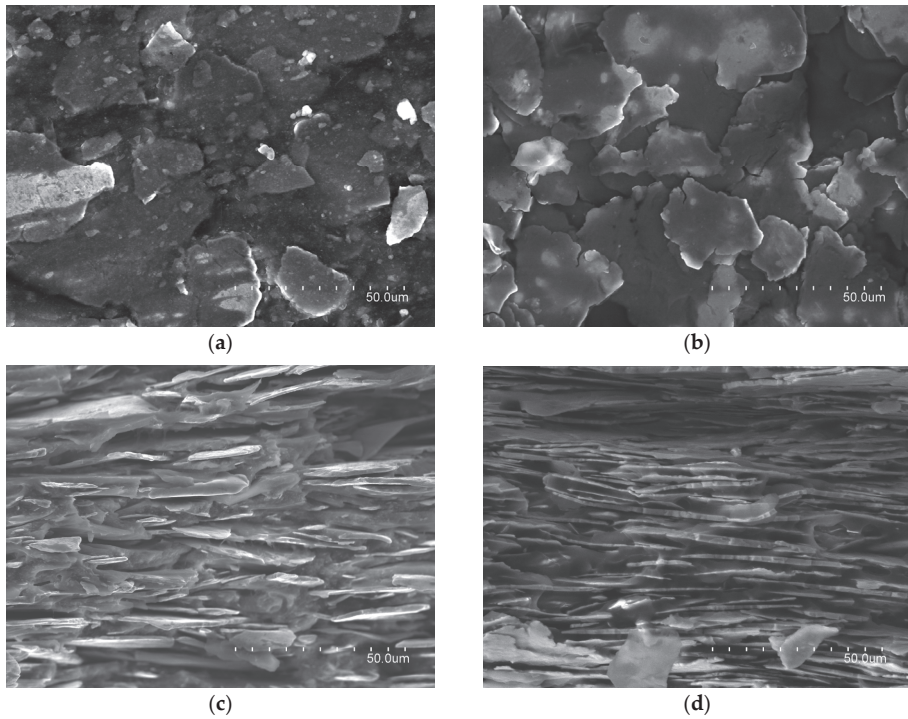


Figure 1. SEM photographs of electromagnetic absorber materials: (a) 304 material composition; (b) 3441 material composition; (c) cross-section of 304 material composition; and, (d) cross-section of 3441 material composition.

These differences between both the characterized materials have also been detected by energy dispersive X-ray (EDX) to carry out the spectroscopy analysis with the S-4800 equipment. Both compositions are mostly based on iron oxide (Fe_2O_3) with a proportion of about 65% and 85% in the case of 304 and 3441 materials, respectively. This fact could imply that 3441 material shows a greater performance to absorb the electromagnetic noise.

One of the most important parameters that describe a material's capacity to absorb electromagnetic noise is the relative permeability (μ_r) [27]. The permeability relates the magnetic flux density to the magnetic field in a defined medium, thus, when an absorber sheet is placed, the magnetic flux is concentrated in it. This is defined by the composite material internal properties and it is represented as through the permeability complex parameter [28]. The losses of the magnetic flux can be quantified by separating it into its complex form, so that the real component (μ') is related to the reflection or inductive part and the imaginary component (μ'') quantifies the effectiveness of the material to absorb the magnetic noise [29]:

$$\mu_r = \mu' - j\mu'' \quad (2)$$

The shielding performance to attenuate or suppress unwanted electromagnetic fields of composite structures can be achieved by the combination of the reflection and absorption losses [30]. The factors that define it are the conductivity, permeability, and thickness of the composite panel, as well as the frequency range of interest. The behavior of these parameters depends on the internal composition of the material. It is usually represented versus the frequency and it can be derived from electromagnetic theory [31,32] as well as obtained experimentally [33,34]. FAS suppress high-frequency noise, making

use of the magnetic loss that is controllable according to the composition and shape of the magnetic material and it is related to the frequency domain separation. Thereby, in order to obtain significant electromagnetic noise attenuation at high-frequency region, it is necessary that the frequency of the ferromagnetic resonance is as high as possible [35].

Therefore, one way of knowing the performance of 3441 and 304 materials is through examining the permeability parameter. Figure 2 represents the relative permeability profiles of 304 and 3441 FAS compositions split into real and imaginary components. As can be observed, 3441 material provided a higher initial permeability (μ_i) than 304 composition, as has been described above, however, both compositions had a high relaxation frequency. Note that relaxation frequency (f_r) is an important parameter because it is the point where real and imaginary parts cross, and thus, the material changes its dominant behavior. The f_r of 3441 material is 163 MHz, whereas the f_r value of 304 material is 2.185 GHz. As can be observed in (b), 3441 composition provided a greater μ'' throughout the frequency range, that is, the ability to absorb electromagnetic noise. The results were obtained with an E4991A Material Analyzer (Keysight, Santa Rosa, CA, USA), together with the 16454A Magnetic Material Text Fixture. This fixture is based on cavity resonance and single-turn inductor theories and allows for measuring the magnetic properties of a material. The sample under test must have a toroidal shape in order to be able to fit inside the fixture, so that a toroidal core is manufactured with the material of each absorber composition. This toroidal sample has an outer diameter of 20 mm, 8 mm of inner diameter, and the thickness is 1 mm. When the sample is placed inside the fixture, an ideal single-turn inductor with no flux leakage is formed; therefore, the permeability can be calculated automatically by the internal software of the equipment from the inductance value of the sample. Thereby, it is possible to obtain direct complex permeability readouts.

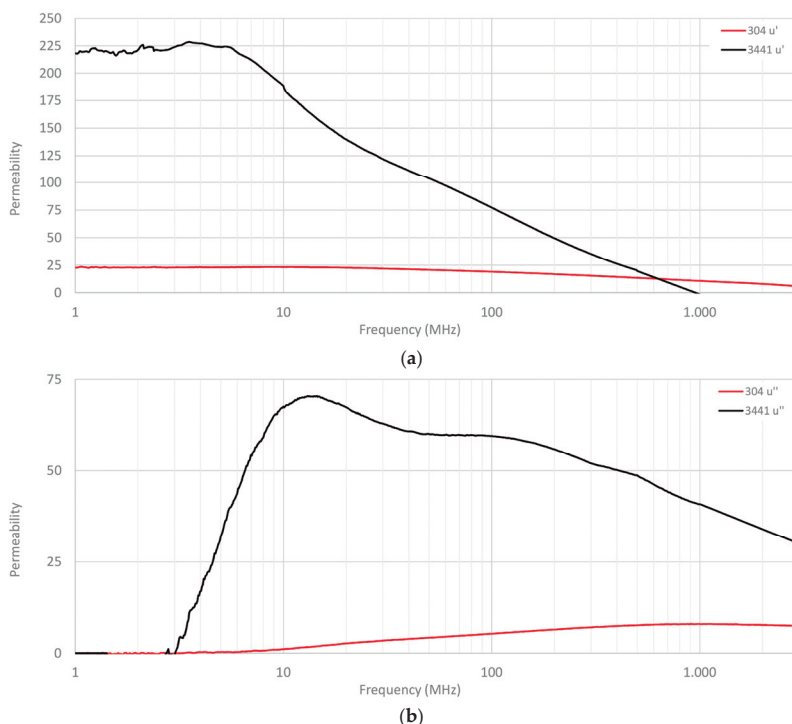


Figure 2. Complex relative permeability profiles of 304 and 3441 materials: (a) real part μ' ; and, (b) imaginary part μ'' .

2.2. Metal Layer Characteristics

Once the FASs had been analyzed and characterized, aluminum and copper metal layers, which were combined with two different absorber compositions, are described in order to study the improvement on the performance of these structures. The metal layers consisted of EMI shielding tapes that were fabricated of a soft aluminum or copper foil backing with an electrically conductive acrylic adhesive. These kinds of materials are usually used for applications that require a great electrical conductivity from the application substrate through the adhesive to the metal surface. Foil tapes with the same dimensions of absorber sheets were used in this study with the aim of covering them completely. In the case of aluminum foil, the surface resistance $R_s = 0.001 \Omega/\text{sq}$ and for copper foil, $R_s = 0.0005 \Omega/\text{sq}$. Both shielding tapes have a thickness $H = 0.04 \text{ mm}$.

2.3. Transmission Attenuation Power Ratio Measurement

Generally, these materials are applied in areas that are very close to the radiation source, thus knowledge of their behavior in the near field region becomes more relevant [1]. This contribution is focused on evaluating the performance of structures based on absorber sheets combined with a metal layer to reduce or suppress conduction electromagnetic noise in the near field range. Consequently, the transmission attenuation power ratio (R_{tp}) was determined following the procedure that is defined in the standard IEC 62333-2 [36] to evaluate the frequency profiles of electromagnetic absorber sheets by using a microstrip line (MSL). The MSL was used as a test fixture for evaluating the attenuation of conducting current noise in a PCB or noise path when a noise suppression sheet is installed. Thereby, the MSL was employed as a transmission line that provides the electromagnetic noise that will be measured to know the sample absorption capability [37].

The standard manufactured MSL with a characteristic impedance of 50Ω was employed in this procedure. The fabricated MSL was based on the characteristics that are described in the standard due to Teflon PTFE substrate with dimensions of 100.0 mm length, 50.0 mm width and 1.6 mm thickness is employed. It consisted of a two layers PCB, where, on the top side, the copper strip conductor with 54.4 mm length, 4.4 mm width, and 0.018 mm thickness is printed. On the bottom side, a ground plane of copper with 0.018 mm thickness is placed and two SMA type connectors are connected are connected one at each end of the strip conductor. The SMA connectors were placed on the bottom layer and they were connected with both ends of the MSL through two vias. These vias are based on a copper conductor that joins different PCB layers; in this case, they are used to join the center conductor of each SMA connector with each end of the strip conductor. The MSL test fixture was used to determine the electromagnetic noise absorbing capability of a certain magnetic film by measuring the reflection and transmission parameters (S_{11} and S_{21} , respectively) with an E5071B Network Analyzer (NA) equipment (Keysight, Santa Rosa, CA, USA), as shown in Figure 3.

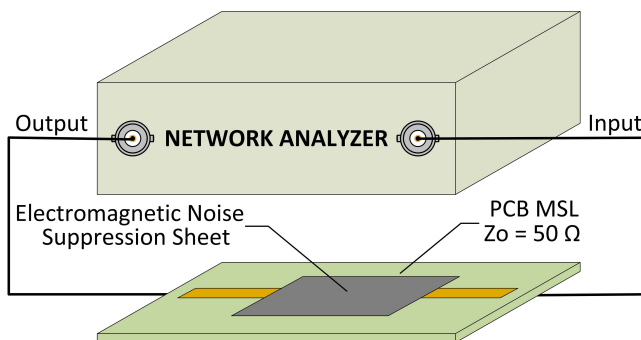


Figure 3. Measurement of reflection and transmission loss through microstrip line (MSL) test fixture.

Once both S_{11} and S_{21} measurements were done, it was possible to calculate the R_{tp} value expressed in decibel units using the equation defined by the standard IEC 62333-2:

$$R_{tp} = -10 \log \left(\frac{10^{S_{21}/10}}{1 - 10^{S_{11}/10}} \right) \text{ dB} \quad (3)$$

where S_{11} is the reflection coefficient, S_{21} is the transmission coefficient, and both parameters are magnitudes in decibels.

The measurement of the MSL transmission characteristics while using a NA made it possible to obtain transmission loss that is associated with magnetic loss of the magnetic material placed on the strip conductor. When a FAS is placed on the transmission line with conducted electromagnetic noise, the high-frequency current is reduced by an additional resistance due to the magnetic dynamic loss [15,38].

2.4. Re-Radiation Measurement Setup

The integration of a metal layer on the absorber sheet could lead to a re-radiation effect, because the electromagnetic noise concentrated into the metal could generate eddy currents that induce a parasitic magnetic flux [39]. Thereby, the measurement of samples re-radiation is presented in the next section with the aim of ensuring they are not emitting an unwanted electromagnetic field. The experimental procedure carried out to evaluate whether the re-radiation parameter was also based on using the MSL as an electromagnetic noise source and the NA equipment, however, in this case, one SMA connector of the MSL was connected to the NA and the other is terminated with a 50 Ω load. A near field probe (NFP) was connected to the second port of the NA and was placed over the center of the strip conductor forming a right angle with it as shown in Figure 4. Subsequently, the S_{21} parameter was evaluated through only measuring the radiated energy by the MSL with the measurement being repeated with the absorber structure placed on the MSL. The distance was set at 1 mm from the strip line to the NFP. Finally, both S_{21} parameters were compared in order to determine if the absorber structure was generating a re-radiation effect.

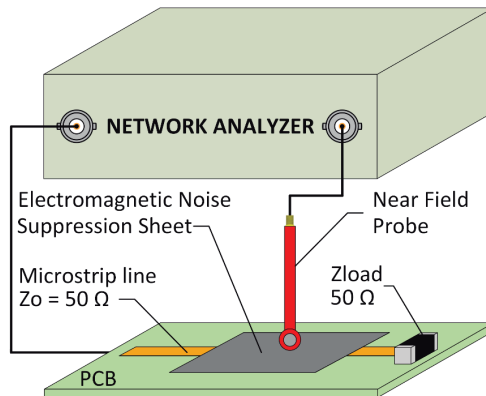


Figure 4. Re-radiation measurement setup.

3. Results and Discussion

Firstly, the transmission attenuation power ratio of both flexible absorber materials under test has been determined accordingly with the IEC standard method. Subsequently, this parameter was also obtained for the structures that are based on an absorber sheet with a metal layer added on its top side in order to analyze the improvement on the performance of these structures, depending on

the complex permeability, absorber film thickness, and type of metal. When considering this, it was possible to evaluate the performance of a high permeability absorber material to provide a solution to filter the conducted electromagnetic noise in the range frequency of 1 MHz to 8.5 GHz and compare it to another material with lower magnetic loss.

3.1. R_{tp} Depending on the Material Composition and Kind of Metal Layer

As has been described in Section 2.3, the transmission attenuation power ratio was determined following the IEC 62333-2 standard based on a microstrip line fixture that simulates a source of electromagnetic conducted interferences. Figure 5 shows the R_{tp} parameter measured when the 304 absorber material with a thickness of 0.3 mm was attached on the microstrip line. The R_{tp} profiles of the structures based on the combination of 304 magnetic film with a Cu layer and Al layer are also represented. This graph demonstrates the ability of the material to attenuate the electromagnetic noise when a metal layer is combined with the 304 absorber composition, being higher than when only the magnetic film is used. Both magnetic and metal structures provided a similar performance, suggesting the difference between combining an Al or a Cu layer with the 304 absorber material is negligible. The structures that combine a metal with an absorber material reached the maximum value about 5 GHz, and, from that frequency, R_{tp} decreased slowly. Nevertheless, 304 profile continuously increased throughout the frequency spectrum analyzed and provided a greater attenuation than the metal and magnetic absorber structures from 7.5 GHz. Note that the maximum difference of R_{tp} between the absorber sheet 304 and both structures based on 304 material with a metal layer attached was about 25 dB and it is taken at 4.8 GHz.

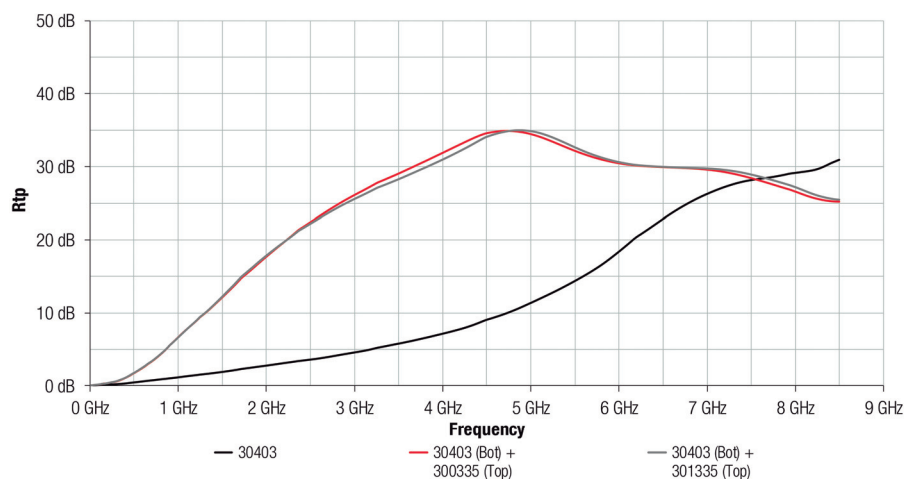


Figure 5. R_{tp} of 30403 absorber sheet without any metal layer (black), 30403 absorber sheet with a Cu layer attached (red) and 30403 absorber sheet with a Al layer attached (grey).

This measurement has been repeated, but in this case, using the 3441 magnetic film that provides a higher permeability than the 304 composition. Figure 6 shows the R_{tp} parameter measured when the 3441 absorber material with a thickness of 0.3 mm was attached on the MSL and when it is combined with a Cu or Al layer. If the 3441 profile is compared to the absorption ability that is provided by 304 composition, it might be concluded that 3441 shows a greater attenuation than 304 up to 6 GHz. Due to its higher permeability, 3441 composition was able to provide a very high attenuation at lower frequencies than 304, reaching the maximum R_{tp} close to 6 GHz. This material provided an abrupt increase at low frequencies, rising to 45 dB from 0 GHz to 2 GHz. From 2 GHz, 3441 trace decreased gradually, providing a higher value of R_{tp} up to 6 GHz than 304 composition. With regard to the effect

of placing an Al or a Cu layer on the 3441 magnetic film, the difference between using a copper layer or aluminum layer were negligibly low, similarly to when a metal layer was combined with 304 absorber sheet, as shown in Figure 5. Another factor that is important to highlight from Figure 6 is that all traces show a similar profile in contrast to Figure 5 where structures based on metal and 304 magnetic film provided a different performance from the 304 composition. This suggests that the performance of 3441 material is not improved when a metal layer is attached on it because of the higher magnetic losses given by 3441 magnetic material.

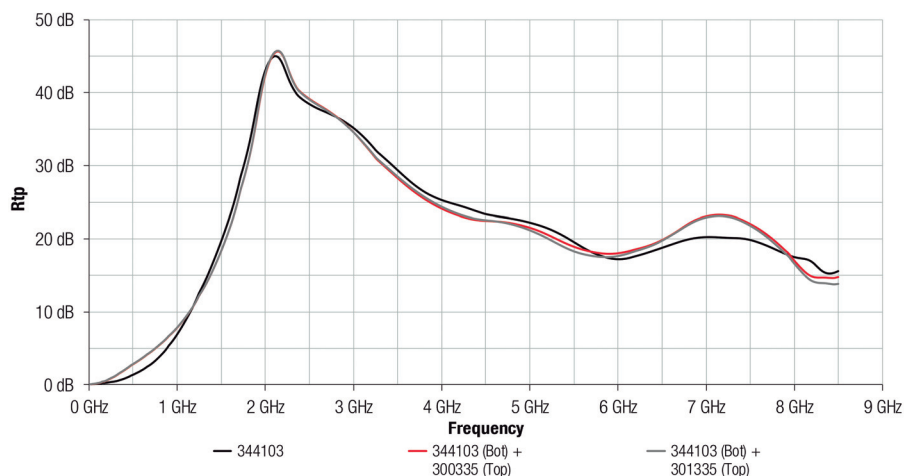


Figure 6. R_{tp} of 344103 absorber sheet without any metal layer (black), 344103 absorber sheet with a Cu layer attached (red,) and 344103 absorber sheet with a Al layer attached (grey).

3.2. R_{tp} Depending on the Material Composition and the Absorber Sheet Thickness

As can be observed from data shown in the last subsection, 304 and 3441 electromagnetic absorber materials did not provide the same behavior when combined with a metal layer. Thereby, 304 composition was analyzed depending on its sheet thickness and combining it with an Al layer, as shown in Figure 7. This graph demonstrates how the greater the thickness of the FAS, generally, the greater the attenuation offered. As regards magnetic films, the maximum R_{tp} value was about 50 dB and was provided by 30405 (0.5 mm thickness) and 30410 (1.0 mm thickness) at 6.3 GHz and 5.0 GHz, respectively. Thus, materials with the same composition were able to offer the same maximum value of attenuation, although when the sheet thickness was increased, and, therefore, the magnetic loss, the maximum peak appeared at lower frequencies. The maximum difference between FAS with metal structures and FAS was 23 dB at 4.8 GHz, in the case of 30403 material; 13 dB at 3.0 GHz for 30405; and, 4.7 dB at 5.0 GHz for 30410. These results suggest that the improvement on the FAS performance with the metal layer attached is more significant when the FAS thickness is lower. Note also that the presence of the metal layer on the absorber generally improved its attenuation performance at lower frequencies.

Figure 8 shows the same comparison, between FAS and FAS with metal structures, as the previous graph, but in this case, the FAS material analyzed corresponds to the 3441 composition. It can be observed how the difference between FAS and FAS with Al structures is significant in the case of thinner sheets: 3441005 (0.05 mm) and 344101 (0.1 mm). Similar to 304 composition, the presence of the metal layer attached on the absorber improved the attenuation performance at lower frequencies for 3441005 and 344101. Specifically, for 344102, the traces were very similar, but the attachment of the metal layer on the absorber improved the maximum peak of R_{tp} provided by 10 dB. However, for the

3441 composition the difference between FAS and FAS with Al structures was practically negligible for sheets with thickness higher than 0.2 mm. Because the 3441 material offers greater magnetic characteristics than 304 material, the effect of placing the metal layer was less significant than 304 in lower sheet thickness. In the case of 304, the effect of metal layer was negligible above 0.5 mm sheet thickness, whereas for the 3441 composition this happened above 0.3 mm sheet thickness.

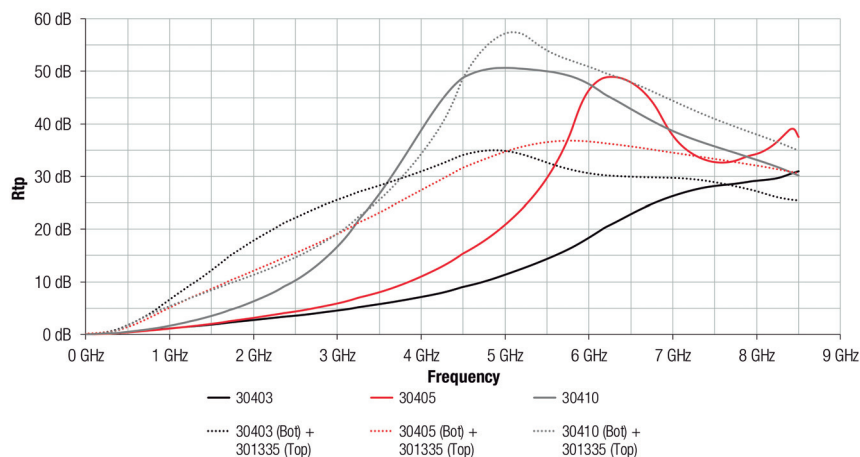


Figure 7. R_{tp} of 304 absorber material with different thicknesses and Al layer integrated.

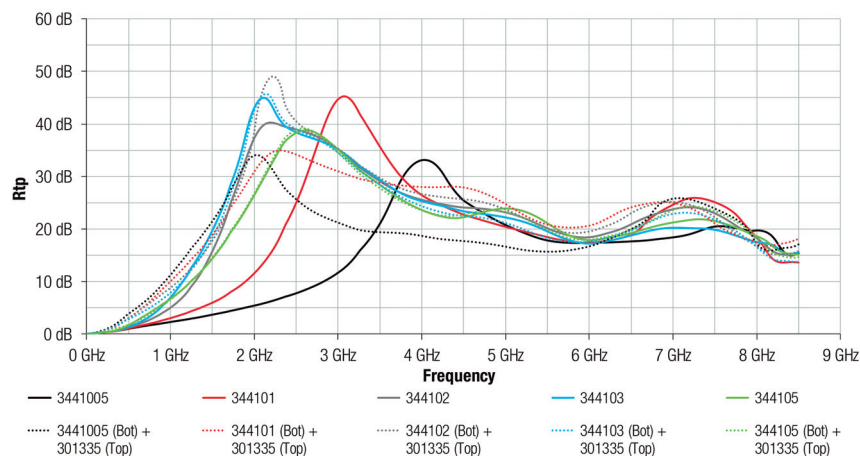


Figure 8. R_{tp} of 3441 absorber material with different thicknesses and Al layer integrated.

3.3. Re-Radiation Analysis

The results of the 304 composition re-radiation based on the measurement setup described in Section 2.4 are shown in Figure 9. From the figure, it is obvious that the ratio of re-radiation from the FAS with metal structure was negligibly low, because, in all thicknesses, when the Al layer was attached on the FAS, the radiated emissions were reduced. For instance, the 30403 composition is similar to the reference (yellow trace) electromagnetic noise measured without any sample placed on the MSL up to 3 GHz. From this frequency point, the difference between re-radiation reference trace and re-radiation with 30403 magnetic film is increasing. On the other hand, the structure of

30403 FAS and Al layer reduced the re-radiation ratio by about 30 dB up to 3 GHz and by about 10 dB at higher frequencies.

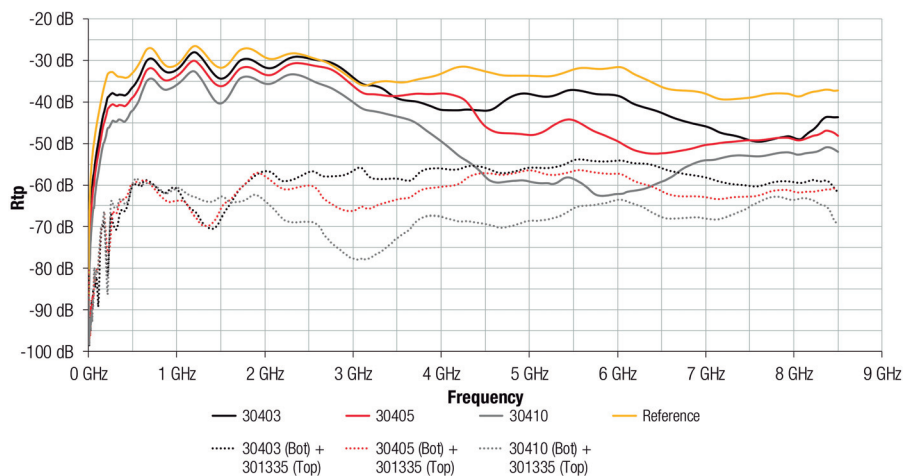


Figure 9. Re-radiation parameter of 304 absorber material with different thicknesses and Al layer integrated.

Figure 10 shows the same comparison as Figure 9, but in this case, 3441 composition is evaluated in terms of re-radiation. The results suggest the same conclusion obtained for 304 material because all the traces show a re-radiation value lower than the reference trace measured without any sample on the MSL. Generally, when the Al layer was combined with the FAS, the re-radiation was reduced. When comparing the 3441 0.3 mm samples, the attenuation of FAS sample was higher from 1 GHz than 304 composition. When the Al layer was attached, this reduction is about 30 dB up to 3 GHz and about 10 dB at higher frequencies.

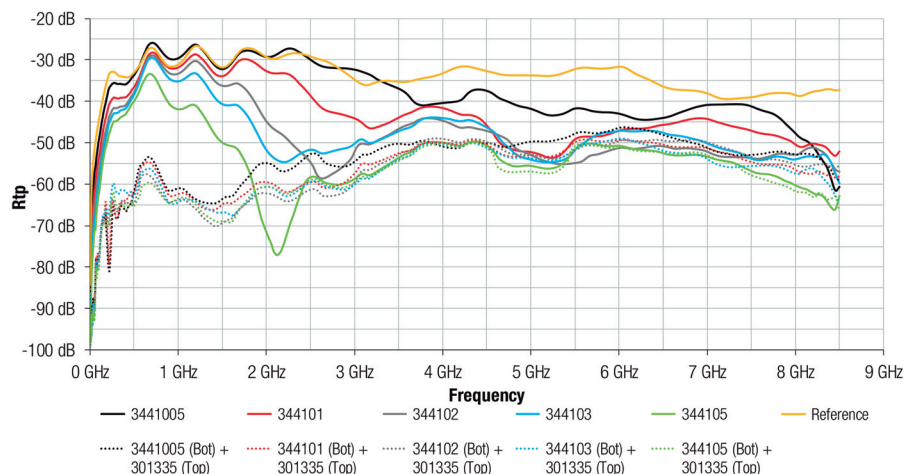


Figure 10. Re-radiation parameter of 3441 absorber material with different thicknesses and Al layer integrated.

4. Conclusions

The noise absorbing properties of two kinds of flexible absorber sheets were analyzed in order to study the improvement on their performance when they are combined with a metal layer. Copper and aluminum layers were combined with both absorber materials and similar results were obtained, so that Al layer were selected to carry out more tests due to it usually representing a more common material and it offers a more competitive cost than Cu.

In terms of R_{tp} , 3441 composition provides a higher performance in the whole frequency spectrum because of it provides a higher magnetic loss than 304 composition. This result matches the relative permeability profiles that are provided for each material. Thus, it is also observed that the higher the thickness of absorber sheet, the higher the attenuation. With regard to the attachment of a metal layer on the absorber material, the results show that the improvement on the performance is more significant in the absorber materials with low magnetic loss. It has been observed when the metal layer has been added in the 30403 material due to the R_{tp} has been increased about 25 dB in the maximum point. Nevertheless, it has not been observed any change when the high-permeability 344103 sheet with a metal layer attached has been analyzed.

Another conclusion that was obtained from the results, is related to the effect of placing a metal layer depending on the thickness of the absorber sheet. It has been proved that an absorber sheet with low thickness shows a greater R_{tp} when the metal sheet is added. This suggests that the performance of absorbers with higher magnetic loss and thickness is not improved when the metal layer is integrated. This demonstrates that the improvement on the performance is negligible when a conductive layer is placed on a thicker absorber sheet, since the magnetic loss that is provided by the absorber is much more significant than the losses provided by the metal layer. Thus, the use of a metal layer provides a higher shielding effectiveness when it is attached to those sheets with low thickness. Accordingly, with this last point, the use of FAS and metal structure makes it possible to save space at the same time that provides high absorption loss without resorting to high-thickness absorber sheets.

Finally, the re-radiation parameter has been analyzed with the aim of ensuring that the presence of a metal layer on the absorber material does not lead to inducing a parasitic magnetic flux. It has been determined that placing the FAS and metal structure, not only it does not re-radiate, but also this combination decreases largely the level of electromagnetic radiated emissions measured in the near field. This is because the isolation is greatly increased when the metal layer is attached on the absorber sheet. Therefore, this opens the way for using the FAS and metal combination in applications with problems that are related to magnetic decoupling.

Author Contributions: Conceptualization, J.V., A.S. and J.T.; Formal analysis, J.V., P.A.M., R.G.-O. and J.S.; Investigation, J.V., A.S., P.A.M., A.A. and J.M.; Methodology, P.A.M., A.A. and J.M.; Project administration, J.T., S.M. and A.G.; Supervision, J.T.; Writing—original draft, J.V., A.S. and J.T.; Writing—review & editing, A.S., J.T., P.A.M., J.M., R.G.-O., J.S., S.M. and A.G.

Acknowledgments: This work was supported by the Catedra Würth-EMC, a research collaboration agreement between the University of Valencia and Würth Elektronik eiSos GmbH & Co. KG.

Conflicts of Interest: The authors declare no conflict of interest. The founding sponsors had no role in the design of the study; in the collection, analyses, or interpretation of data; in the writing of the manuscript, and in the decision to publish the results.

References

1. Piersanti, S.; de Paulis, F.; Orlandi, A.; Connor, S.; Liu, Q.; Archambeault, B.; Dixon, P.; Khorrami, M.; Drewniak, J.L. Near-Field Shielding Performances of EMI Noise Suppression Absorbers. *IEEE Trans. Electromagn. Compat.* **2017**, *59*, 654–661. [[CrossRef](#)]
2. Paul, C.R. *Introduction to Electromagnetic Compatibility*, 2nd ed.; Wiley Interscience: Hoboken, NJ, USA, 2006; ISBN 978-047-175-500-5.
3. Matsushita, N.; Nakamura, T.; Abe, M. Spin-sprayed Ni–Zn–Co ferrite films with high $\mu_r > 100$ in extremely wide frequency range 100 MHz–1 GHz. *J. Appl. Phys.* **2003**, *93*, 7133–7135. [[CrossRef](#)]

4. Idris, F.M.; Hashim, M.; Abbas, Z.; Ismail, I.; Nazlan, R.; Ibrahim, I.R. Recent developments of smart electromagnetic absorbers based polymer-composites at gigahertz frequencies. *J. Magn. Magn. Mater.* **2016**, *405*, 197–208. [[CrossRef](#)]
5. Nisanci, M.H.; De Paulis, F.; Di Febo, D.; Orlandi, A. Synthesis of composite materials with conductive aligned cylindrical inclusions. In Proceedings of the Progress in Electromagnetics Research Symposium (PIERS), Kuala Lumpur, Malaysia, 27–30 March 2012; pp. 646–649.
6. Lal, K.; Singh, V. Broad-Band EMI Suppression Absorber. In Proceedings of the Antenna Test & Measurement Society (ATMS India—2017), Hyderabad, India, 6–8 February 2017.
7. Koledintseva, M.Y.; Drewniak, J.L.; DuBroff, R.E.; Rozanov, K.N.; Archambeault, B. Modeling of shielding composite materials and structures for microwave frequencies. *Prog. Electromagn. Res. B* **2009**, *15*, 197–215. [[CrossRef](#)]
8. Nisanci, M.H.; de Paulis, F.; Di Febo, D.; Orlandi, A. Sensitivity analysis of electromagnetic transmission, reflection and absorption coefficients for biphasic composite structures. In Proceedings of the 2014 International Symposium on Electromagnetic Compatibility (EMC Europe), Gothenburg, Sweden, 1–4 September 2014; pp. 438–443.
9. De Paulis, F.; Nisanci, M.H.; Koledintseva, M.Y.; Drewniak, J.L.; Orlandi, A. Derivation of homogeneous permittivity of composite materials with aligned cylindrical inclusions for causal electromagnetic simulations. *Prog. Electromagn. Res. B* **2012**, *37*, 205–235. [[CrossRef](#)]
10. Nisanci, M.H.; De Paulis, F.; Orlandi, A. Synthesis of composite materials with conductive and/or lossy spherical inclusions. In Proceedings of the 2013 International Symposium on Electromagnetic Compatibility (EMC Europe), Brugge, Belgium, 2–6 September 2013; pp. 593–598.
11. Shimada, Y.; Yamaguchi, M.; Ohnuma, S.; Itoh, T.; Li, W.D.; Ikeda, S.; Kim, K.H.; Nagura, H. Granular thin films with high RF permeability. *IEEE Trans. Magn.* **2003**, *39*, 3052–3056. [[CrossRef](#)]
12. Rizza, C.; Ciattoni, A.; De Paulis, F.; Palange, E.; Orlandi, A.; Columbo, L.; Prati, F. Reconfigurable photoinduced metamaterials in the microwave regime. *J. Phys. D Appl. Phys.* **2015**, *48*, 135103. [[CrossRef](#)]
13. De Paulis, F.; Nisanci, M.H.; Orlandi, A.; Koledintseva, M.Y.; Drewniak, J.L. Design of homogeneous and composite materials from shielding effectiveness specifications. *IEEE Trans. Electromagn. Compat.* **2014**, *56*, 343–351. [[CrossRef](#)]
14. Ryu, G.B.; Kim, S.S. Numerical analysis on power loss mechanism of $\text{Fe}_{55}\text{Al}_{18}\text{O}_{27}$ thin films for conduction noise through microstrip line. *J. Appl. Phys.* **2009**, *105*, 07A5081–07A5083. [[CrossRef](#)]
15. Yoshida, S.; Ono, H.; Ando, S.; Tsuda, F.; Ito, T.; Shimada, Y.; Masumoto, T. High-frequency noise suppression in downsized circuits using magnetic granular films. *IEEE Trans. Magn.* **2001**, *37*, 2401–2403. [[CrossRef](#)]
16. Hayt, W.H.; Buck, J.A. *Engineering Electromagnetics*; McGraw-Hill: New York, NY, USA, 2001; ISBN 978-007-338-066-7.
17. Ott, H.W. *Electromagnetic Compatibility Engineering*; John Wiley & Sons: Hoboken, NJ, USA, 2009; ISBN 978-04-7050-850-3.
18. Kondo, K.; Chiba, T.; Ono, H.; Yoshida, S.; Shimada, Y.; Matsushita, N.; Abe, M. Conducted noise suppression effect up to 3 GHz by NiZn ferrite film plated at 90 °C directly onto printed circuit board. *J. Appl. Phys.* **2003**, *93*, 7130–7132. [[CrossRef](#)]
19. Kim, S.T.; Cho, H.S.; Kim, S.S. Conducted noise attenuation by iron particles-rubber composites attached on microstrip line. In Proceedings of the IEEE International Magnetism Conference (INTERMAG), Nagoya, Japan, 4–8 April 2005; pp. 1101–1102.
20. Kim, S.; Park, Y.; Kim, S. The influence of magnetic and dielectric loss on the noise absorption of iron particles-rubber composites attached to a microstrip line. *Met. Mater. Int.* **2008**, *14*, 233–237. [[CrossRef](#)]
21. Kim, S.; Kim, S. Conduction noise absorption by ITO thin films attached to microstrip line utilizing Ohmic loss. *J. Appl. Phys.* **2010**, *108*, 0249041–0249046. [[CrossRef](#)]
22. Kim, S. Conduction noise absorption by Sn-O thin films on microstrip lines. *Korean J. Met. Mater.* **2011**, *49*, 329–333. [[CrossRef](#)]
23. Lovat, G.; Burghignoli, P.; Celozzi, S. Shielding Properties of a Wire-Medium Screen. *IEEE Trans. Electromagn. Compat.* **2008**, *50*, 80–88. [[CrossRef](#)]
24. Silveirinha, M.; Fernandes, C. Effective Permittivity of Metallic Crystals: A Periodic Green's Function Formulation. *Electromagnetics* **2003**, *23*, 647–663. [[CrossRef](#)]

25. Diaz, R.E.; Merrill, W.M.; Alexopoulos, N.G. Analytic framework for the modeling of effective media. *J. Appl. Phys.* **1998**, *84*, 6815–6826. [[CrossRef](#)]
26. Koledintseva, M.; Rawa, P.C.; Dubroff, R.; Drewniak, J.; Rozanov, K.; Archambeault, B. Engineering of composite media for shields at microwave frequencies. In Proceedings of the 2005 International Symposium on IEEE Electromagnetic Compatibility, Chicago, IL, USA, 8–12 August 2005; pp. 169–174.
27. Goldman, A. *Modern Ferrite Technology*, 2nd ed.; Springer Science & Business Media: Pittsburgh, PA, USA, 2006; ISBN 978-0-387-28151-3.
28. Suarez, A.; Victoria, J.; Alcarria, A.; Torres, J.; Martinez, P.A.; Martos, J.; Soret, J.; Garcia-Olcina, R.; Muetsch, S. Characterization of Different Cable Ferrite Materials to Reduce the Electromagnetic Noise in the 2–150 kHz Frequency Range. *Materials* **2018**, *11*, 174. [[CrossRef](#)] [[PubMed](#)]
29. Sharma, A.; Rahman, N.; Obol, M.; Afsar, M. Precise characterization and design of composite absorbers for wideband microwave applications. In Proceedings of the European Microwave Conference, Paris, France, 28–30 September 2010; pp. 160–163.
30. Brander, T.; Gerfer, A.; Rall, B.; Zenkner, H. *Trilogy of Magnetics: Design Guide for EMI Filter Design, SMP & RF Circuits*, 4th ed.; Swiridoff Verlag: Künzelsau, Germany, 2010; ISBN 978-3-89929-157-5.
31. Nisanci, M.H.; De Paulis, F.; Koledintseva, M.Y.; Drewniak, J.L.; Orlandi, A. From Maxwell Garnett to Debye Model for Electromagnetic Simulation of Composite Dielectrics-Part II: Random Cylindrical Inclusions. *IEEE Trans. Electromagn. Compat.* **2012**, *54*, 280–289. [[CrossRef](#)]
32. De Paulis, F.; Nisanci, M.; Koledintseva, M.Y.; Drewniak, J.L.; Orlandi, A. From Maxwell Garnett to Debye Model for Electromagnetic Simulation of Composite Dielectrics Part I: Random Spherical Inclusions. *IEEE Trans. Electromagn. Compat.* **2011**, *53*, 933–942. [[CrossRef](#)]
33. Nicolson, A.M.; Ross, G.F. Measurement of the Intrinsic Properties of Materials by Time-Domain Techniques. *IEEE Trans. Instrum. Meas.* **1970**, *19*, 377–382. [[CrossRef](#)]
34. Barry, W. A Broad-band, automated, stripline technique for the simultaneous measurement of complex permittivity and permeability. *IEEE Trans. Microw. Theory Tech.* **1986**, *34*, 80–84. [[CrossRef](#)]
35. Yoshida, S.; Kondo, K.; Ono, H. High-frequency noise suppression using ferrite-plated film. *NEC Tech. J.* **2006**, *1*, 77–81.
36. International Electrotechnical Commission. IEC 62333-2: 2006 (E), *Noise Suppression Sheet for Digital Devices and Equipment Part 2: Measuring Methods*; IEC: Geneva, Switzerland, 2006; ISBN 978-288-912-593-7.
37. Suarez, A.; Victoria, J.; Alcarria, A.; Torres, J. Characterization of electromagnetic noise suppression sheet for aerospace applications. In Proceedings of the ESA Workshop on Aerospace EMC, Valencia, Spain, 23–25 May 2016; pp. 1–6.
38. Tsuda, F.; Ono, H.; Shinohara, S.; Sato, R. Effect of installing magnetic-polymer-composite sheeting on transmission line to suppress conducted-electromagnetic noise. In Proceedings of the 2005 International Symposium on IEEE Electromagnetic Compatibility, Washington, DC, USA, 21–25 August 2000; pp. 867–870.
39. Ono, H.; Ito, T.; Yoshida, S.; Takase, Y.; Hashimoto, O.; Shimada, Y. Noble magnetic films for effective electromagnetic noise absorption in the gigahertz frequency range. *IEEE Trans. Magn.* **2004**, *40*, 2853–2857. [[CrossRef](#)]



5.3 Scientific conference article IV: Designing the layers structure

Title: Board-level shielding with magnetic absorber sheet.

Authors: Jorge Victoria, Adrián Suárez, Pedro A Martínez, Antonio Alcarria, Andrea Amaro, José Torres.

Published in: 2022 International Symposium on Electromagnetic Compatibility - EMC EUROPE, IEEE. Gothenburg, Sweden.

DOI: 10.1109/EMCEurope51680.2022.9901317

Description: The International Symposium on Electromagnetic Compatibility - EMC EUROPE is an international conference with a high scientific level supported by IEEE and the EMC Society. It is an annual conference that promotes EMC research, innovation and international cooperation. The submitted contributions are subjected to the peer review process to assess the quality of the manuscript before it is published in the IEEE Xplore database, one of the most comprehensive interdisciplinary engineering databases in the world.

Synopsis:

This contribution was presented at the 2022 "IEEE EMC Europe" conference. In it, we evaluate the possibility, based on the results of the previous article, of using a combination of an NSS sheet, a metal sheet, and an adhesive sheet for electromagnetic shielding in printed circuit boards.

The classical solution for PCB shielding is an open-sided metal box covering the area of the PCB that requires shielding. It must be soldered to a ground plane covering the sixth side of the box, thus forming a Faraday cage. By combining the magnetic absorption of the NSS with the reflection and absorption effects of eddy currents from the metal layer, we aim to achieve an equally effective solution with practical improvements in design and application.

To evaluate and compare the electromagnetic shielding effectiveness of both solutions, we designed an experiment based on a printed circuit that generates electromagnetic fields over a wide frequency range and allows for the insertion of different solutions. Measurements are taken using an EMScan device connected to a spectrum analyzer.

The shielding results obtained with a metal box soldered to the ground plane (classical BLS solution), NSS sheets, and various combinations of NSS sheets of different thicknesses, as well as aluminum and copper sheets, are compared. It is concluded that the combination of NSS with metal provides greater attenuation over a wider frequency range than NSS alone, and there are no significant differences between the use of

aluminum or copper. The results of the hybrid compound are comparable, although inferior to those obtained with the metal box. However, the compound has the advantage of not requiring a specifically designed printed circuit for proper soldering to the reference plane, making it an interesting solution without the need for redesign.

Board-level shielding with magnetic absorber sheet

Jorge Victoria
Product Management
Würth Elektronik eiSos
Waldenburg, Germany
jorge.victoria@we-online.de

Adrian Suarez
Department of Electronic Engineering
University of Valencia
Valencia, Spain
0000-0002-4961-9627

Pedro A. Martinez
Department of Electronic Engineering
University of Valencia
Valencia, Spain
pedro.a.martinez@uv.es

Antonio Alcarria
Product Management
Würth Elektronik eiSos
Waldenburg, Germany
antonio.alcarria@we-online.de

Andrea Amaro
Department of Electronic Engineering
University of Valencia
Valencia, Spain
andrea.amaro@uv.es

Jose Torres
Department of Electronic Engineering
University of Valencia
Valencia, Spain
jose.torres@uv.es

Abstract— The ongoing trend to miniaturize electronic devices with the aim of providing more advanced functionalities and greater performances makes the detection of electromagnetic interference (EMI) a recurring problem. These requirements result in design restrictions that make it complicated to use basic EMI shielding techniques. Consequently, innovative shielding solutions are needed. Thereby, the board-level shielding (BLS) solutions are widely used in printed circuit board (PCB) applications to reduce the intra-system EMI of integrated circuits (ICs) and improve the immunity of the electronic devices. This contribution focuses on analyzing a magnetic absorber sheet combined with a metal layer as a board-level shield solution. Using this combination is expected to obtain higher shielding effectiveness than using only a magnetic sheet by obtaining the absorbing properties of the magnetic material and the losses mechanism of a metal, such as reflection and eddy current losses. One of the main advantages of using this hybrid structure is that it does not require redesigning the electronics since it can be stuck over the EMI source. Therefore, a magnetic material with different thicknesses is combined with metal layers. These hybrid combinations are compared with the performance of a shielding cabinet in order to determine its performance. The results presented are based on the spectral and spatial magnetic near-field distribution measurement.

Keywords— board-level shielding (BLS), hybrid material, magnetic near-field, magnetic absorber sheet, conductive shielding

I. INTRODUCTION

The continuous implementation of new advanced functionalities and the miniaturization of electronic devices for embedded systems has become a serious difficulty in terms of electromagnetic compatibility (EMC). This evolution usually involves the use ICs that operates with high-frequency clocks, the integration of communication circuits, the reduction of the device housing, and, thus, the reduction of PCB size and thickness that leads to a higher component integration [1]. These design principles are often used to achieve a device with better performance and features. However, they increase the likelihood of generating complex EMI problems. The undesired magnetic decoupling between two near circuits, where a noisy IC or component generates a stray field that affects another near component that acts like a victim, represents one of these problems [2]. Fig. 1(a) shows an example of EMI problems caused by near-field interferences between elements of the same PCB (intra-decoupling) and Fig. 1(b) when the interference is produced between two electronic circuits placed one on top of the other (inter-decoupling).

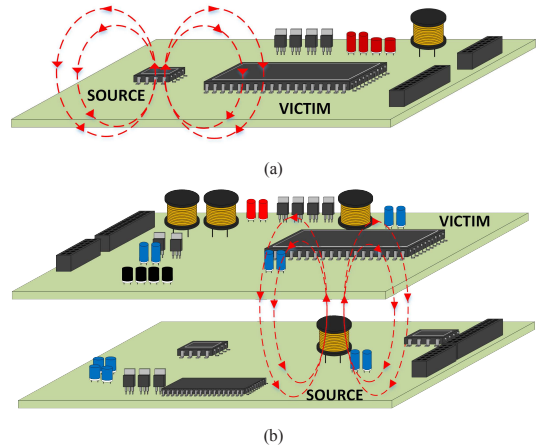


Fig. 1. Representation of EMI problems in the board-level caused by an underused magnetic decoupling. (a) Intra-decoupling problem. (b) Inter-decoupling problem.

Thereby, the use of board-level shields to control the interferences emitted by a certain noisy IC or component inside a PCB is continuously growing [3]. Some of the most relevant techniques for determining the shielding effectiveness (SE) of a board-level shield (BLS) are under examination in the IEEE collaborative project P2716 Guide for the Characterization of the Effectiveness of Printed Circuit Board Level Shielding [4]. One of the most widely used BLS solutions consists of a shielding cabinet, a metal case that helps to isolate a component or a specific area of the PCB by forming a Faraday cage, providing five of the necessary six walls [5]. The shielding cabinet should be connected to the ground plane of the PCB to obtain the sixth wall that encloses completely the component to be shielded. Another widely used shielding solution is applying magnetic absorber sheets (also known as noise suppression sheets), although this solution does not usually attenuate the shielding cabinet [6]. In this contribution, we analyze the performance of a hybrid shielding solution based on combining a magnetic absorber material with a conductive layer as an alternative solution to reduce near-field interferences. The main advantage of this BLS construction is that it can be applied over a noisy IC or component without a redesign of the PCB since it does not need to introduce a footprint.

Consequently, the SE of this hybrid shielding solution is analyzed by comparing it with the results obtained by other BLS, such as a magnetic absorber sheet or a shielding cabinet.

This comparison is carried out by measuring the spatial magnetic near-field distribution and the spectral response.

II. HYBRID BLS CHARACTERIZATION

The magnetic absorber material selected to be combined with a conductive layer is a host matrix of ferrite-polymer composites based on a silicon rubber matrix with embedded inclusions. These inclusions are iron particles in the form of flakes prepared by the mechanical forging of spherical iron powders while using an attrition mill. When the inclusions and the spatial periods are tiny compared with the wavelength of the electromagnetic field generated by the noise source, the composite materials can be considered homogeneous materials [7], [8]. Hence, this kind of material can be characterized by the inclusions' geometrical and physical properties, the host medium, and the orientation of the inclusions regarding the host matrix. From the standpoint of the magnetic properties, the material used in this research provides an initial permeability $\mu_i = 38$, as shown in Fig. 2. It is interesting to analyze the material in terms of the complex relative permeability that separates the μ_r into the real and imaginary components. The real component μ_r' represents the inductance ability of the material to concentrate and redirect the magnetic flux. Otherwise the imaginary component μ_r'' quantifies the losses or effectiveness to absorb the interferences [9].

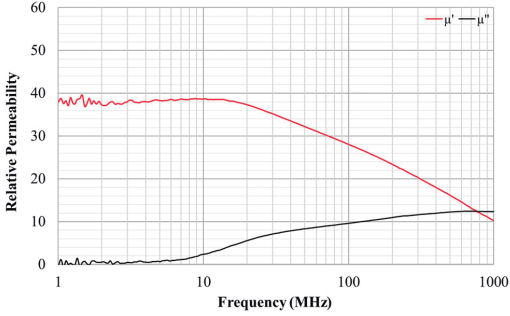


Fig. 2. Relative permeability of the magnetic absorber material analyzed.

The dielectric properties also influence these materials since they can also play a non-negligible role in field distribution. Fig. 3. shows the permittivity components measured by using a parallel conducting plates fixture connected to a material analyzer equipment.

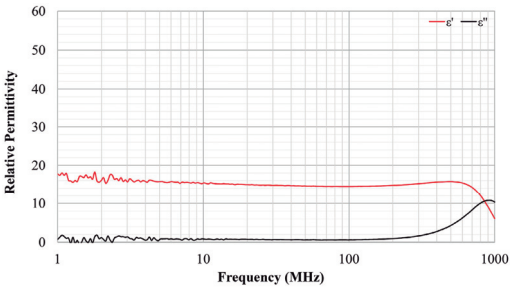


Fig. 3. Relative permittivity of the magnetic absorber material analyzed.

The conductive material that is attached to the magnetic absorber sheet is based on a metal layer of copper (surface

resistance, $R_s = 0.0005 \Omega/\text{sq}$) or aluminum ($R_s = 0.001 \Omega/\text{sq}$), having a thickness, $t = 0.04 \text{ mm}$.

Thereby, the magnetic material yields attenuation mainly through the losses determined by its magnetic properties, whereas the metal layer can reduce the interferences by means of the eddy currents induced on the metal and providing attenuation through the reflection mechanism. The use of magnetic materials also prevents the appearance of stray fields because the electromagnetic noise concentrated into the metal layer could generate eddy currents that induce a parasitic magnetic flux and could cause undesired interferences by the re-radiation mechanism [7].

III. MEASUREMENT SETUP

The distribution of the magnetic field is measured with an EM scanner (ISM-L4G-Xi-M7). This system is a passive device that couples the near-field emissions received from a device under test (DUT). Subsequently, the scanner measures the emissions generated by the EMI source PCB that integrates an oscillator IC in the bottom layer that provides a 40 MHz square signal. This signal is propagated through a spiral track that is implemented in the top layer of the PCB. Thereby, this PCB acts as an EMI interference source that emits a certain field that is acquired with the scanner. The measurement of the coupled field caused by the EMI source PCB are carried out with a spectrum analyzer synchronized with the scanner, as shown in Fig. 4. The software used (EMxpert) compensates the insertion loss of each matrix probe that composes the scanner throughout the frequency range analyzed to display a proportional H-field value in terms of the amplitude (dBuV) provided by each of the cells of the scanner. Each scanner cell corresponds to an individual near field probe (NFP), and it is spaced 7.5 mm in array distribution, providing an effective resolution of 3.75 mm [10]. The measurements obtained from the scanner are represented through the frequency spectrum and the spatial near-field magnetic radiation diagram. The frequency range considered to measure the H-field generated by the EMI source PCB with the scanner is 10-750 MHz with a resolution bandwidth of 100 kHz and without introducing an attenuator factor. The max-hold trace detector determines the H-field acquisition of each cell. The starting frequency has been selected below the fundamental harmonic of the oscillator. The surroundings limit the upper frequency to 750 MHz since RF signals are coupled in the measurement setup.

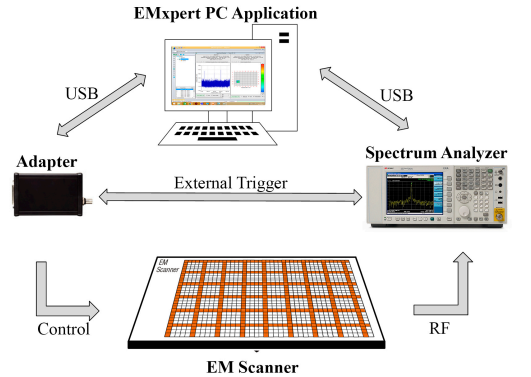


Fig. 4. EM Scanner measurement setup.

In order to keep the exact distance between the scanner surface and the EMI source PCB, a 5 mm fixed gap has been introduced. The characterization is performed by placing the EMI source PCB on the selected area of the EM scanner in order to measure the field emitted considering four scenarios:

- 1) Reference measurement without applying any shielding.
- 2) Measuring the field when the magnetic absorber sheet is applied.
- 3) Measuring the field when the hybrid magnetic and conductive structure is applied.
- 4) Measuring the field with the shielding cabinet soldered to the EMI source PCB.

Therefore, the board-level shielding solutions are applied on the spiral track located at the top layer, between the scanner and the EMI source PCB. Fig. 5 shows the four analyzed scenarios to determine the SE provided by each of the solutions considered.

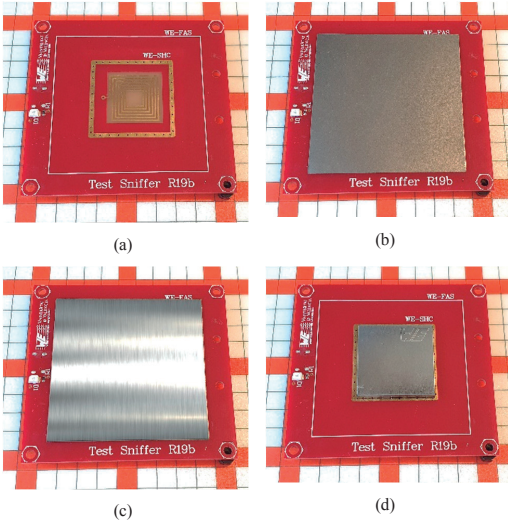


Fig. 5. Setup of the EMI source PCB considering the four measurement scenarios. (a) Reference measurement without applying any BLS (top view). (b) Magnetic absorber sheet applied. (c) Hybrid construction by combining a magnetic absorber material with a conductive layer attached. (d) Shielding cabinet applied.

IV. RESULTS AND DISCUSSION

This section focuses on showing the results corresponding to the measurement of the magnetic field emitted by the EMI source PCB considering the four scenarios described in Section III. A comparison of the SE provided by a magnetic absorber material with different sheet thicknesses combined with several conductive layers. Finally, the performance of the best hybrid combination of magnetic and conductive materials is compared with the results provided by a shielding cabinet.

Firstly, the behavior of the EMI source PCB without applying any board-level shielding solution (reference value) is performed in order to show the reference signal. Fig. 6 shows the spatial magnetic near-field distribution measurement and the frequency spectrum. The worst radiation value (red color) represented in the spatial magnetic near-field distribution diagram corresponds with the highest harmonic peak (64.3 dBuV @200 MHz).

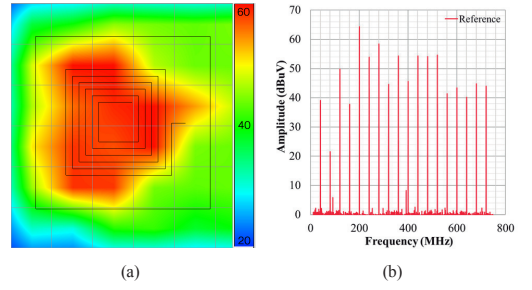


Fig. 6. Near-field radiated emissions of the EMI source PCB measured with the EM scanner. (a) Spatial magnetic near-field distribution. (b) Frequency spectrum.

The first study case is the measurement of the EMI source PCB by applying a magnetic absorber sheet with $t = 0.2$ mm, as is shown in Fig. 7(a). Thereby, this material is combined with an aluminum layer of 0.04 mm (Fig. 7(b)) and a copper layer of 0.04 mm (Fig. 7(c)). By comparing the reference value with the field emitted by the EMI source PCB when it is shielded by applying the magnetic absorber sheet, it is possible to observe that the maximum radiation (64.3 dBuV) is reduced up to 53.3 dBuV. When the conductive layer is attached to the magnetic absorber sheet, the near-field measured is significantly reduced up to about 38 dBuV. Both hybrid aluminum and copper construction alternatives show a similar response; thus, the following measurements and comparisons are carried out by considering only the hybrid board-level shielding solution based on the magnetic absorber material combined with an aluminum layer.

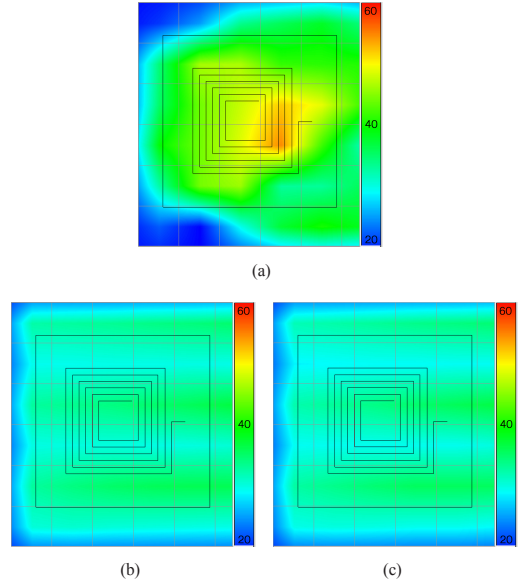


Fig. 7. Near-field radiated emissions of the EMI source PCB attaching different combinations of a magnetic absorber material and metal layers. (a) Magnetic absorber material sheet ($t = 0.2$ mm). (b) Magnetic absorber material sheet ($t = 0.2$ mm) with an aluminum layer attached ($t = 0.04$ mm). (c) Magnetic absorber material sheet ($t = 0.2$ mm) with a copper layer attached ($t = 0.04$ mm).

Another parameter to be considered in the construction of the hybrid BLS is the thickness of the conductive layer. Fig. 8 shows the measurement of the spatial near-field distribution by considering two different aluminum layer thicknesses: 0.08 mm and 0.2 mm. From this comparison, it is possible to observe that increasing the thickness of the conductive layer does not improve the performance of the hybrid construction. The mechanisms of the conductive material to reduce the near-field interferences are based on its ability to reflect the undesired signals and the generation of eddy currents.

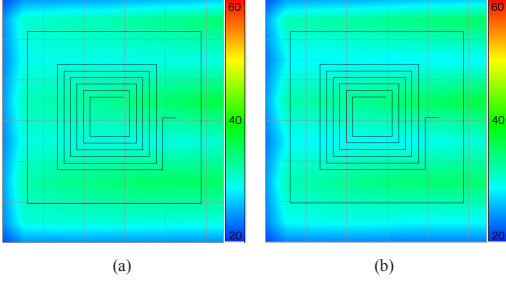


Fig. 8. Near-field radiated emissions of the EMI source PCB attaching a magnetic absorber material with aluminum metal layers with different thicknesses. (a) Magnetic absorber material sheet ($t = 0.2$ mm) with an aluminum layer attached ($t = 0.08$ mm). (b) Magnetic absorber material sheet ($t = 0.2$ mm) with an aluminum layer attached ($t = 0.2$ mm).

Fig. 9 shows the SE provided by two magnetic absorber sheets with higher thickness. Fig. 9(a) represents a maximum near-field interference of 52.2 dBuV when a magnetic absorber sheet is with $t = 0.3$ mm. The near-field distribution measured by applying a magnetic absorber sheet with $t = 0.5$ mm is shown in Fig. 9(c), having a maximum value of 50.7 dBuV. Fig. 9(b) and Fig. 9(d) show the results obtained when these two magnetic absorber materials are combined with an aluminum layer ($t = 0.04$ mm). It is possible to observe that increasing the magnetic absorber sheets by 0.02 mm improves the SE by 1.5 dB. Thereby, the magnetic absorber sheet with $t = 0.5$ mm attenuates the original maximum value of interference without applying any shielding solution in 13.6 dB. By analyzing the near-field distributions measured when the aluminum layer is introduced, it is verified that the use of the hybrid construction yields more significant shielding attenuation than only the magnetic absorber material. In both hybrid combinations it is observed similar maximum near-field results, 38.0 dBuV for the construction with a magnetic material with $t = 0.3$ mm and 35.5 dBuV with $t = 0.5$ mm, respectively.

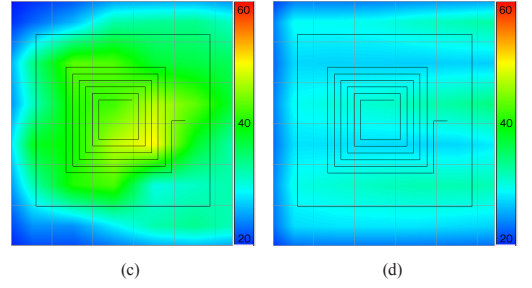
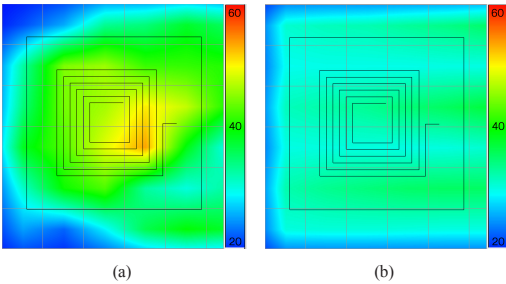
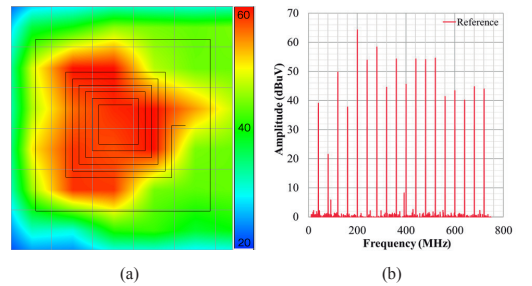


Fig. 9. Near-field radiated emissions of the EMI source PCB, evaluating different thicknesses of the magnetic absorber sheet. (a) Magnetic absorber material sheet ($t = 0.3$ mm). (b) Magnetic absorber material sheet ($t = 0.3$ mm) with an aluminum layer attached ($t = 0.04$ mm). (c) Magnetic absorber material sheet ($t = 0.5$ mm). (d) Magnetic absorber material sheet ($t = 0.5$ mm) with an aluminum layer attached ($t = 0.04$ mm).

Once it has been determined that applying a conductive layer on a magnetic absorber sheet increases its SE significantly, this hybrid BLS is compared with a shielding cabinet. Thereby, Fig. 10 compares the four scenarios described in Section III by analyzing them, considering the near-field emissions diagram and the frequency spectrum. The application of a thick magnetic absorber sheet ($t = 1.0$ mm) reduces the maximum emissions peak from 64.3 dBuV to 46.5 dBuV, achieving an attenuation of 17.7 dB. It practically suppresses the red and yellow colors in the near-field emissions diagram (Fig. 10(c)). Subsequently, when the aluminum layer combined with this absorber material is applied over the EMI source PCB, it is possible to observe the effectiveness of the hybrid solution to reduce near-field interferences. The frequency spectrum of the hybrid sheet (Fig. 10(f)) shows that all harmonics have been significantly attenuated. The hybrid solution introduces an attenuation of 30.5 dB since the maximum emission peak provided in this scenario is 33.8 dBuV. It results in suppressing the red, yellow, and green colors in the near-field diagram (Fig. 10(e)). Finally, the results obtained when the shielding cabinet is applied to the EMI source PCB are shown in Fig. 10(g) and (h). The frequency spectrum shows how the harmonics have been significantly attenuated, especially those in the lower frequency region. The near-field distribution shows that the shielded area (the spiral track) is colored by dark blue, which means that this BLS provides the highest attenuation (31.6 dB). Nevertheless, it is essential to highlight that pasting the hybrid solution over the source of emissions shows a similar SE to the shielding cabinet that requires soldering it to the PCB.



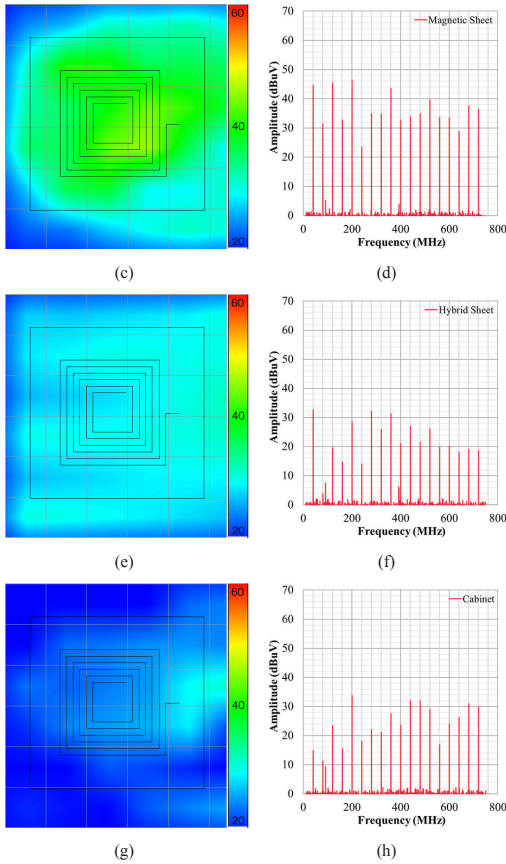


Fig. 10. Near-field radiated emissions of the EMI source PCB, evaluating different BLs. (a) Spatial magnetic near-field distribution of the EMI source PCB. (b) Frequency spectrum of the EMI source PCB. (c) Spatial magnetic near-field distribution of the magnetic absorber material sheet ($t = 1.0$ mm). (d) Frequency spectrum of the magnetic absorber material sheet ($t = 1.0$ mm). (e) Spatial magnetic near-field distribution of the hybrid sheet (magnetic layer with $t = 0.5$ mm and aluminum layer with $t = 0.04$ mm). (f) Frequency spectrum of the hybrid sheet (magnetic layer with $t = 0.5$ mm and aluminum layer with $t = 0.04$ mm). (g) Spatial magnetic near-field distribution of the shielding cabinet. (h) Frequency spectrum of the shielding cabinet.

V. CONCLUSIONS

The performance of a hybrid board-shield solution based on combining a magnetic absorber material with a metal layer has been analyzed. The results presented show that adding a conductive layer to a magnetic absorber material can significantly improve the SE provided.

From the results obtained, it is possible to verify that the attenuation provided by adding an aluminum layer is quite similar to introducing a copper layer. This is because both have high conductivity, making it possible to similarly reduce

the interferences by reflection and eddy currents mechanisms. Besides, it has been verified that increasing the thickness of the conductive layer does not result in improving the SE of the hybrid structure.

The performance of the hybrid BLS has also been characterized by modifying the thickness of magnetic absorber material. It has been determined that increasing the magnetic absorber sheet's thickness makes it possible to improve the attenuation ratio, but it is not very significant when the conductive layer is attached since it introduces a considerably higher attenuation. Finally, the hybrid structure has been compared with a shielding cabinet. It has been determined that both board-level solutions are able to provide an attenuation of about 30 dB.

Consequently, the hybrid structure is an interesting board-level shielding alternative since it is able to yield a similar SE to the shielding cabinet in the frequency range studied. The main advantage of this BLS construction is that it can be applied over a noisy IC or component without redesigning the PCB since it does not need to introduce a footprint.

REFERENCES

- [1] A. Suarez *et al.*, "Performance Study of Split Ferrite Cores Designed for EMI Suppression on Cables," *Electronics*, vol. 9, no. 12, p. 1992, Nov. 2020, doi: 10.3390/electronics9121992.
- [2] P. A. Martinez *et al.*, "Design and Study of a Wide-Band Printed Circuit Board Near-Field Probe," *Electronics*, vol. 10, no. 18, p. 2201, Sep. 2021, doi: 10.3390/electronics10182201.
- [3] J. Victoria, A. Suarez, P. A. Martinez, A. Alcarria, A. Gerfer and J. Torres, "Improving the Efficiency of NFC Systems Through Optimizing the Sintered Ferrite Sheet Thickness Selection," *IEEE Transactions on Electromagnetic Compatibility*, vol. 62, no. 4, pp. 1504-1514, Aug. 2020, doi: 10.1109/TEM.2020.3003800.
- [4] IEEE Project P2716. Guide for the Characterization of the Effectiveness of Printed Circuit Board Level Shielding.
- [5] A. C. Marvin, J. F. Dawson, H. Xie, L. Dawson and A. Venkateshaiah, "An Experimental Study of the Variability of the Shielding Effectiveness of Circuit Board Shields," in *2020 International Symposium on Electromagnetic Compatibility - EMC EUROPE*, 2020, pp. 1-5, doi: 10.1109/EMCEUROPE48519.2020.9245741.
- [6] Y. Liu, R. He, V. Khilkevich and P. Dixon, "Shielding Effectiveness of Board Level Shields with Absorbing Materials," in *2019 IEEE International Symposium on Electromagnetic Compatibility, Signal & Power Integrity (EMC+SIPI)*, 2019, pp. 84-89, doi: 10.1109/ISEMC.2019.8825197.
- [7] J. Victoria *et al.*, "Transmission Attenuation Power Ratio Analysis of Flexible Electromagnetic Absorber Sheets Combined with a Metal Layer," *Materials*, vol. 11, no. 9, p. 1612-1626, Sep. 2018.
- [8] G. Lovat, P. Burghignoli and S. Celozzi, "Shielding Properties of a Wire-Medium Screen," *IEEE Transactions on Electromagnetic Compatibility*, vol. 50, no. 1, pp. 80-88, Feb. 2008.
- [9] A. Suarez *et al.*, "Effectiveness Assessment of a Nanocrystalline Sleeve Ferrite Core Compared with Ceramic Cores for Reducing Conducted EMI," *Electronics*, vol. 8, no. 7, pp. 1-21, Jul. 2019, doi.org/10.3390/electronics8070800.
- [10] Z. Ji, Y. Tengfei and Z. Xiaohui, "Analyse and research of radiated emission on PCBs," in *2011 International Conference on Electronics, Communications and Control (ICECC)*, Ningbo, China, 2011, pp. 727-730, 10.1109/ICECC.2011.6066397.

5.4 Scientific article III: Design and validation of the hybrid solution

Title: Advanced Characterization of a Hybrid Shielding Solution for Reducing Electromagnetic Interferences at Board Level.

Authors: Jorge Victoria, Adrián Suárez, Pedro A Martínez, Andrea Amaro, Antonio Alcarria, José Torres, Roberto Herráiz, Víctor Solera, Víctor Martínez, Raimundo García-Olcina.

Published in: Electronics (MDPI), vol. 13, no. 3 (2024).
DOI: 10.3390/electronics13030598

Impact factor (2022): JCR: 2.900; SJR: 0.628

Quartile (2022): JCR: Q2 (category: Engineering, Electrical & Electronic)
SJR: Q2 (category: Electrical and Electronic Engineering)

Citations: 0 (WoS, accessed on March 2024).

Description: Electronics (ISSN 2079-9292; CODEN: ELECGJ) is an international peer-reviewed open access journal on the science of electronics and its applications published semimonthly online by MDPI. The impact factor, quartile and rank information have been obtained from Journal Citation Reports (JCR) and Scimago Journal Rank (SJR) databases according to the publication year (2024). The citations have been consulted in the Web of Science database.

Synopsis:

In the latest published article, we designed and validated the hybrid solution for board-level shielding.

Firstly, we characterized the selected NSS by its permeability, permittivity, and shielding effectiveness, as well as the shielding effectiveness of aluminum and copper materials for the metal layer.

To quantify the SE of the final solution, we designed and implemented a new measurement system. We used a 2 cm transmission line connected to a signal generator as the source of electromagnetic emissions and a magnetic field probe at a fixed distance as the receiver. By applying different BLS solutions, we measured the SE magnitude at each frequency.

We created a finite element model of the designed system and, using the NSS models generated in this thesis, simulated the shielding of different combinations: NSS alone, a hybrid solution of NSS with a metal sheet, and a metal box soldered to the ground plane.

By comparing the experimental results with the simulated ones, we demonstrate the validity of our models.








The generated simulation allows us to optimize the thickness of the NSS to achieve maximum SE when combined with the metal sheet.

Finally, thanks to the simulation, we analyzed the distribution of the magnetic field in different situations. We observed a risk of reradiation at the edges of the hybrid solution, which can be eliminated by excessively increasing the covered area to cover the radiation source.

This article demonstrates the validity of the simulation and the models and their utility in the design and analysis of various solutions. It also confirms that the designed hybrid solution offers SE results comparable to those of the classical solution while adding significant advantages in terms of application, space, and ease of use without the need for redesign.

Article

Advanced Characterization of a Hybrid Shielding Solution for Reducing Electromagnetic Interferences at Board Level

Jorge Victoria ^{1,2} , Adrian Suarez ^{1,*} , Pedro A. Martinez ¹ , Andrea Amaro ¹ , Antonio Alcarria ^{1,2}, Jose Torres ^{1,*} , Roberto Herraiz ¹ , Victor Solera ¹, Víctor Martinez ² and Raimundo Garcia-Olcina ¹ 

- ¹ Department of Electronic Engineering, University of Valencia, 46100 Burjassot, Spain; jorge.victoria@we-online.de (J.V.); pedro.a.martinez@uv.es (P.A.M.); andrea.amaro@uv.es (A.A.); antonio.alcarria@we-online.de (A.A.); roberto.herraiz@uv.es (R.H.); victor.solera@uv.es (V.S.); raimundo.garcia@uv.es (R.G.-O.)
- ² EMC Shielding & Grounding Team, Würth Elektronik eiSos, 74638 Waldenburg, Germany; victor.martinez@we-online.de
- * Correspondence: adrian.suarez@uv.es (A.S.); jose.torres@uv.es (J.T.)

Abstract: The development of new advanced functionalities, miniaturization, and the aim of obtaining optimized performance in electronic devices significantly impacts their electromagnetic compatibility (EMC). As electronic components become more densely packed on a printed circuit board (PCB), unintended coupling between components can cause electromagnetic interference (EMI). These requirements result in design restrictions that make using a board level shield (BLS) essential in reducing intra-system EMI in PCB designs. This contribution focuses on studying and characterizing a BLS solution based on combining a noise suppression sheet (NSS) with an aluminum layer to reduce intra-system EMI coupling. This hybrid solution has the advantage of providing a shielding option that does not require any electronic redesign. It does not need a footprint or a ground connection as it can be affixed over the EMI source. The solution is expected to provide higher attenuation levels than using only an NSS by combining the absorbing properties of the magnetic material and the loss mechanism of the metal. In order to verify the effectiveness of the hybrid BLS proposed solution, the magnetic near-field emissions of an EMI source are analyzed in this study. The experimental measurements and simulated results demonstrate a significant increase (51.6 dB at 1 GHz) in the shielding effectiveness (SE) provided by the proposed solution compared to a conventional NSS.

Keywords: board level shield (BLS); electromagnetic interference (EMI); electromagnetic compatibility (EMC); finite element method (FEM) simulation; shielding effectiveness (SE); hybrid shielding



Citation: Victoria, J.; Suarez, A.; Martinez, P.A.; Amaro, A.; Alcarria, A.; Torres, J.; Herraiz, R.; Solera, V.; Martinez, V.; Garcia-Olcina, R. Advanced Characterization of a Hybrid Shielding Solution for Reducing Electromagnetic Interferences at Board Level. *Electronics* **2024**, *13*, 598. <https://doi.org/10.3390/electronics13030598>

Academic Editor: Antonio Orlandi

Received: 28 December 2023

Revised: 22 January 2024

Accepted: 30 January 2024

Published: 31 January 2024



Copyright: © 2024 by the authors. Licensee MDPI, Basel, Switzerland. This article is an open access article distributed under the terms and conditions of the Creative Commons Attribution (CC BY) license (<https://creativecommons.org/licenses/by/4.0/>).

1. Introduction

The ongoing trend to increase complexity, integration, and connectivity has characterized the evolution of electronic devices. This evolution has introduced important challenges in the field of electromagnetic compatibility (EMC) [1–3]. The miniaturization of electronic components, driven by advancements in microelectronics, has led to devices with smaller form factors. While this enhances the portability of electronic devices, it also necessitates careful design considerations to manage the proximity of components and prevent unwanted coupling [4,5]. Specifically, the process of combining multiple functions into a single integrated circuit (IC) can generate even more challenges related to EMC. High-density ICs require advanced shielding techniques to address electromagnetic considerations [6,7]. This situation is critical when the device holds a wireless communication technology since it amplifies the risk of electromagnetic interference, and there is a need for robust EMC strategies to ensure reliable operation [8,9]. To reduce electromagnetic interference (EMI), one should consider using the systems approach. This involves applying advanced grounding, optimized layout design, and filtering and shielding techniques throughout the design process [10,11].

Effective management of EMI problems requires the ability to eliminate or reduce coupling. To achieve this, the coupling may be decreased using spatial separation between the interference source and the victim circuit or their orthogonalization [12–14]. Nevertheless, if these methods are not feasible due to miniaturization requirements, applying an electromagnetic shield is necessary [15]. An ideal shield should be an infinitely conducting enclosure without any openings, but real enclosures require them for ventilation, controls, or cables [16].

A board level shield (BLS) is a specially designed shielded enclosure that provides localized shielding to protect electronic devices on a printed circuit board (PCB) [17]. The main purpose of the BLS is to ensure that there is no interference between its contents and other components nearby on the same PCB or in the same electronic system [17–19]. Given the tiny size of a typical BLS, it can be characterized by its effectiveness in reducing EMI in the (very) near field [20]. It is interesting to determine the effectiveness of a BLS in reducing near-field problems, such as undesired magnetic decoupling between two adjacent circuits [21–23].

The shielding cabinet (also known as a shielding can) is the most common component used for BLS. By connecting to the reference plane of the PCB, it provides five of the six walls required to form a Faraday cage [19,24]. Another widely employed option for shielding is the use of a noise suppression sheet (NSS) [25,26]. An NSS is not generally as effective as shielding cabinets in attenuating EMI, although it offers the distinct advantage of being easily applicable during the validation stage. Unlike cabinets, which require a footprint to be included on the PCB, it is unnecessary to carry out modifications to the PCB to apply an NSS [27,28]. In addition to being an advantageous solution during the validation stage, it is easy to incorporate in the production stage, and it can be implemented as a final solution for a product.

The objective of this study is to analyze the effectiveness of a hybrid BLS that combines a conductive metal layer with a magnetic absorber material. The metal layer reduces interferences via eddy currents induced on the metal while also providing attenuation through the reflection mechanism. The magnetic material produces attenuation mainly through the losses determined by its magnetic properties [29]. The use of magnetic materials also prevents the appearance of eddy currents generated in the metal layer, which could cause unwanted interference through the re-radiation mechanism. Applying the hybrid BLS should result in higher attenuation than an NSS [30]. Moreover, the hybrid BLS does not require the inclusion of a footprint in the PCB. The hybrid BLS can be conveniently affixed over the EMI source, whether it be an IC or a certain area of the PCB that causes EMI problems [31]. In order to assess the effectiveness of reducing magnetic near-field interferences, a thorough analysis of the hybrid BLS is conducted and compared with an NSS and a shielding cabinet.

The IEEE Standard P2716 [17], “Guide for the Characterization of the Effectiveness of Printed Circuit Board Level Shielding”, is the first standard document that considers the specific topic of determining the shielding effectiveness (SE) of a BLS using standardized and non-standardized procedures. It provides comprehensive guidelines and outlines standardized measurement techniques, such as the SAE ARP6248 [32], which employs a stripline measuring method, and the reverberation method [33–35]. One of the alternative techniques proposed involves using a stripline within a BLS as an EMI source and another stripline outside the BLS as an external antenna [36]. This technique helps to determine the onboard coupling between the external and internal antennas when the BLS is applied [17,18]. Meanwhile, the standard IEC 62333-2 outlines methods for characterizing an NSS. Specifically, it describes how to determine the decoupling ratio parameter that specifies the reduction in coupling when a noise suppression sheet is applied [28,37].

The method of measurement developed in this study combines the use of stripline antennas proposed in the IEEE Standard P2716 and the decoupling procedure described in the IEC 62333-2. A PCB that contains a microstrip line serves as a reference source of EMI. This microstrip line can be shielded using a BLS. The emissions in a specific area outside

the BLS are determined with a magnetic near-field probe (H-NFP) [22]. This technique allows us to measure the magnetic field (H-field) in a particular region close to the BLS to determine the field that can be coupled to a nearby element. The advantages of using this measurement procedure are the possibility of measuring other BLSs besides an NSS and improving the dynamic range in the measurement. This last issue may not be critical when measuring the NSS, but it might be problematic when characterizing conductive shielding, as it typically provides a higher value of SE.

The measuring procedure is carried out both experimentally and through a simulated finite element method (FEM) model that replicates the experimental setup. This is an essential issue because when the results of a simulation match the experimental results, it makes it possible to explore variations in the initial validated scenario that would be difficult to measure experimentally.

This manuscript is structured into six sections that present a comprehensive analysis of the proposed hybrid BLS. Section 2 outlines the main parameters of the materials that constitute the hybrid BLS. In Section 3, the experimental measurement setup used for the magnetic near-field measurement is featured. Section 4 defines the FEM simulation model that is developed to determine the magnetic near-field emissions. Subsequently, in Section 5, the results obtained from the experimental measurement setup and simulations are reported. This section also presents a comparative analysis of the performance of the hybrid BLS with other alternatives, such as an NSS and a shielding cabinet. Finally, in Section 6, the main conclusions of this research are summarized.

2. Shielding Material Characterization

2.1. Hybrid BLS Solution

In order to improve the shielding of a specific part of a PCB, the most common technique used is a conductive shielding cabinet. Metal materials are effective at providing significant SE levels when applied properly. However, the NSS is becoming more popular in solving complex EMI problems. This is because it offers a lightweight solution with high flexibility. The main advantage of NSSs is that they can be adapted to achieve complex shapes and are easily assembled with adhesive onto a specific component or surface without adding a footprint in the PCB [25].

The proposed hybrid BLS solution consists of an NSS combined with an attached aluminum metal layer, as shown in Figure 1. It consists of an adhesive non-conductive layer for fixing the hybrid BLS to the EMI source. This is followed by a layer of magnetic absorber material ($t = 1.0$ mm), an adhesive layer ($t = 0.1$ mm), and an aluminum foil layer ($t = 0.04$ mm) [31].

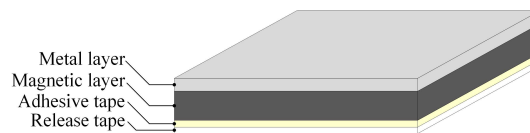


Figure 1. Layers that form the hybrid BLS.

This hybrid solution has the advantage of not requiring any redesign of the electronics as it can be affixed to the EMI source in a customized shape and size. Unlike shielding cabinets, it does not cause cavity resonance problems as it does not form a complete Faraday cage. Adding the metal layer is expected to obtain higher attenuation than using just an NSS. The attenuation of the EMI in the hybrid BLS is determined by the interaction of its constituent materials. The magnetic material primarily causes attenuation through the losses determined by its magnetic properties, mainly defined by its permeability [38]. On the other hand, the metal layer can reduce interferences through eddy currents induced on the surface and provide attenuation through the reflection mechanism. The use of magnetic material in the hybrid structure further prevents the occurrence of undesired interference

through the re-radiation mechanism caused by eddy currents generated in the surface and the capacitive coupling produced, as shown in Figure 2a,b [31]. Thereby, this structure may extend the working bandwidth of these materials and obtain a more significant attenuation than each of these materials could provide individually.

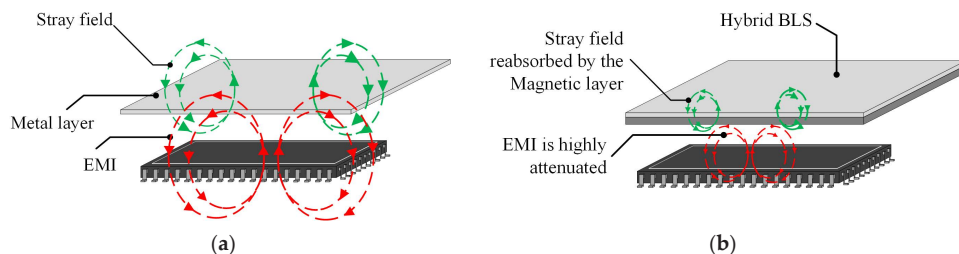


Figure 2. EMI reduction using the hybrid BLS: (a) applying only the metal layer as a shield; (b) applying the metal layer combined with a magnetic one (hybrid BLS).

2.2. Magnetic Material Characterization

Magnetic absorbing materials are metamaterials that convert electromagnetic interference into heat, which ultimately reduces the strength of the magnetic field. These materials are effective in reducing EMI depending on factors such as frequency, thickness, and dimensions. [29,39]. The selected magnetic absorber material, to be combined with a conductive layer, contains iron particles homogeneously distributed throughout a polymer matrix. In the presence of an H-field, the iron particles present in the polymer matrix are magnetized and absorb the magnetic energy. If the size of particles and spatial periods is significantly smaller than the wavelength of the electromagnetic field produced by the EMI source, then the material can be considered homogeneous [28,29].

To comprehend the mechanism by which a magnetic material can reduce EMI, it is essential to consider its permeability (μ) [40,41]. The complex relative permeability of a material can be partitioned into real and imaginary components, which are dependent on the frequency, as shown in Figure 3. The selected magnetic absorber material included in the hybrid BLS proposed has a thickness of $t = 1.0$ mm and an initial permeability of $\mu_i = 100$.

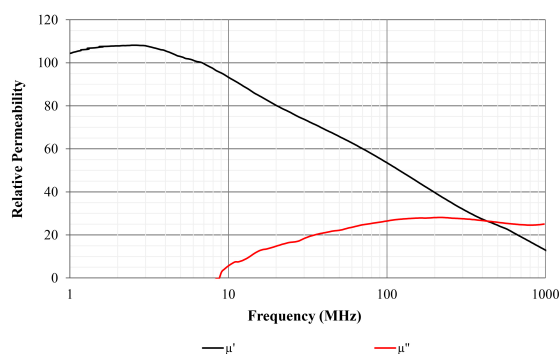


Figure 3. Relative permeability of the magnetic absorber material selected.

Another intrinsic material property worth mentioning is the electrical permittivity (ϵ_r). This is an essential material property that shows how a material can resist the formation of electric fields when an external field is applied. It has two components: the real part (ϵ_r') shows how a material can store electrical energy, while the imaginary part (ϵ_r'') represents dielectric losses due to energy dissipation in the material. Figure 4 shows the permittivity

components of the selected material, measured using a parallel conducting plates fixture, connected to a material analyzer equipment. As expected, the magnetic properties are more relevant in this kind of material.

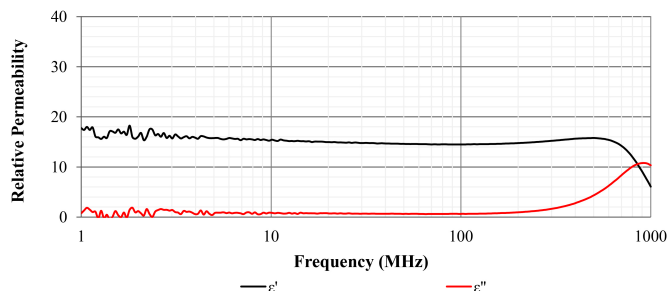


Figure 4. Relative permittivity of the magnetic absorber material analyzed.

2.3. Conductive Material Characterization

Aluminum and copper materials are usually used as shielding solutions because they are highly conductive. These materials generally are used to manufacture components such as shielding tapes or textiles. Although copper may be preferred for its superior electrical conductivity, aluminum might be selected for being lightweight and cost-effective. Additionally, aluminum has better corrosion resistance than copper due to the protective oxide layer it forms.

In order to observe the performance of aluminum material compared to copper material in the frequency range of interest, aluminum and copper layers with a thickness of $t = 0.04$ mm are compared in terms of SE. This characterization is carried out by following the ASTM D4935-18 standard [42]. It defines the test method for measuring the electromagnetic shielding effectiveness of planar materials in a narrow frequency range from 30 MHz to 1.5 GHz. The method lies in measuring the insertion loss (IL) that results when introducing test samples in a coaxial two-conductor transmission line holder, supporting the transverse EM (TEM) propagation mode. This test method is effective in determining the SE of conductive materials in a narrow frequency range from 30 MHz to 1.5 GHz. The holder is connected to a vector network analyzer (VNA) equipment that is used to determine the IL parameter, as shown in Figure 5. The procedure requires two types of specimens that must have the same thickness in order to take SE measurements: the reference and the load specimens. The difference between the measurements of the load and the reference specimens provides the measurement of the SE.

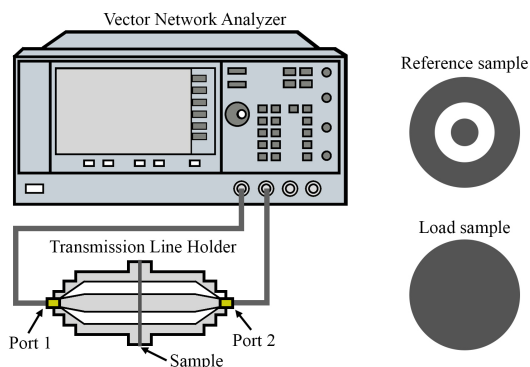


Figure 5. Measurement test setup for measuring the shielding effectiveness of planar materials based on the ASTM D4935-18 procedure and sample geometries and dimensions.

The SE measurement can be expressed as the difference between the IL expressed in dB of the load ($IL_{dB,l}$) and reference specimens ($IL_{dB,r}$), as follows:

$$SE_{dB} = IL_{dB,l} - IL_{dB,r}. \quad (1)$$

Figure 6 shows the SE of the two shielding metal layers measured according to the ASTM D4935-18 standard. Given that the behavior of both materials is identical across the entire bandwidth, aluminum is validated as the material to incorporate into the final hybrid BLS.

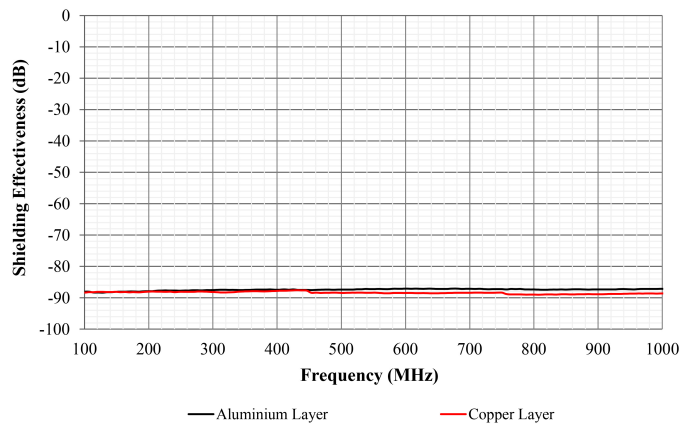


Figure 6. Shielding effectiveness parameter obtained for aluminum and copper materials by using the ASTM D4935-18 standard procedure.

3. Experimental Measurement Procedure

In this study, a novel method of measurement is proposed that utilizes the stripline antennas, as suggested in the IEEE P2716, in conjunction with the decoupling procedure, as described in IEC 62333-2. According to the fundamental diagram of an EMC problem, the microstrip line serves as the source of EMI, while the H-NFP is the victim element. The EMI source is implemented by a PCB that holds a microstrip line, which acts as a reference emission level. The H-NFP is used to measure the H-field emissions in a particular region close to the EMI source. Specifically, the location of the H-NFP is adjusted to the center of the microstrip line, which was found to be the area of maximum emission. As the H-NFP introduces approximately 30 dB of attenuation, obtaining measurements of maximum emissions is crucial in order to have a significant dynamic range in the experimental measurement setup. The distance between the H-NFP and the microstrip line must be as close as possible without touching the NSS or hybrid BLS under test. Considering this statement and the thickness of the hybrid BLS, the distance is fixed at 1.4 mm. By applying different BLSs, emissions are measured and compared with the reference measurement without using any BLS. Thereby, it is possible to quantify the SE provided by the BLS applied to the EMI source.

The developed method significantly enhances the dynamic range of the measurement setup. Using a microstrip line as an EMI source instead of an H-NFP significantly improves the dynamic range of the measurement since, generally, an H-NFP can introduce about 30 dB of attenuation [22]. Thus, the results are significantly attenuated if two H-NFPs are used both as a source and receiver (as defined by the IEC 62333-2). When measuring the NSS, the issue mentioned in the text might not be critical. However, it could be problematic while characterizing conductive shielding as it usually provides a higher value of SE. The proposed method has an added advantage over the IEC 62333-2 as it allows us to measure other BLSs apart from the NSS.

The EMI source consists of a PCB that includes a $50\ \Omega$ microstrip line, as shown in Figure 7. On the bottom side of the PCB, a ground plane with a 0.035 mm thickness is added, and two SMA connectors are attached, one at each end of the strip conductor. The SMA connectors are located on the bottom layer and connected to both ends of the microstrip line through two vias. One SMA connector is connected to a signal generator equipment (SG), while the other one is connected to a matched $50\ \Omega$ load. The SG is configured to power the EMI source with a parametric signal ranging from 100 MHz to 1 GHz .

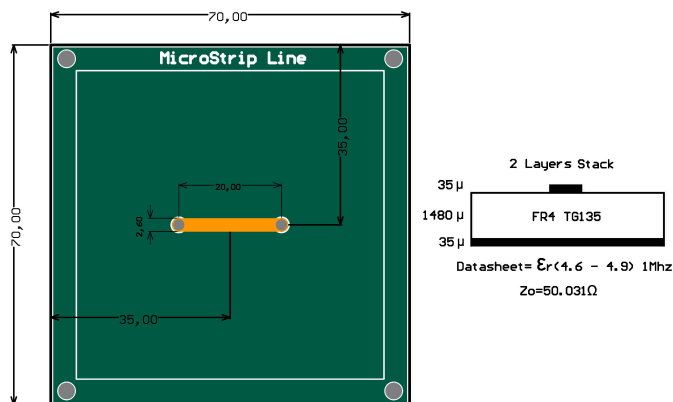


Figure 7. Characteristics of the PCB that holds the microstrip line employed as EMI source.

The H-NFP is placed at a right angle with the EMI source and connected to spectrum analyzer (SA) equipment to measure the emissions, as shown in Figure 8.

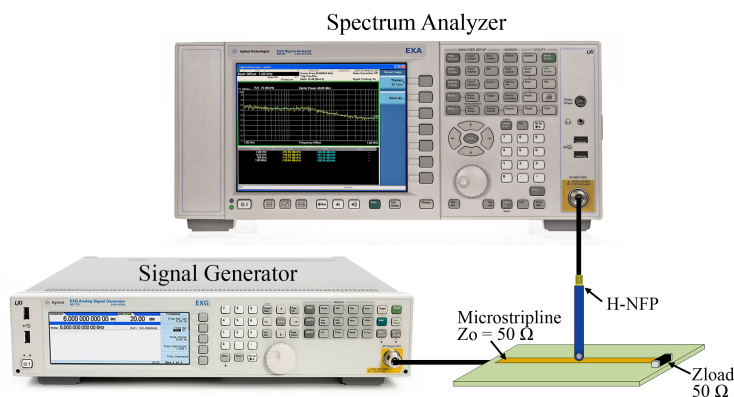


Figure 8. Description of the experimental measurement method used.

The XF-R 3-1 from Langer EMV GmbH is the H-NFP selected since it is able to measure the emissions in a specific area. The XF-R 3-1 is specifically designed to directly and accurately measure H-fields on a particular component or assembly, with high resolution. Figure 9 depicts the H-field correction factor of the XF-R 3-1 probe in terms of $(\text{dB}\mu\text{A}/\text{m})/\text{dB}\mu\text{V}$. It is used for the transformation of voltage measurements obtained through the SA into magnetic field results. A significant advantage of the proposed measurement setup is that it makes it possible to compare the experimental results with those obtained from the simulation model.

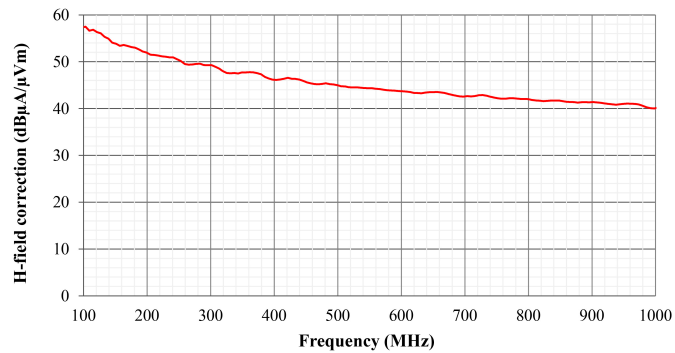


Figure 9. Correction H-field factor of the XF-R 3-1 H-NFP.

Therefore, given the H-NFP response and the measurements obtained with the SA, (2) and (3) are used to determine the experimental results in H-field units (dBA/m):

$$H \left[dB \frac{\mu A}{m} \right] = U_{out} [dB \mu V] + K_H \left[dB \frac{\mu A}{m} \right] \quad (2)$$

$$H \left[dB \frac{A}{m} \right] = H \left[dB \frac{\mu A}{m} \right] - 120 \quad (3)$$

where U_{out} represents the voltage that the H-NFP provides to the SA and K_H correction factor represented in Figure 9.

4. Simulation Model Definition

The FEM simulation is created using the software Ansys Electromagnetics Suite 2022 R1 HFSS 3D's electronics simulation platform (Ansys Electronics Desktop). The experimental measurement setup has been replicated to assess the distribution of near H-fields when different BLSs are applied to the EMI source. In the model, the SG equipment used for powering the EMI source PCB is implemented as a lumped port that is connected to one end of a microstrip line. This port emulates the signal emitted by the SG equipment and sets the power and frequency to the same values used for the experimental measurements. The other end of the microstrip line is matched with a 50 Ω load, replicating the experimental model. The following scenarios are assessed to evaluate the performance of the hybrid BLS:

1. Reference measurement: H-field without applying any shielding component;
2. H-field when only the NSS is applied;
3. H-field when the hybrid BLS is applied;
4. H-field when a 30 mm × 30 mm shielding cabinet is applied.

Note that the NSS has been modeled from the relative permeability and permittivity defined in Section 2. The hybrid BLS also utilizes the same model as the NSS and adds an aluminum layer defined by the electrical conductivity parameter (3.6×10^7 S/m).

These scenarios make it possible to assess the performance of the hybrid BLS in comparison to the reference level. Additionally, the hybrid BLS can be compared with the NSS without the inclusion of the aluminum layer. Finally, the effectiveness of the hybrid BLS can be evaluated by comparing it with a shielding cabinet, which is one of the most widely used and effective solutions.

4.1. Near-Field Distribution Simulation

The results obtained from the simulation model are verified by comparing them with those obtained from the experimental setup. This is carried out by analyzing the H-field parameter measured at the selected distance from the EMI source. The simulation

environment provides the resulting measurement by maintaining the same position of H-NFP as in the experimental setup. It is important to note that when the results of a simulation match those of an experiment, it becomes possible to explore different variations in the initial validated scenario that may be difficult to measure experimentally. Once the simulation model is verified, the near-field distribution generated by the EMI source can be analyzed to observe the considered scenarios. The initial size of the NSS and hybrid BLS sheets is chosen to be 60×60 mm to measure only the H-field produced by the microstrip line. The near-field distribution is also studied by applying the hybrid BLS with different sample dimensions on the EMI source. The obtained results provide insights to optimize the size of the hybrid BLS. Consequently, scenario 3 is modified by testing shorter ($30 \text{ mm} \times 30 \text{ mm}$) and larger ($100 \text{ mm} \times 100 \text{ mm}$) dimensions of the hybrid BLS.

The scenarios defined to study the near-field distribution generated by the EMI source are shown in Figure 10. Figure 10a shows the reference scenario 1 without applying any shielding. Scenario 2 is represented in Figure 10b, where the $60 \text{ mm} \times 60 \text{ mm}$ NSS is applied to the EMI source. In Figure 10c, the hybrid BLS with dimensions of $60 \text{ mm} \times 60 \text{ mm}$ is used (scenario 3). Figure 10d represents scenario 4, where a shielding cabinet is connected to the ground plane of the EMI source. Additionally, the models of Figure 10e,f show the hybrid BLS with shorter and larger dimensions, respectively.

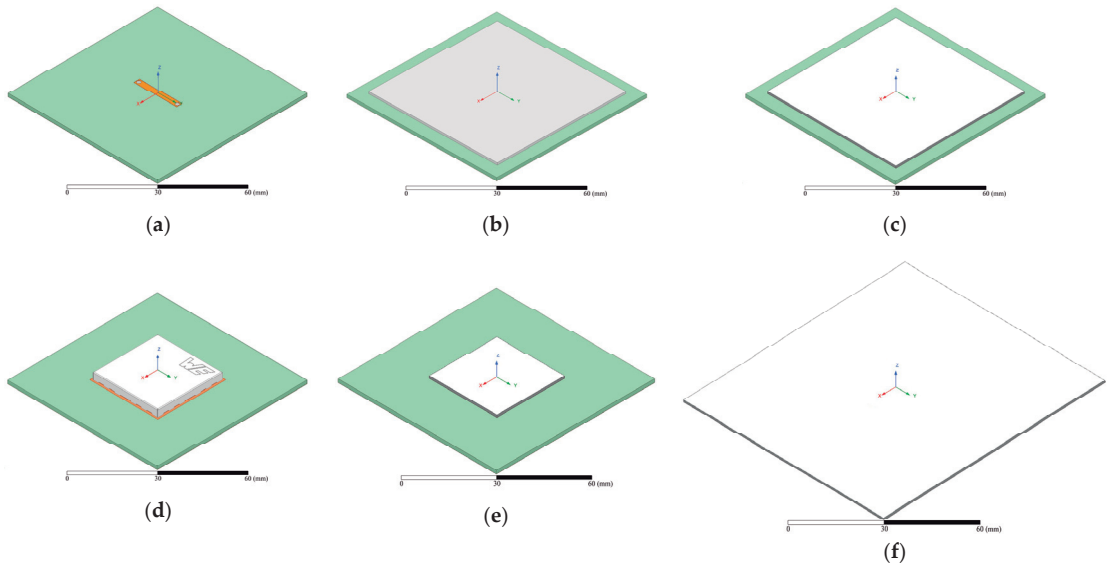


Figure 10. Definition of the scenarios analyzed in this manuscript, considering the EMI source PCB: (a) reference measurement without applying any BLS; (b) NSS applied ($60 \text{ mm} \times 60 \text{ mm}$); (c) hybrid construction by combining a magnetic absorber material with an aluminum layer attached ($60 \text{ mm} \times 60 \text{ mm}$); (d) shielding cabinet applied ($30 \text{ mm} \times 30 \text{ mm}$); (e) applying a hybrid sheet with smaller dimensions ($30 \text{ mm} \times 30 \text{ mm}$); (f) applying a hybrid sheet with larger dimensions ($100 \text{ mm} \times 100 \text{ mm}$).

4.2. Frequency Response Simulation

The use of filtering and shielding techniques is effective in reducing EMI, although it is essential to ensure that they do not affect the intended working signals. Thereby, the transmission attenuation ratio [29] for scenarios 1, 2, and 3 proposed is simulated and analyzed through the S21 parameter. A signal is injected into the microstrip line, covering a frequency range up to 1.0 GHz, that is received at its other end. Scenario 1 is expected to have a flat response of around 0 dB. On the other hand, the NSS and the hybrid BLS

are expected to have a response similar to a low-pass filter. The most noteworthy result from this measurement is the point at which the hybrid BLS can start affecting the signals present in the area it covers.

5. Results and Discussion

This section focuses on the analysis of the hybrid BLS to reduce near-field EMI problems. The results obtained from the experimental measurement setup and those provided by the simulation model are compared through the near H-field parameter. There are two main purposes for this comparison. The first purpose is to analyze the accuracy of the reference measurement (scenario 1) in order to ensure that the simulation model has been designed properly. The second purpose is to validate the model of the magnetic absorber material that has been created using the permeability and permittivity parameters. This second point is crucial in evaluating the performance of the hybrid BLS since the magnetic material defined is one of its layers. Figure 11 shows the results obtained for the first three scenarios described in Section 4. It represents the experimental (solid traces) and computed (dotted traces) H-field provided by the EMI source and measured at the same specific position.

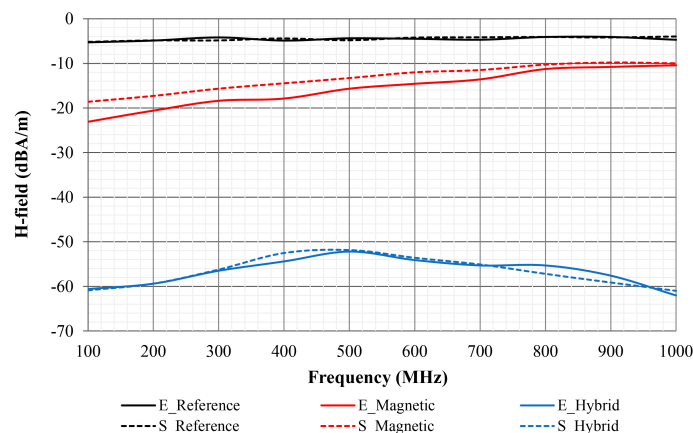


Figure 11. Comparison of the H-field (1.4 mm from EMI source) obtained by FEM simulation and experimentally measured for the scenarios studied.

Based on the obtained results, it has been confirmed that both the simulation model and the magnetic material are accurately designed. The black traces in the graph represent the reference measurement for scenario 1. The experimental measurement shows a mean H-field of -4.7 ± 0.6 dB A/m, whereas the simulated measurement is -4.6 ± 0.6 dB A/m. Therefore, it can be concluded that there is a strong correlation between the experimental and simulated measurement setups.

Scenario 2, which represents the use of the NSS, validates that this material has been adequately modeled since the simulated and experimental result trends are very similar. The model is observed to be more precise in the high-frequency region, with the largest disparity observed in the lowest frequency studied (4.58 dB at 100 MHz). When the NSS is applied to the EMI source, it reduces the H-field measured to -23.1 dB A/m at 100 MHz and -10.4 dB A/m at 1.0 GHz, according to the experimental results. The maximum SE provided by this solution is observed in lower frequencies since the H-field measurement decreases with increasing frequency. The experimental data show that the SE provided by the NSS is -17.8 dB at 100 MHz.

According to the experimental results, the modeled hybrid BLS has a significant match. The maximum error observed is 1.9 dB at 400 MHz and 800 MHz. In the rest of the frequency range studied, the difference is less than 0.5 dB. Comparing the H-field attenuation generated by applying the hybrid BLS with that obtained using only magnetic

material, it is evident that the former is more effective. At 100 MHz and 1 GHz, the H-field is reduced to -60 dBA/m, resulting in an SE of 37.5 dB and 51.6, respectively. These results demonstrate that the hybrid structure can provide a significant SE value.

The scope of this analysis is limited to the frequencies specified by the simulation model, owing to the measurement of permeability and permittivity data up to 1.0 GHz. The trend of the NSS reveals that the higher the frequency, the slower the SE is reduced. Conversely, the trend of the hybrid BLS suggests a more substantial attenuation of SE in the higher frequency range compared to the characterized region.

5.1. Near-Field Distribution Results

The simulation model allows for an analysis of performance regarding the distribution of the H-field. This analysis considers the scenarios outlined in Section 4. Figure 12 illustrates the strength of the H-field on the Y-Z plane, which is the plane perpendicular to the PCB substrate. This H-field is generated by the EMI source at 500 MHz. In scenario 1, the H-field is distributed over the microstrip line, as shown in Figure 12a. As explained above, the maximum H-field is concentrated in the center of the microstrip line. However, it does not generate an H-field in the area under the PCB because it is blocked by the ground reference plane included under the stripline. In scenario 2, the introduction of the NSS causes a slight attenuation of the H-field, as shown in Figure 12b. This result is in line with the findings presented in Figure 11. In scenario 3, the H-field is significantly attenuated when the hybrid BLS is attached to the EMI source, as demonstrated in Figure 12c. This situation is similar to the one presented in Figure 12d when the shielding cabinet is applied (scenario 4). Note that in this case, a significant part of the field is enclosed inside the cabinet area. As expected from the results shown in Figure 11, the attenuation provided by the hybrid BLS is notable and may be comparable with the cabinet's effectiveness. Moreover, the hybrid BLS has an advantage over a shielding cabinet as it can be easily attached to the source of interference without requiring the electronics to be redesigned by introducing a footprint.

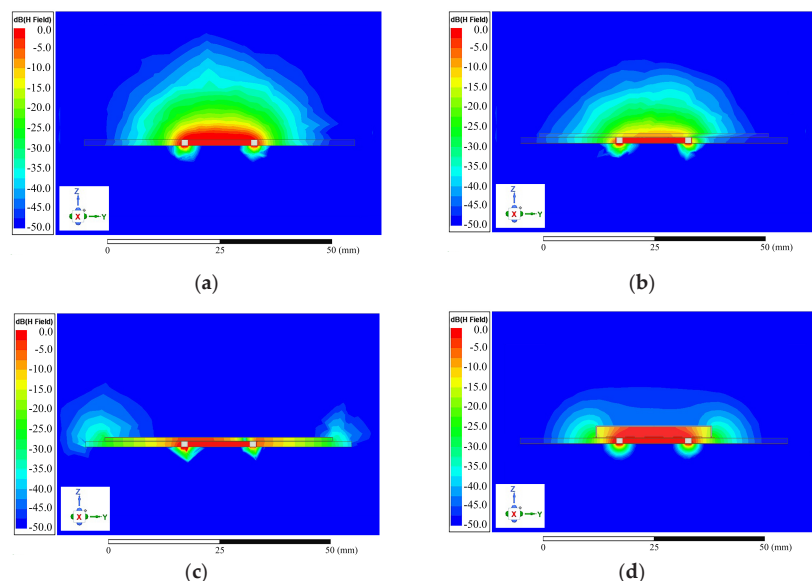


Figure 12. Analysis of the near H-field distribution for the first four scenarios to compare the effectiveness of the hybrid BLS with the other two solutions, considering the EMI source PCB: (a) reference measurement without applying any BLS; (b) NSS applied (60 mm \times 60 mm); (c) hybrid BLS applied (60 mm \times 60 mm); (d) shielding cabinet applied (30 mm \times 30 mm).

The hybrid BLS and the shielding cabinet test results revealed that some of the H-field is re-radiated from the component edges. To further investigate this situation, scenario 3 has been modified by varying the dimensions of the hybrid BLS sheet. The simulation results for the two sheet dimensions, $30\text{ mm} \times 30\text{ mm}$ and $100\text{ mm} \times 100\text{ mm}$, defined in Section 4, are shown in Figure 13. When the hybrid BLS sheet is reduced, the results are similar to those shown in Figure 12. It can be observed that the near H-field distribution of the hybrid BLS, which has the same dimensions as the shielding cabinet, also significantly attenuates the emissions generated by the EMI source. However, it should be noted that the stray field generated in the edges of the hybrid BLS of size $30 \times 30\text{ mm}$ has increased compared to the $60 \times 60\text{ mm}$ sheet. Moreover, as seen in Figure 13a, the edge of the sheet is closer to the microstrip line, and the re-radiated H-field is affecting it, which may lead to undesired couplings. If the hybrid BLS sheet is extended to overlap the EMI source PCB, the re-radiated H-field will be generated at the edge of the PCB instead of the sheet's edge. Additionally, the H-field will be re-radiated only toward the area located under the PCB, as the hybrid BLS protects the area situated over the PCB. Specifically, in this case, due to the proximity of the aluminum layer of the hybrid BLS and the copper ground plane of the PCB, a capacitive undesired effect occurs, which results in re-radiation. The re-radiating effect is produced when a discontinuity between both parallel conductive planes is produced. Therefore, it is essential to properly select the dimensions of the hybrid BLS to avoid the edge re-radiating effect that may affect the area or component that wants to be shielded.

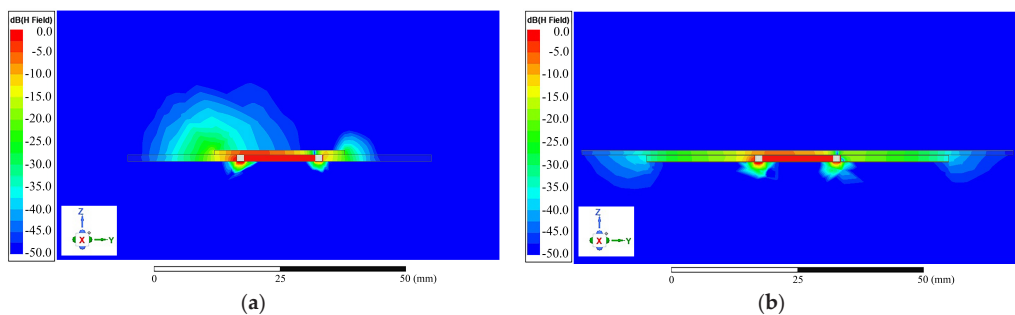


Figure 13. Analysis of the near H-field distribution to compare the influence of the hybrid BLS sheet dimensions: (a) applying a hybrid sheet with shorter dimensions ($30\text{ mm} \times 30\text{ mm}$); (b) applying a hybrid sheet with larger dimensions ($100\text{ mm} \times 100\text{ mm}$).

5.2. Frequency Response Analysis

Figure 14 shows the outcome of the frequency response analysis of the transmission attenuation ratio. This is carried out by placing a BLS on the microstrip line of the EMI source PCB. As anticipated, scenario 1 (red trace) indicates a constant response across the entire frequency range studied. This is because when no BLS is applied to the microstrip line, it is expected to have an even response of approximately 0 dB. The NSS and hybrid BLS act as a low-pass filter. As a result, scenario 2 (black trace) demonstrates that the transmitted signal becomes attenuated beyond 200 MHz. The worst attenuation result is produced at 1.0 GHz, and the value is 0.8 dB. The hybrid BLS, whose dimensions are the defined by scenario 3 (orange trace), becomes attenuated from 110 MHz and experiences the maximum attenuation at 1.0 GHz, which corresponds to 2.4 dB.

If the criterion selected to determine the cutoff frequency is an attenuation of -3.0 dB , it can be confirmed that for the hybrid BLS, this value is reached at a frequency higher than the one studied. This indicates that this solution can be deemed optimal at least up to 1.0 GHz since it does not affect the desired signal.

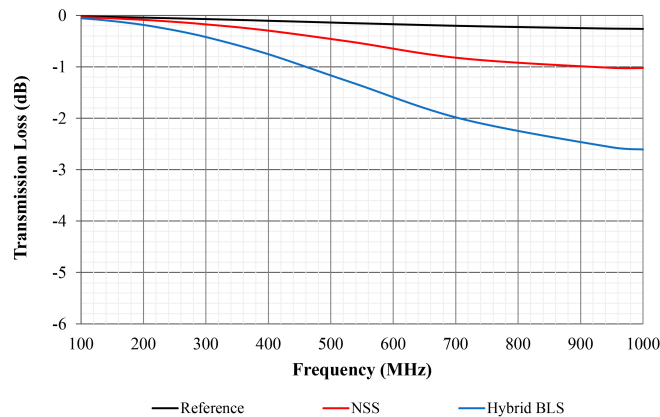


Figure 14. Transmission loss ratio to study the influence of applying a specific BLS on the intended (desired) signal.

6. Conclusions

The hybrid BLS solution based on combining an NSS with an aluminum layer to reduce intra-system EMI coupling was presented. The main layers contained in the hybrid BLS were described and characterized. This proposed shield was analyzed in terms of its ability to reduce intra-system EMI coupling. The hybrid BLS was modeled and evaluated through a simulation model that emulates the experimental measurement technique employed to determine the near H-field emissions. Based on the obtained results, it was confirmed that both the simulation model and the magnetic material were accurately designed.

The hybrid BLS presented a significant attenuation of the near H-field (up to 51.6 dB at 1 GHz) when applied to the EMI source. Hence, it is verified that the SE is more than that provided using the NSS. The near H-field distribution diagrams reveal that the attenuation provided by the hybrid BLS is notable and may be comparable with the shielding cabinet's effectiveness. Additionally, the re-radiation caused by the use of the hybrid BLS was studied, concluding that it is essential to select the dimensions of the hybrid BLS to avoid the edge re-radiating effect affecting the area that needs to be shielded or other near elements.

Consequently, the hybrid BLS represents an interesting solution since it is able to yield similar results to the shielding cabinet in the frequency range studied. Moreover, the hybrid BLS has an advantage over a shielding cabinet as it can be easily attached to the source of interference without requiring the electronics to be redesigned by introducing a footprint.

Author Contributions: Conceptualization, J.V., A.S., A.A. (Antonio Alcarria) and J.T.; methodology, R.G.-O., A.A. (Antonio Alcarria) and P.A.M.; software, P.A.M., J.V., V.S. and A.S.; validation, A.A. (Andrea Amaro), V.M. and R.G.-O.; formal analysis, J.V., V.S. and R.H.; investigation, J.V., A.S., P.A.M., J.T. and A.A. (Andrea Amaro); data curation, A.A. (Andrea Amaro), R.H., V.S. and V.M.; writing—original draft preparation, J.V., A.S., P.A.M., A.A. (Andrea Amaro) and J.T.; writing—review and editing, J.T., A.A. (Antonio Alcarria), R.H., V.M. and R.G.-O.; supervision, J.T., A.S. and R.G.-O.; project administration, J.T., J.V. and A.A. (Antonio Alcarria); funding acquisition, J.T. and J.V. All authors have read and agreed to the published version of the manuscript.

Funding: The APC was funded by the Universitat de València (20150151).

Data Availability Statement: Data are contained within the article.

Conflicts of Interest: The authors declare no conflicts of interest. The funders had no role in the design of the study; in the collection, analyses, or interpretation of data; in the writing of the manuscript; or in the decision to publish the results.

References

- Valenzuela, R. Novel Applications of Ferrites. *Phys. Res. Int.* **2012**, *2012*, 591839. [\[CrossRef\]](#)
- González-Vizuete, P.; Domínguez-Palacios, C.; Bernal-Méndez, J.; Martín-Prats, M.A. Simple Setup for Measuring the Response to Differential Mode Noise of Common Mode Chokes. *Electronics* **2020**, *9*, 381. [\[CrossRef\]](#)
- Gil-de-Castro, A.; Rönnerberg, S.K.; Bollen, M.H.J.; Moreno-Muñoz, A. Study on Harmonic Emission of Domestic Equipment Combined with Different Types of Lighting. *Int. J. Electr. Power Energy Syst.* **2014**, *55*, 116–127. [\[CrossRef\]](#)
- Kim, J.; Rotaru, M.D.; Baek, S.; Park, J.; Iyer, M.K.; Kim, J. Analysis of Noise Coupling from a Power Distribution Network to Signal Traces in High-Speed Multilayer Printed Circuit Boards. *IEEE Trans. Electromagn. Compat.* **2006**, *48*, 319–330. [\[CrossRef\]](#)
- Crovetti, P.; Musolino, F. Interference of Spread-Spectrum EMI and Digital Data Links under Narrowband Resonant Coupling. *Electronics* **2020**, *9*, 60. [\[CrossRef\]](#)
- Archambeault, B.; Brench, C.; Connor, S. Review of Printed-Circuit-Board Level EMI/EMC Issues and Tools. *IEEE Trans. Electromagn. Compat.* **2010**, *52*, 455–461. [\[CrossRef\]](#)
- Kapoor, D.; Sangwan, V.; Tan, C.M. Electromagnetic hotspots identification in integrated circuits. *Prog. Electromagn. Res. Lett.* **2019**, *86*, 121–128. [\[CrossRef\]](#)
- Victoria, J.; Suarez, A.; Martinez, P.A.; Alcarria, A.; Gerfer, A.; Torres, J. Improving the Efficiency of NFC Systems Through Optimizing the Sintered Ferrite Sheet Thickness Selection. *IEEE Trans. Electromagn. Compat.* **2020**, *62*, 1504–1514. [\[CrossRef\]](#)
- Suganya, A.; Natarajan, R. Polarization Insensitive Dual Band FSS for S-Band and X-Band Applications. *Prog. Electromagn. Res. Lett.* **2023**, *110*, 37–45. [\[CrossRef\]](#)
- Ott, H.W. *Electromagnetic Compatibility Engineering*; John Wiley & Sons: Hoboken, NJ, USA, 2009.
- Paul, C.R. *Introduction to Electromagnetic Compatibility*, 2nd ed.; Wiley Interscience: Hoboken, NJ, USA, 2006.
- Kat, Y.; Morita, S.; Shiomi, H.; Sanada, A. Ultrathin Perfect Absorbers for Normal Incident Waves Using Dirac Cone Metasurfaces With Critical External Coupling. *IEEE Microw. Wirel. Compon. Lett.* **2020**, *30*, 383–386. [\[CrossRef\]](#)
- Tan, Z.; Yi, J.; Cheng, Q.; Burokur, S.N. Design of Perfect Absorber Based on Metagratings: Theory and Experiment. *IEEE Trans. Antennas Propag.* **2023**, *71*, 1832–1842. [\[CrossRef\]](#)
- Tan, Z.; Yi, J.; Chen, X.; Lin, M.; Jiang, Z.H.; Werner, D.H.; Burokur, S.N. Fully Analytical Design of Dual-Wire PCB Metagratings for Beam Steering and Splitting. *IEEE Trans. Antennas Propag.* **2023**, *71*, 5452–5456. [\[CrossRef\]](#)
- Vance, E.F.; Graf, W. The Role of Shielding in Interference Control. *IEEE Trans. Electromagn. Compat.* **1988**, *30*, 294–297. [\[CrossRef\]](#)
- Suarez, A.; Dawson, J.F.; Ariën, Y.; Catrysse, J.; Pissort, D.; Marvin, A.C. An Overview of the IEEE P2715 Guide for the Characterization of the Shielding Effectiveness of Planar Materials. *IEEE Electromagn. Compat. Mag.* **2023**, *12*, 78–88. [\[CrossRef\]](#)
- IEEE P2716/D2; IEEE Guide for the Characterization of the Effectiveness of Printed Circuit Board Level Shielding. IEEE: Piscataway, NJ, USA, 2022.
- Marvin, A.; Dawson, J.; Robinson, M. Experimental Verification of Board Level Shielding Variability at Microwave Frequencies. In Proceedings of the 2021 IEEE International Joint EMC/SI/PI and EMC Europe Symposium, Virtual, 26 July–20 August 2021; IEEE: Piscataway, NJ, USA, 2021; pp. 883–888.
- Marvin, A.C.; Dawson, J.F.; Xie, H.; Dawson, L.; Venkateshaiah, A. An Experimental Study of the Variability of the Shielding Effectiveness of Circuit Board Shields. In Proceedings of the 2020 International Symposium on Electromagnetic Compatibility-EMC Europe, Rome, Italy, 23–25 September 2020; IEEE: Piscataway, NJ, USA, 2020; pp. 1–5.
- Pissort, D. IEEE Standard P2716 Update: Characterization of the Effectiveness of Printed Circuit Board Level Shielding. *IEEE Electromagn. Compat. Mag.* **2021**, *10*, 97–98. [\[CrossRef\]](#)
- Perotoni, M.B.; Silva, L.A.; Silva, W.; Santos, K.M.G. Near-field measurement system based on a software defined radio. *Prog. Electromagn. Res. Lett.* **2022**, *102*, 87–94. [\[CrossRef\]](#)
- Filipašić, M.; Dadić, M. A Two-Turn Shielded-Loop Magnetic Near-Field PCB Probe for Frequencies up to 3 GHz. *Sensors* **2023**, *23*, 7308. [\[CrossRef\]](#)
- Mansour, R.; Benjelloun, N.; Kadi, M. Characterization of the Shielding Effectiveness of Composite Materials Using Electromagnetic Methods Covering a Wide Frequency Range. *Prog. Electromagn. Res. M* **2023**, *118*, 117–126. [\[CrossRef\]](#)
- Kim, J.; Park, H.H. A Novel IC-Stripline Design for Near-Field Shielding Measurement of On-Board Metallic Cans. *IEEE Trans. Electromagn. Compat.* **2017**, *59*, 710–716. [\[CrossRef\]](#)
- Piersanti, S.; de Paulis, F.; Orlandi, A.; Connor, S.; Liu, Q.; Archambeault, B.; Dixon, P.; Khorrami, M.; Drewniak, J.L. Near-Field Shielding Performances of EMI Noise Suppression Absorbers. *IEEE Trans. Electromagn. Compat.* **2017**, *59*, 654–661. [\[CrossRef\]](#)
- Seo, Y.; Ko, S.; Ha, H.; Qaiser, N.; Leem, M.; Yoo, S.J.; Jeong, J.H.; Lee, K.; Hwang, B. Stretchable carbonyl iron powder/polydimethylsiloxane composites for noise suppression in gigahertz bandwidth. *Compos. Sci. Technol.* **2022**, *218*, 109150. [\[CrossRef\]](#)
- Liu, Y.; He, R.; Khilkevich, V.; Dixon, P. Shielding Effectiveness of Board Level Shields with Absorbing Materials. In Proceedings of the 2019 IEEE International Symposium on Electromagnetic Compatibility, Signal & Power Integrity (EMC+SIPI), New Orleans, LA, USA, 22–26 July 2019; IEEE: Piscataway, NJ, USA, 2019; pp. 84–89.
- Deutschmann, B.; Khan, J.S.; Winkler, G.; Victoria, J. Reduction of Electromagnetic Emission from ICs Using Soft Flexible Ferrite Sheets. In Proceedings of the 2021 13th International Workshop on the Electromagnetic Compatibility of Integrated Circuits (EMC Compo), Bruges, Belgium, 8–11 March 2022; IEEE: Piscataway, NJ, USA, 2022; pp. 19–24.

29. Victoria, J.; Suarez, A.; Torres, J.; Martinez, P.; Alcarria, A.; Martos, J.; Garcia-Olcina, R.; Soret, J.; Muetsch, S.; Gerfer, A. Transmission Attenuation Power Ratio Analysis of Flexible Electromagnetic Absorber Sheets Combined with a Metal Layer. *Materials* **2018**, *11*, 1612. [[CrossRef](#)]
30. Victoria, J.; Suarez, A.; Martinez, P.A.; Alcarria, A.; Amaro, A.; Torres, J. Board-Level Shielding with Magnetic Absorber Sheet. In Proceedings of the 2022 International Symposium on Electromagnetic Compatibility-EMC Europe, Gothenburg, Sweden, 5–8 September 2022; IEEE: Piscataway, NJ, USA, 2022.
31. Alcarria, A.; Suarez, A.; Martinez, P.A.; Victoria, J.; Amaro, A.; Torres, J. Magnetic-Metallic board-level shielding hybrid solution evaluation. In Proceedings of the 2020 International Symposium on Electromagnetic Compatibility-EMC Europe, Rome, Italy, 23–25 September 2020; IEEE: Piscataway, NJ, USA, 2023; pp. 1–5.
32. SAE ARP6248; Stripline Test Method to Characterize the Shielding Effectiveness of Conductive EMI Gaskets up to 40 GHz. SAE International: Warrendale, PA, USA, 2022.
33. IEC 61967-8; Integrated Circuits—Measurements of Electromagnetic Emissions—Part 8: Measurement of Radiated Emissions—IC Stripline Method. International Electrotechnical Commission: Geneva, Switzerland, 2011.
34. Sabine, W.C. *Collected Papers on Acoustics*; University of California Libraries: Berkeley, CA, USA, 1922.
35. Serra, R.; Marvin, A.C.; Moglie, F.; Primiani, V.M.; Cozza, A.; Arnaut, L.R.; Huang, Y.; Hatfield, M.O.; Klingler, M.; Leferink, F. Reverberation Chambers a La Carte: An Overview of the Different Mode-Stirring Techniques. *IEEE Electromagn. Compat. Mag.* **2017**, *6*, 63–78. [[CrossRef](#)]
36. Somolinos, D.R.; Gallardo, B.P.; Sanz, D.L.; Estévez, J.C.; Mena, V.D.; Martínez, D.P. Characterization of Adhesive and Fastener Carbon Fiber Composite Joints Based on a Microstrip Transmission Line Method. In Proceedings of the 2022 International Symposium on Electromagnetic Compatibility-EMC Europe, Gothenburg, Sweden, 5–8 September 2022; IEEE: Piscataway, NJ, USA, 2022; pp. 102–107.
37. IEC 62333-2: 2006 (E); Noise Suppression Sheet for Digital Devices and Equipment Part 2: Measuring Methods. IEC: Geneva, Switzerland, 2006; ISBN 9782889125937.
38. Snelling, E.C. *Soft Ferrites, Properties and Applications*, 2nd ed.; Butterworth: Boston, MA, USA, 1988.
39. Lovat, G.; Burghignoli, P.; Celozzi, S. Shielding Properties of a Wire-Medium Screen. *IEEE Trans. Electromagn. Compat.* **2008**, *50*, 80–88. [[CrossRef](#)]
40. Li, D.; Hu, X.; Gao, B.; Yin, W.-Y.; Chen, H.; Qian, H. Highly Transparent Tunable Microwave Perfect Absorption for Broadband Microwave Shielding. *Prog. Electromagn. Res.* **2023**, *176*, 35–44. [[CrossRef](#)]
41. Borecki, M.; Sroka, J. Evaluation of the Effectiveness of Ferrite Characteristics Measurements Based on the CISPR 17 Standard. *IEEE Trans. Magn.* **2022**, *58*, 2800708. [[CrossRef](#)]
42. ASTM D4935-18; Standard Test Method for Measuring the Electromagnetic Shielding Effectiveness of Planar Materials. ASTM International: West Conshohocken, PA, USA, 2018.

Disclaimer/Publisher's Note: The statements, opinions and data contained in all publications are solely those of the individual author(s) and contributor(s) and not of MDPI and/or the editor(s). MDPI and/or the editor(s) disclaim responsibility for any injury to people or property resulting from any ideas, methods, instructions or products referred to in the content.

5.5 Summary

Using the tools and knowledge generated in this work, we have designed, produced, and tested a new product for board-level shielding. It presents different advantages compared with other solutions and shows excellent potential for upcoming challenges following the electronics market trends.

Chapter 6. CONCLUSIONS AND TECHNOLOGICAL TRANSFER

This final chapter presents the general and specific conclusions drawn from this doctoral thesis. In addition, this chapter presents the transfer to the industry of the results and knowledge derived from this Ph.D. study.

6.1 Conclusions

The magnetic absorbers have been thoroughly studied, analyzed, and evaluated in this doctoral thesis, demonstrating their usefulness for EMI control. Furthermore, this doctoral thesis provides a comprehensive characterization of the materials through different experimental measurement methods and simulation models, allowing for determining their performance from the perspective of magnetic properties, dimensions, and position in the electronic device to be protected.

Measurements of permeability, resistivity, and permittivity have enabled us to characterize the materials' electromagnetic properties. Through implemented measurements of transmission losses, absorption, and decoupling, we have been able to assess the absorbent sheets' performance for EMI prevention. We have also utilized a matrix of magnetic field probes (EMScan) to measure the effect of different absorbers on the distribution of the magnetic field.

Additionally, we have designed a new system to quantify the effectiveness of electromagnetic shielding that is valid for magnetic absorber sheets and other BLS solutions.

Using the characterization measurements performed, we have generated finite element simulation models of the different absorption sheets studied (FSFS, NSS, hybrid solution). We have also simulated the measurement systems, allowing us to validate the models by comparing the simulation results with the experimental ones. The models have helped us to optimally solve EMI problems in near-field communication (NFC) systems. The solutions obtained through simulation have also been corroborated by experimental measurements and used in combination with the Smith Chart and the equivalent circuit of the communication system.

The experimental methods designed and the validated simulation models have allowed us to design and evaluate a new solution for electromagnetic shielding in printed circuits. This solution is based on combining an NSS and an aluminum layer. Both the selection of materials and their thicknesses have been carried out with the knowledge, simulations, and measurements presented in this work. Simulation also allows us to observe the effect of this hybrid solution on the distribution of electromagnetic fields, enabling us to optimize its dimensions for each given problem.

Thus, the hypothesis of this doctoral thesis is demonstrated: electromagnetic absorption sheets enable the solution of complex EMI problems at the PCB level. The measurement and simulation tools generated, combined with the flexibility in the development of new compounds based on ferrimagnetic materials, lay the foundation for addressing present and future challenges in the field of electromagnetic compatibility.

6.2 Technological transfer

The technological transfer of the results of this doctoral thesis has been carried out at various levels.

6.2.1 Measurement setups

In this work, we have designed and implemented different measurements to better understand magnetic absorber sheets and their performance against EMI. Those measurement setups, with the documentation needed to perform and understand them, have been transferred and installed in various laboratories of Würth Elektronik, either at its headquarters in Waldenburg (Germany), its quality center in Shenzhen (China), or at the laboratory of the EMC Chair WE-UV. They will be used to characterize existing and future material compositions.

The shielding effectiveness measurement system designed in this work will add valuable information to the specifications of magnetic absorber sheets, shielding cabinets, and other solutions or materials for BLS.

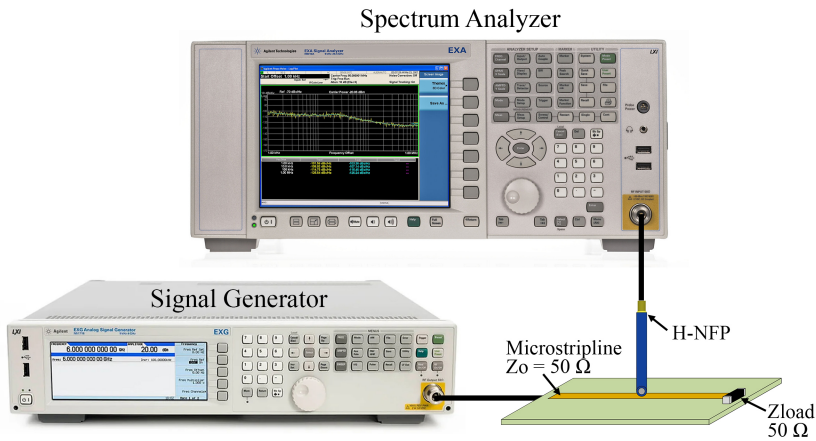
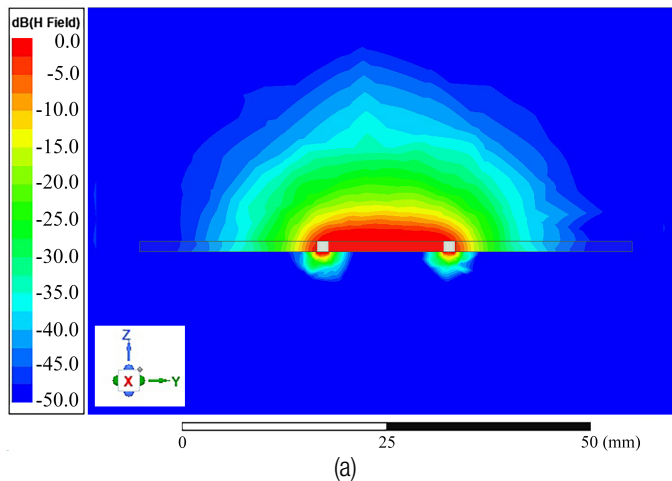


Figure 6.1. Measurement setup designed to determine the SE parameter.

6.2.2 Simulation models

The models of the NSS and FSFS materials generated and verified during this thesis have been implemented in the simulation software ANSYS user library. These models are also available to download from the WE homepage. With these models, designers can select the right material, thickness, and shape of the absorber sheets and observe the changes in magnitude and distribution of the magnetic fields when applying the different solutions.



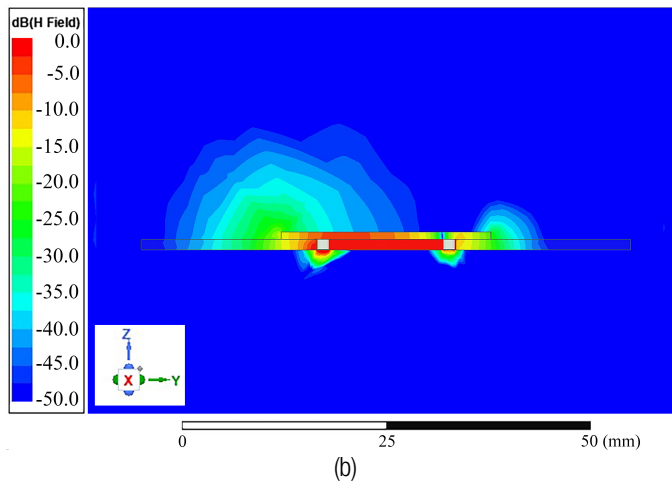


Figure 6.2. H-field results obtained from the simulation model created for the new hybrid shielding solution: (a) EMI source reference; (b) EMI source shielded with the EMI Patch.

The design and inclusion of the WE material models in other simulation platforms are under preparation.

6.2.3 Education

Different application notes and seminars have been written and presented, along with the knowledge generated in this work. These are some examples:

- Application note: ANP016 Going Wireless with Magnetic Shielding.
- Application note: ANP022 Selection and Characteristics of WE-FSFS (Flexible Sintered Ferrite Sheet).
- Seminar EMV Stuttgart 2019: EMI Reduction with Magnetic Absorbers.
- Seminar EMC Live 2019: EMI Reduction with Magnetic Absorbers.
- Seminar PCIM Nürnberg 2022: Study of Combined Solutions for Thermal Management and Electromagnetic Shielding: Shielding Cabinets, EMI Absorbers and Thermal Gap Fillers.
- Workshop IEEE EMC Dresden 2015: NFC/RFID Selective shielding.

6.2.4 Product design and development: EMI Patch™

Following WE's internal process for product development and release and based on the hybrid solution for board-level shielding designed in this work, EMI Patch™ has been launched successfully.



Figure 6.3. WE internal process diagram.

One lamination step has been added to the NSS production process for the addition of the aluminum layer and, optionally, the isolation.

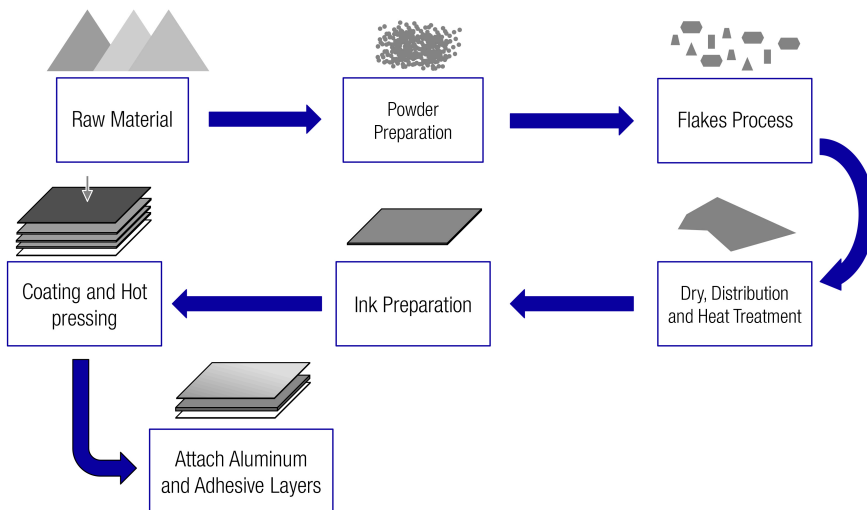


Figure 6.4. Manufacturing procedure for the EMI Patch product (hybrid shielding sheet).

The product portfolio starts with different sizes of the following combinations:

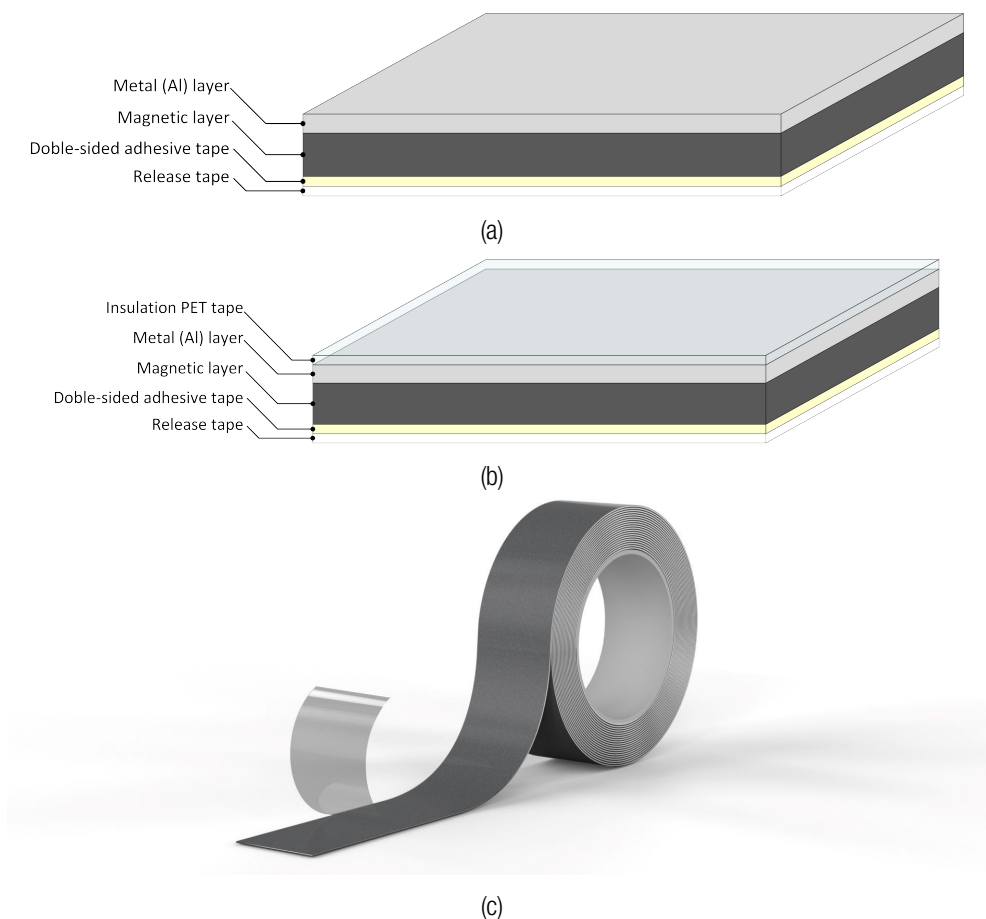


Figure 6.5. EMI Patch product (hybrid shielding sheet): a) layers structure without isolating the top metal layer; b) layers structure isolating the top metal layer; c) final product sample.

The non-isolated version allows the connection of the aluminum layer to a ground plane or metallic enclosure for grounding. On the other hand, the isolated version avoids any possibility of a short circuit due to the inclusion of the EMI Patch™ in a critical PCB region.

REFERENCES

1. *Electromagnetic Compatibility Directive*, European Commission 2014/30/EU (EMCD), 2014.
2. Rohde & Schwarz. *Precompliance EMI debug: Accelerating time-to-market with EMI Debugging & Troubleshooting Simplified* (2020). Accessed: Mar. 1, 2024. [Online]. Available: https://cdn.rohde-schwarz.com/pws/campaigns/rsa/Rohde_Schwarz_Precompliance_EMI_Debug_AppNote_V1.pdf
3. H. W. Ott, *Electromagnetic Compatibility Engineering*. New York, NY, USA: Wiley, 2011.
4. J.Smit and H.P.J.Wijn, *Ferrites - Physical properties and technical applications*. Eindhoven, Holland: N.V. Philips' Gloeilampenfabrieken, 1959.
5. T. Brander, A. Gerfer, B. Rall and H. Zenkner, *Trilogy of Magnetics: Design Guide for EMI Filter Design SMPS & RF Circuits*. Waldenburg, Germany: Würth Elektronik, 2018.
6. C. Kittel and A. H. Mitchell, "Ferromagnetic Relaxation and Gyromagnetic Anomalies in Metals," *Phys. Rev.*, vol. 101, no. 1611. 1956, doi: 10.1103/PhysRev.101.1611.
7. A. Goldman, *Modern Ferrite Technology*. New York, NY, USA: Springer, 2006.
8. Würth Elektronik (Jorge Victoria). *Application note: Selection and Characteristics of WE-FSFS (Flexible Sintered Ferrite Sheet)* (2014). Accessed: Mar. 1, 2024. [Online]. Available: https://www.we-online.com/components/media/o109046v410%20ANP022Selection_and_Characteristics_of_WE-FSFS_5k_9images%20%281%29.pdf
9. Würth Elektronik (Jorge Victoria). *Application note: Characterization Methods for Flexible Absorber Sheets WE-FAS* (2018). Accessed: Mar. 1, 2024. [Online]. Available: https://www.we-online.com/components/media/o122566v410%20ANP059a_EN_Characterization_Methods_for_Flexible_Absorber_Sheets_WE-FAS%20%281%29.pdf
10. Keysight Technologies. *Application brief: Materials Testing: Magnetic Material Measurement* (2014). Accessed: Mar. 1, 2024. [Online]. Available: <https://www.keysight.com/zz/en/assets/7018-04460/application-notes/5991-4714.pdf>
11. *Standard Test Methods for DC Resistance or Conductance of Insulating Materials*, ASTM D257-14, 2014.
12. Prostat Corporation. *Concentric Ring PRF-911 Operations Manual* (2007). Accessed: Mar. 1, 2024. [Online]. Available: https://www.coreinsight.co.kr/images/down/PRF-911_MANUAL.pdf

13. Keysight Technologies. *Application note: Basics of Measuring the Dielectric Properties of Materials* (2020). Accessed: Mar. 1, 2024. [Online]. Available: <https://www.keysight.com/zz/en/assets/7018-01284/application-notes/5989-2589.pdf>
14. P. A. Martinez et al., "Design and study of a wide-band printed circuit board near-field probe", *Electronics*, vol. 10, no. 18, Sep. 2021.
15. *Noise suppression sheet for digital devices and equipment – Part 2: Measuring methods*, IEC 62333-2, 2006.

Appendix A. SCIENTIFIC CONTRIBUTIONS

This section includes a list of all the scientific publications and conferences derived from this Ph.D. work in chronological order.

A.1 Peer-reviewed scientific articles in journals

J. Victoria, A. Suarez, J. Torres, P. Martinez, A. Alcarria, J. Martos, et al., "Transmission Attenuation Power Ratio Analysis of Flexible Electromagnetic Absorber Sheets Combined with a Metal Layer", *Materials*, vol. 11, no. 9, pp. 1612-1626, Sep. 2018, doi: 10.3390/ma11091612.

J. Victoria, A. Suarez, P. A. Martinez, A. Alcarria, A. Gerfer and J. Torres, "Improving the Efficiency of NFC Systems Through Optimizing the Sintered Ferrite Sheet Thickness Selection," in *IEEE Transactions on Electromagnetic Compatibility*, vol. 62, no. 4, pp. 1504-1514, Aug. 2020, doi: 10.1109/TEMPC.2020.3003800.

J. Victoria, A. Suárez, P. A Martinez, A. Amaro, A. Alcarria, J. Torres *et al.*, "Advanced Characterization of a Hybrid Shielding Solution for Reducing Electromagnetic Interferences at Board," *Electronics*, vol. 13, no. 3, Jan. 2024, doi: 10.3390/electronics13030598.

A.2 Peer-reviewed scientific articles in conferences

A. Suarez, J. Victoria, A. Alcarria and J. Torres, "Characterization of electromagnetic noise suppression sheet for aerospace applications," *2016 ESA Workshop on Aerospace EMC (Aerospace EMC)*, Valencia, Spain, 2016, pp. 1-6, doi: 10.1109/AeroEMC.2016.7504546.

A. Suarez, J. Victoria, A. Alcarria, J. Torres, P. A. Martinez, J. Soret, et al., "Characterization of Flexible Absorber Sheets with an EMC Scanner System," *SAAEI 2017 Proceedings*, Valencia, Spain, 2017.

J. Victoria, P. A. Martinez, A. Suarez, A. Alcarria, S. Mirasol and J. Torres, "Design approach for high efficiency NFC systems with magnetic shielding materials", *2020 International Symposium on Electromagnetic Compatibility - EMC EUROPE*, pp. 1-7, 2020, doi: 10.1109/EMCEUROPE48519.2020.924586.

J. Victoria, A. Suarez, P. A. Martinez, A. Alcarria, A. Amaro and J. Torres, "Board-level shielding with magnetic absorber sheet," *2022 International Symposium on Electromagnetic Compatibility – EMC Europe*, Gothenburg, Sweden, 2022, pp. 74-78, doi: 10.1109/EMCEurope51680.2022.9901317.

Appendix B. LIST OF ABBREVIATIONS

This section includes a list of all the abbreviations included in this Ph.D. work in alphabetical order.

ASTM	American society for testing and materials
BLS	Board-level shielding
dB	Decibels
EMC	Electromagnetic compatibility
EMI	Electromagnetic interference
EU	European Union
FEM	Finite element method
FMR	Ferromagnetic resonance
FSFS	Flexible sintered ferrite sheet
IC	Integrated circuit
IEC	International electrotechnical commission
MAS	Magnetic absorber sheet
NFC	Near field communication
NSS	Noise suppression sheet
PCB	Printed circuit board
PET	Polyethylene terephthalate
RF	Radio frequency
SE	Shielding effectiveness
SEM	Scanning electron microscopy
UV	University of Valencia
VNA	Vector network analyzer
WE	Würth Elektronik
WPC	Wireless power charger